NBS TECHNICAL NOTE

415

Thermal Radiation Property Measurement Techniques

S. T. Dunn, J. C. Geist, D. G. Moore,
H. E. Clark, and J. C. Richmond

U.S. DEPARTMENT OF COMMERCE
National Bureau of Standards

THE NATIONAL BUREAU OF STANDARDS

The National Bureau of Standards[1] provides measurement and technical information services essential to the efficiency and effectiveness of the work of the Nation's scientists and engineers. The Bureau serves also as a focal point in the Federal Government for assuring maximum application of the physical and engineering sciences to the advancement of technology in industry and commerce. To accomplish this mission, the Bureau is organized into three institutes covering broad program areas of research and services:

THE INSTITUTE FOR BASIC STANDARDS . . . provides the central basis within the United States for a complete and consistent system of physical measurements, coordinates that system with the measurement systems of other nations, and furnishes essential services leading to accurate and uniform physical measurements throughout the Nation's scientific community, industry, and commerce. This Institute comprises a series of divisions, each serving a classical subject matter area:

—Applied Mathematics—Electricity—Metrology—Mechanics—Heat—Atomic Physics—Physical Chemistry—Radiation Physics—Laboratory Astrophysics[2]—Radio Standards Laboratory,[2] which includes Radio Standards Physics and Radio Standards Engineering—Office of Standard Reference Data.

THE INSTITUTE FOR MATERIALS RESEARCH . . . conducts materials research and provides associated materials services including mainly reference materials and data on the properties of materials. Beyond its direct interest to the Nation's scientists and engineers, this Institute yields services which are essential to the advancement of technology in industry and commerce. This Institute is organized primarily by technical fields:

—Analytical Chemistry—Metallurgy—Reactor Radiations—Polymers—Inorganic Materials—Cryogenics[2]—Materials Evaluation Laboratory—Office of Standard Reference Materials.

THE INSTITUTE FOR APPLIED TECHNOLOGY . . . provides technical services to promote the use of available technology and to facilitate technological innovation in industry and government. The principal elements of this Institute are:

—Building Research—Electronic Instrumentation—Textile and Apparel Technology Center—Technical Analysis—Center for Computer Sciences and Technology—Office of Weights and Measures—Office of Engineering Standards Services—Office of Invention and Innovation—Clearinghouse for Federal Scientific and Technical Information.[3]

---

[1] Headquarters and Laboratories at Gaithersburg, Maryland, unless otherwise noted; mailing address Washington, D. C., 20234.
[2] Located at Boulder, Colorado, 80302.
[3] Located at 5285 Port Royal Road, Springfield, Virginia, 22151.

NBS TECHNICAL NOTE 415

ISSUED APRIL 27, 1967

Thermal Radiation
Property Measurement Techniques

S. T. Dunn, J. C. Geist, D. G. Moore,
H. E. Clark, and J. C. Richmond

Institute for Basic Standards
National Bureau of Standards
Washington, D.C., 20234

CONTENTS

LIST OF ILLUSTRATIONS

THERMAL RADIATION PROPERTY MEASUREMENT TECHNIQUES

S. T. Dunn, J. C. Geist, D. G. Moore, H. E. Clark and J. C. Richmond

This is an annual summary report of work completed on NASA Contract R-09-022-032. The work comprised (1) completion of the development and calibration of a rotating cylinder procedure for measuring normal spectral emittance of non-conducting materials at temperatures in the range of 1200 to 1600 °K, (2) analysis and calibration of an ellipsoidal mirror reflectometer, and (3) a study of the relation between surface roughness and geometric distribution of flux reflected from a surface.

Key Words: Averaging spheres, diffuse reflectance, emissivity, emittance, flux averaging devices, infrared reflectance, spectral reflectance, spectral emittance, specular reflectance.

1 Introduction

This is the yearly report on the NASA contract No. R-09-022-032. The group working on the NASA contract has the following long-range objectives:

(a) To develop accurate and versatile methods of measuring thermal radiative properties throughout the electromagnetic spectrum of interest to the theoretician and heat transfer analyst.

(b) To provide close liaison between the field of thermal radiative property measurements and the field of thermal radiative heat transfer.

(c) To study the relation of thermal radiative properties of engineering surfaces and fundamental properties of matter (composition and structure).

(d) To advance the state of the art of thermal radiative heat transfer computations by developing more accurate techniques.

At present two experimental instruments are funded on this contract: the Rotating Cylinder Equipment for spectral emittance measurements from 1 to 15μm and temperatures from 1200 to 1800 °K; and the Ellipsoidal Mirror Reflectometer for spectral reflectance measurements from 0.4 to about 8μm in the approximate temperature range of 300 to 800 °K. Both of these instruments seem to provide the most accurate data available over their useful wavelength and temperature ranges. In addition, the ellipsoidal mirror reflectometer provides the necessary reflectance optics to measure directional hemispherical reflectance, bi-directional reflectance, and directional annular cone reflectance.

The rotating cylinder equipment measures normal spectral emittance by utilizing a specimen, in the form of a hollow cylinder, which rotates in a furnace having a water-cooled viewing port. Energy radiated by the specimen through the port is focused on one entrance slit of a double-beam spectrophotometer while energy from a blackbody furnace at the same temperature as the specimen is focused on the other slit. The instrument then plots the flux ratio of the two beams as a function of wavelength. This ratio, when corrected for instrument response, gives the normal spectral emittance.

The paper covering the summary and analysis of this instrument has been reviewed and accepted

for publication as an NBS Technical Note. In addition, D. G. Moore presented the basic conclusions of the paper at the September, 1965, meeting of the American Ceramic Society in French Lick, Indiana. Basically the paper describes the design and construction of equipment to measure the spectral normal emittance of polycrystalline ceramic oxide specimens in the wavelength region 1 - 15μm and at temperatures of 1200, 1400, and 1600 °K. Specimens consisted of small hollow cylinders that were rotated at 100 RPM in a furnace cavity equipped with a water-cooled viewing port. The emittances were determined by comparing the flux from the specimen to that from a laboratory blackbody furnace at the same temperature. Error sources were investigated and, where possible, the measurement uncertainties associated with each source were evaluated. The overall accuracy of measurements made with the equipment was estimated to be ±0. 02 in emittance.

A series of six measurements (two measurements each on three specimens) was made on commercially pure specimens of alumina, thoria, magnesia, and zirconia. All four materials showed similar behavior in that the emittances were low in the shorter wavelength regions and high at the longer wavelengths. Also, the temperature coefficients of spectral emittance were positive for all four material. The coefficients, however, varied with the materials; those for thoria were appreciably higher than those for the others. In all cases coefficients were greater at short wavelengths than at long. The measured emittances were consistent with emittance computed from room-temperature reflectances measured on the same materials. Also, the data for alumina were consistent with recently reported absorption coefficients for sapphire. The data were reduced on the computer, and the standard deviations (due to both sample differences and instrument error) were calculated. The average of the standard deviations for these measurements was about 0. 007 emittance units.

The ellipsoidal mirror reflectometer was initially constructed in 1960, under a project sponsored by the Marshall Space Flight Center. The original detector used with the equipment was a Golary cell detector of large sensitive area (1-cm diameter), used with the sensitive diaphragm in a horizontal position. The detector proved to be highly microphonic, and usable signal-to-noise ratios were not attained in spite of elaborate precautions to isolate the equipment from air-borne and structure-borne noise.

Work on the equipment was transferred to Air Force sponsorship during the period November 1962 through October 1964, and is reported in NBS Technical Notes 252 and 267.

The principal accomplishments prior to initiation of the present contract were (1) the Golay cell was demonstrated to be definitely unsuitable for use in this instrument; (2) the thermopile detector, procured to replace the Golay cell detector, was shown to have serious variations in areal and angular sensitivity; and (3) several different diffusing devices were developed for use with the thermopile detector.

During the current contract year, the instrument was further developed and analysed. Continued work on the ellipsoidal mirror reflectometer awaits the development of the interferometer spectrometer as outlined later in this report.

The remainder of the work done under Contract No. R-09-022-032 was performed in completion of past contracts with Marshall Space Flight Center (H-41986 and H-71435) or as logical extensions of our NASA-NBS mission.

2   Nomenclature

Before discussing the various measurement techniques in this report, the terms discussed must be specifically defined. During the past year, several members of this section have participated in discussions leading to a system of nomenclature for reflectance terms which we are presently refining before presentation to the various nomenclature committees and in the various technical journals.

2. 1 Reflectance

Reflectance, ρ, in general, is defined as the ratio of reflected flux to incident flux. Since this ratio will vary with the geometric and spectral distribution of both the incident and reflected flux, the term reflectance must be suitably modified in order to define precisely the quantity referred to.

2. 1. 1 <u>Naming:</u> A two adjective naming system is suggested for the various geometrical kinds of reflectance, where the first adjective modifying reflectance refers to incident conditions and the second adjective refers to the collection (or exit) conditions. The adjectives proposed are:

Hemispherical: Perfectly diffuse incidence when applied to incident condition and nonselective collection when applied to exit condition.

Conical: Incident from or collected over a finite solid angle smaller than a hemisphere. The size, shape, if other than a right circular cone, and direction of the axial ray of the solid angle or angles involved must be specified.

Directional: This means incident from or collected over an infinitesimal solid angle in a given direction.

2. 1. 2 <u>Symbols:</u> The following simplified convention is suggested for writing symbols for the various reflectances. To define the incident and collection conditions, the reflectance symbol ρ should be followed by parentheses which contain this information. To facilitate a minimum amount of symbolism, a set of ground rules is given.

θ, φ, g refer to the incident conditions where θ is the angle from the normal to the surface, φ is the azimuthal angle from some reference on the specimen, and g refers to the geometry of the finite solid angle; θ', φ', g' represent the collection conditions.

2π refers to hemispherical incidence or collection.

The use of θ, φ, or θ', φ' implies directional incidence or directional collection, respectively.

g or g' implies conical incidence or conical collection, respectively.

Table I gives the nine terms for reflectance and their symbols.

Table I Reflectance Terminology

Name	Symbol
bi-hemispherical reflectance	$\rho(2\pi; 2\pi)$
hemispherical–conical reflectance	$\rho(2\pi; g')$
hemispherical–directional reflectance	$\rho(2\pi; \theta', \varphi')$
conical–hemispherical reflectance	$\rho(g; 2\pi)$
bi-conical reflectance	$\rho(g; g')$
conical-directional reflectance	$\rho(g; \theta', \varphi')$
directional-hemispherical reflectance	$\rho(\theta, \varphi; 2\pi)$
directional-conical reflectance	$\rho(\theta, \varphi; g')$
directional-directional reflectance	$\rho(\theta, \varphi; \theta', \varphi')$

The terms radiance factor, β, and reflectance factor, R, can be used with the same symbols indicated for reflectance, ρ, in Table I. The radiance factor is always a directional property, while the reflectance factor is always a conical or hemispherical property. Radiance factor β, is defined as the ratio of the reflected radiance of a specimen in a given direction θ', φ'; to that of the ideal

completely reflecting perfectly diffusing surface, identically irradiated. (For a perfectly diffusing surface, the reflected radiance does not vary with direction.) Reflectance factor is defined as the ratio of the reflectance of a specimen under specified conditions of irradiation and collection, to that of the ideal perfectly reflecting completely diffusing surface, under identical conditions of irradiation and collection.

2.1.3 **Reflectance relationships:** The most used terms in reflectance are defined below; the definition of the other terms in Table I obviously follows these same lines.

Radiance-irradiance quotient: The radiance-irradiance quotient, ℓ, is defined first because of its symmetry in θ, φ and θ', φ' and second because of its usefulness in other definitions.

$$\ell(\theta, \varphi; \theta', \varphi') = \frac{L'(\theta', \varphi')}{L(\theta, \varphi) \cos\theta \, d\omega} \tag{1}$$

where θ is the polar angle, φ is the azimuth with respect to a convenient reference. The primes denote collection directions and the unprimed letters the incident directions. $L(\theta, \varphi)$ denotes radiance in the direction θ, φ. Radiance, as used here, is identical to the term intensity as used in the heat transfer literature.

Radiance (i.e. $\partial^2 P / \cos\theta \, \partial A \, \partial\omega$ where P is power, A is the area of the emitting surface and ω is the solid angle of collection) has been shown to be invariant along a path in a loss-less system [2]. Other authors, at various times, have called $\ell(\theta, \varphi; \theta', \varphi')$:

1) bi-angular reflectance, 2) reflectance function, and 3) partial remission factor.

Reference 1 and 2 present a detailed discussion with additional references of the reciprocity of the radiance-irradiance quotient (i.e. $\ell(\theta, \varphi; \theta', \varphi') = \ell(\theta', \varphi'; \theta, \varphi)$.

Bi-directional reflectance

$$\rho(\theta, \varphi; \theta', \varphi') = \frac{L(\theta', \varphi') \cos\theta' \, d\omega'}{L(\theta, \varphi) \cos\theta \, d\omega} \tag{2}$$

Directional hemispherical reflectance, $\rho(\theta, \varphi; 2\pi)$: This is the ratio of the flux reflected into the hemisphere above the surface to that incident from an infinitesimal solid angle in the direction θ, φ.

$$\rho(\theta, \varphi; 2\pi) = \frac{\int_H L'(\theta', \varphi') \cos\theta' \, d\omega'}{L(\theta, \varphi) \cos\theta \, d\omega} \tag{3}$$

This could also be written as:

$$\rho(\theta, \varphi; 2\pi) = \int_H \ell(\theta, \varphi; \theta', \varphi') \cos\theta' \, d\omega' \tag{4}$$

Of course, experimentally we measure the reflectance for a small group of directions centered on θ, φ. Thus, we depend on $\rho(\theta, \varphi; 2\pi)$ to change only slowly with small changes in θ, φ. In general, the study of this variable has only begun. Further, past experience in the visible spectrum $(0.4 - 7.\mu)$ is not necessarily applicable either to the ultraviolet or the infrared regions of the spectrum.

Hemispherical directional reflectance $\rho(2\pi; \theta', \varphi')$: This is the ratio of flux reflected into an infinitesimal solid angle, $d\omega'$ in the direction θ', φ' to that incident diffusely over the hemisphere.

$$\rho(2\pi; \theta', \varphi') = \frac{L'(\theta', \varphi') \cos\theta' \, d\omega'}{\pi L} \tag{5}$$

where $\int_H L(\theta, \varphi) \cos\theta \, d\omega = \pi L$.

Further, $\rho(2\pi; \theta', \varphi')$ is not equal to $\rho(\theta, \varphi; 2\pi)$.

Bi-hemispherical reflectance: the ratio of flux reflected into the hemisphere above the surface to the incident flux, which is perfectly diffuse over the hemisphere. This is

$$\rho(2\pi; 2\pi) = \frac{\int_H L'(\theta', \varphi') \cos\theta' \, d\omega'}{\pi L} \tag{6}$$

or

$$\rho(2\pi; 2\pi) = 1/\pi \int_H \beta(2\pi; \theta', \varphi') \cos\theta' \, d\omega' \tag{7}$$

Directional specular component of reflectance, $\rho_s(\theta, \varphi)$: the ratio of the flux reflected into a small solid angle $d\omega'$ in the specular direction ($\theta' = \theta$ and $\varphi' = 180° + \varphi$) over and above the diffuse component in that direction, to the flux incident from the direction θ, φ. This is a very difficult term to realistically assess for common engineering materials since the separation of specularly reflected flux from the diffusely reflected flux is difficult. Further reference 3 indicates that this term probably has little use in the heat transfer calculations.

Diffuse component of reflectance, $\rho_D(\theta, \varphi; 2\pi)$, is equal to the directional hemispherical reflectance minus the specular component of reflectance [i. e. $\rho_D(\theta, \varphi; 2\pi) = \rho(\theta, \varphi; 2\pi) - \rho_s(\theta, \varphi)$]. The problems in determining the directional specular component of reflectance similarly affect the definition of the diffuse component of reflectance.

These definitions lead to the following well known conclusion for a surface in equilibrium with an isothermal enclosure [4].

In a hohlraum

$$\epsilon(\theta, \varphi) = 1 - \beta(2\pi; \theta', \varphi') \tag{8}$$

From conservation of energy

$$\alpha(\theta, \varphi) = 1 - \rho(\theta, \varphi; 2\pi) \tag{9}$$

From reciprocity

$$\rho(\theta, \varphi; 2\pi) = \beta(2\pi; \theta', \varphi') \tag{10}$$

Therefore, from 8, 9 and 10

$$\alpha(\theta, \varphi) = \epsilon(\theta, \varphi) \tag{11}$$

The above definitions frequently consider the unidirectional case, while in practice we almost always measure a reflectance for a small solid angle centered in the direction θ, φ or θ', φ'. What size solid angle is small enough to measure $\rho(\theta, \varphi)$ depends on $\ell(\theta, \varphi; \theta', \varphi')$; this is dependent on so many surface and material variables that a general statement on the size of measurement solid angle is impossible. The experimentalist must exhibit care in choosing the instrument solid angle, depending on the samples to be measured, wavelength range of interest, energy limitations, information desired, etc. Further, the above definitions do not discuss the conical case where the solid angles are between the hemispherical case and the unidirectional case. Thus it is necessary to integrate the incident radiance function over the solid angle of interest, by using the appropriate weighting factor, such as $\rho(\theta, \varphi; 2\pi)$.

The spectral conditions refer to the wavelength (spectral) distribution of the incident flux and the wavelength (spectral) response of the detector. If only a narrow wavelength band of incident flux, centered about the wavelength λ, is used, the reflectance is referred to as spectral reflectance, $\rho(\lambda)$. In this case, the spectral response of the detector is assumed to be flat over the narrow wavelength band involved, and need not be specified. If a broad wavelength band of incident flux is used, the measured reflectance is a function of both the spectral distribution of the source and the spectral response of the detector. If the product of the spectral distribution of the source and the spectral

response of the detector approximates the spectral distribution of solar energy, the measured reflectance may be referred to as solar reflectance; if the product approximates the CIE photophic spectral luminous efficience curve, the measured reflectance may be referred to as luminous reflectance for an "equal energy" source.

The radiance factor, β, and reflection factor, R, are important because they are the properties measured by most infrared reflectometers. For hemispherical collection, the reflectance factor is numerically equal to the reflectance

$$\rho(g; 2\pi) = \beta(g; 2\pi)$$
$$\rho(\theta, \varphi; 2\pi) = \beta(\theta, \varphi; 2\pi) \tag{12}$$
$$\rho(2\pi; 2\pi) = \beta(2\pi; 2\pi)$$

There are also certain reciprocal relationships that hold when the solid angles of irradiation and collection are interchanged while the incident radiance remains constant. For the following equations $\theta = a$, $\varphi = b$, $\theta' = c$, $\varphi' = d$, $g = e$, $g' = f$.

$$R(2\pi; f) = R(f; 2\pi)$$
$$\beta(2\pi; c, d) = R(c, d; 2\pi)$$
$$R(e; 2\pi) = R(2\pi; e)$$
$$\rho(a, b; c, d) = \rho(c, d; a, b) \tag{13}$$
$$\beta(a, b; c, d) = \beta(c, d; a, b)$$
$$R(e; f) = R(f; e)$$

It should be noted that only one kind of reflectance is included in these reciprocal relationships.

2.2 Emittance Definitions

Emittance (and absorptance) definitions are simpler since only one angular condition need be specified.

Thermal emittance, ϵ, is defined as the ratio of the radiant flux per unit area emitted by a specimen at a given temperature and under given geometric and spectral conditions, to that emitted by a blackbody radiator at the same temperature and under the same spectral and geometric conditions.

Absorptance, α, is defined as the ratio of absorbed flux to incident flux. Absorptance will vary with the spectral and geometric conditions of irradiation. The following comments regarding emittance apply also to absorptance, except that the geometric and spectral conditions refer to incident flux rather than to emitted flux. The term total absorptance refers to absorptance for radiation emitted by a blackbody radiator at a given temperature which should be specified, as α_T (1000 °K).

The geometric conditions refer to the size of the emitting area, the size of the solid angle, ω, over which the emitted flux is measured, and the direction, θ, φ, of the centroid of that solid angle from the emitting surface. The angle θ is measured from the given direction to the normal to the emitting surface and the angle φ is the azimuth angle of the given direction from some reference on the specimen. When the solid angle is a complete hemisphere, 2π steradians, the emittance is referred to as <u>hemispherical emittance,</u> ϵ_H. When the solid angle is small, its size usually is not specified, and the emittance is referred to as <u>directional emittance,</u> $\epsilon(\theta, \varphi)$; or if the direction is normal to the emitting surface, as <u>normal emittance,</u> ϵ_N. The azimuth angle, φ, is specified only for surfaces in which ϵ varies with azimuth angle, such as fibrous materials, textiles, oriented crystals and grooved surfaces.

The spectral conditions refer to the wavelength range of the radiant flux that is measured. If all wavelengths are measured, the emittance is referred to as <u>total emittance,</u> ϵ_T. Since emittance, and particularly total emittance, varies with temperature, total emittance is frequently plotted as a function of temperature to give a total emittance curve. If only a narrow wavelength band of flux is measured, centered about a wavelength, λ, the emittance is referred to as spectral emittance, $\epsilon(\lambda)$
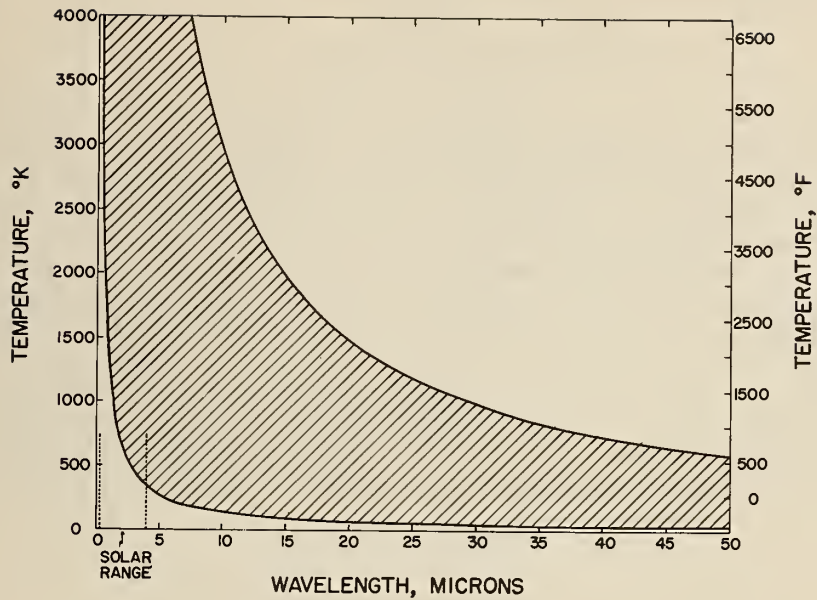
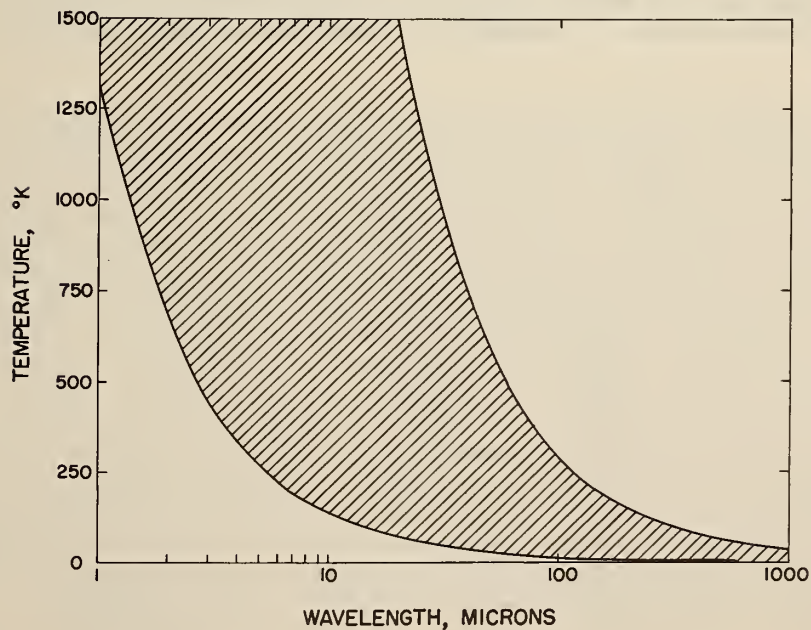Figure 1. Ninety-nine Percent Energy Bands for High Temperatures

Figure 2. Ninety-nine Percent Energy Bands for Low Temperatures

7

at wavelength λ   Spectral emittance is frequently plotted as a function of wavelength to give a spectral emittance curve.

2.3 Spectral Range of Interest

With the above types of reflectances, absorptances and emittances defined on a monochromatic basis, it is necessary to know the wavelengths at which these properties should be measured. If one considers the problem of heat transfer, it is apparent that the wavelengths of interest are those at which the principal amount of energy is transmitted. The cross-hatched areas of figures 1 and 2 indicate the wavelength band encompassing 99 percent of the flux emitted by a blackbody source at the indicated temperature. These graphs indicate that for high temperatures the band is very small and centered near the visible (0.4 to 0.7μm); as the temperature decreases, the center of the band shifts to longer wavelengths, and it becomes much wider, so that at very low temperatures it is extremely wide and centered far out in the infrared. Thus, the wavelength of interest varies with application; the space program of satellite temperature control is primarily concerned with the 0.25 to 35μm region, which encompasses the principal flux from the sun, that emitted and reflected by the earth, and that emitted by the spacecraft. The theorist for most studies is not too concerned with the wavelengths measured, but mostly with having a very wide band of wavelengths from which to choose.

3   Ellipsoidal Mirror Reflectometer

3.1 Theory of the Ellipsoidal Mirror Reflectometer

This section describes the conceptual design and operation of an ellipsoidal mirror reflectometer, which was developed to minimize the problems experienced during previous attempts to measure accurately infrared reflectance. Further, during the development of this instrument, the versatility of measurement was stressed to enable absolute or relative measurement of $\rho(\theta, \varphi; 2\pi)$, $\rho(\theta, \varphi; \theta', \varphi')$, ρ(specular), ρ(non-specular), and ρ(directional annular cone)[1]. Initially, the instrument is intended for use in the near infrared, where sufficient energy is available from a silicon carbide source (Globar) to actuate thermopile detectors. Eventually, the instrument will be utilized throughout the 0.2 to 500μm range.

Figure 3, which illustrates the basic design of this instrument, shows a SiC element as the source. The flux from the SiC source is chopped by a 11.3 c/s chopper before entering a [prism] monochromator; the monochromatic beam is then refocused (by two mirrors, one an optically flat, front surface, aluminum mirror with no overcoat, and the other a 36-inch radius of curvature, front surface, spherical mirror) through a small entrance hole onto the first focal point of an ellipsoidal mirror. The ellipsoidal mirror is 12 1/4 inches in diameter and 3 5/8 inches high, the first focal point is in the plane of the edge of the mirror, and the second focal point is 17 inches below the first focal point. The detector signal is amplified by a thermocouple synchronous amplifier. To measure the incident flux, the detector is placed at the first focal point (see figure 4). The reflected flux is measured by placing the detector at the second focal point and the sample at the first focal point; the reflected flux leaves the sample and is focused by the ellipsoidal mirror onto the detector at the second focal point. Thus, after correcting for system losses, the absolute directional diffuse reflectance is measured for $\theta = 7°$. When the instrument is operated in the relative mode, the detector is always at the second focal point and two measurements are made, one with a sample at the first focal point, the other with a reflectance standard at the first focal point. As in other methods of reflectance measurement, the relative measurement tends to eliminate the effects of atmospheric absorption and reduce the effect of the other errors; however, it also requires the use of nonexistent reflectance standards.

This instrument has the same inherent losses as the other systems, with the following exceptions:

---

[1] A detailed list of terms used throughout this section appears at the end of the section.

CHOPPED FLUX FROM MONOCHROMATOR

ENTRANCE HOLE

SPECULARLY REFLECTING ELLIPSOIDAL MIRROR

FIRST FOCAL PLANE

FIRST FOCAL POINT

N

7°

SECOND FOCAL POINT

Figure 4. Optics of the Ellipsoidal Mirror

36" RADIUS SPHERICAL MIRROR

ELLIPSOIDAL MIRROR

DETECTOR AT SECOND FOCAL POINT

MONOCHROMATOR

SPECIMEN

SIDE VIEW

45° ALUMINUM FRONT SURFACE MIRROR

MONOCHROMATOR

CHOPPER

GLOBAR SOURCE

SOURCE OPTICS
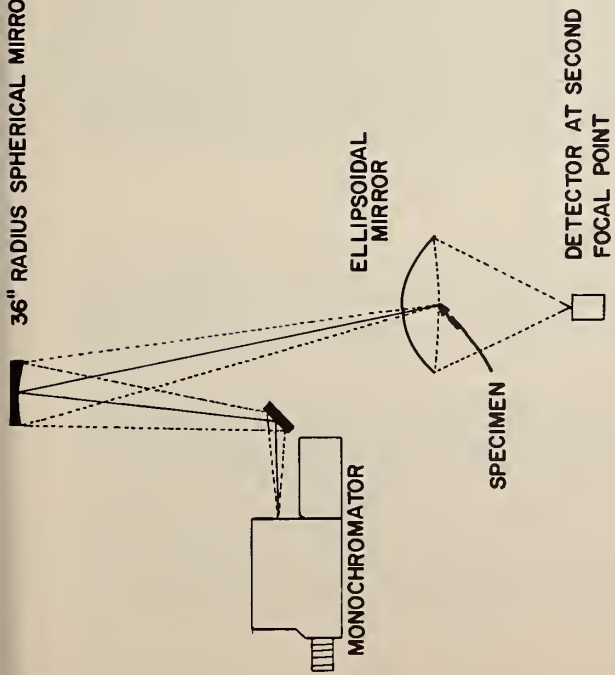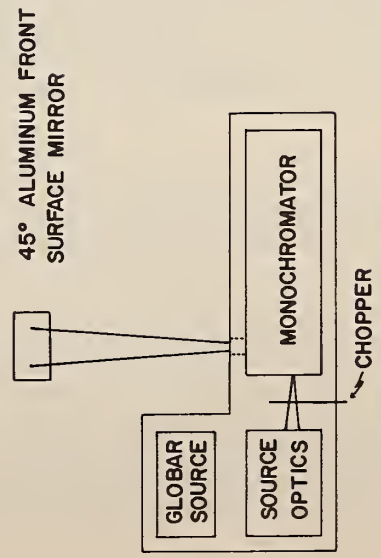
PARTIAL TOP VIEW

Figure 3. General Optical System of the Ellipsoidal Mirror Reflectometer

9

a. Aberrations are reduced to a minimum, since all measurements are centered around true focal points rather than conjugate focal points [5].

b. The reflected energy is now concentrated in a small cone (24° half-angle), instead of over the entire hemisphere, which reduces errors due to angular sensitivity. (See Appendix C, Flux Averaging Devices).

c. The detector and sample are widely separated (17 inches), which will allow heating and cooling of the sample over large temperature ranges.

d. Further, the unique optics involved in the use of the ellipsoidal mirror will allow accurate calibration of mirror and hole losses for all but the most radically distributed reflected flux (such as that from a diffraction grating).

3.2 Measurement Capabilities

This reflectometer is primarily designed for the measurement of $\rho(\theta, \varphi; 2\pi)$; however, the unique optics of the ellipsoidal mirror allow accurate description of the distribution of the reflected flux because the areal distribution of the reflected energy crossing the first focal plane is related precisely to the goniometric distribution of the reflected flux. That is, every direction (θ', φ') from the first focal point in the hemisphere above the first focal plane is represented by a point P in the first focal plane, and every solid angle centered in the direction θ', φ' is represented by an area about P. This implies the ability to select the energy that the detector views by blanking out the unwanted energy with a shield placed in the first focal plane. With this procedure, a specular component can be measured which has a solid angle determined by the open area of the shield placed in the first focal plane. Similarly, the bi-directional reflectance (i.e., $\rho(7°, \varphi; \theta', \varphi')$) could be measured by the same procedure (i.e., by varying the position of the hole in the shield). Measurement of the directional annular cone reflectance is accomplished through use of a set of circular disks centered on the sample, which allows sufficient data for calculation of this reflectance. Further, this ability to measure the distribution of the reflected flux will aid greatly in making precise corrections for the system losses.

Due to energy limiting factors, especially the need for flux averaging devices, the instrument was initially used in the 1.5 to 7.0μm region. Further, since absolute measurements were taken in the laboratory atmosphere, eight wavelengths and corresponding band passes were chosen which do not include the absorption bands of water and CO_2. These wavelengths are 1.5, 2.0, 2.5, 3.5, 4.5, 5.5, 6.5 and 7.0 microns. The width of the band passes varies from about 0.2μm for the shorter wavelengths to about 0.5μm for the longest wavelength setting. These large band passes will not in general be a hindrance, since the materials studied do not have absorption bands or radical changes of reflectance in the wavelength range, 1.5 to 7.0μm.

3.3 Description of System Losses

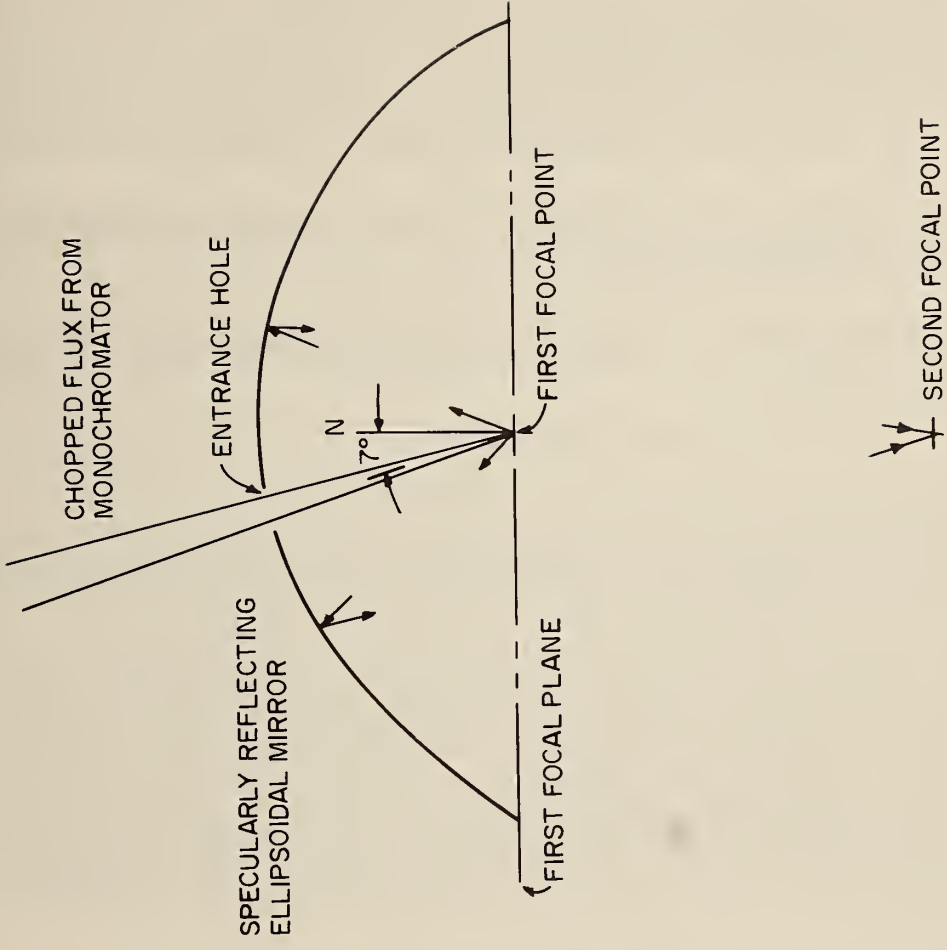In order to attain a high degree of accuracy, the flux losses in the system must be accounted for precisely. Thus, this section qualitatively describes these losses for future use in a flux balance of the system.

Ellipsoidal Mirror Losses (F_α): Energy is absorbed by the ellipsoidal mirror; therefore the reflectance of the mirror coating must be known. This reflectance may vary with angle of incidence on the mirror, and, hence, position on the mirror. The angle of incidence varies from 0° at the apex to 35° at the edge of the mirror. There also will be losses from scattering due to scratches, dust, and other imperfections of the mirror surface.

Hole Losses (F_H): Some of the reflected flux will escape through the hole in the mirror which

admits the incident beam. This loss varies with geometric distribution of the reflected flux. Previous instruments have been unable to accurately establish this loss, which does not necessarily lie between the condition of no loss for a specular sample and a loss based on a diffuse configuration factor from the sample to the entrance hole. For most engineering surfaces, this loss will be higher than would be computed for a diffuse reflector since such surfaces reflect a predominant amount of flux about the specular direction, which may include the direction of the hole.

Sample Shielding ($F_{SP} - F_{SR}$): Flux leaving the sample normal to its surface will be re-reflected to the sample, and hence be blocked from reaching the detector. Most of this will be lost, but some may be multiply reflected by the sample and mirror and reach the detector.

Sample Holder Losses (F_H): Those parts of the sample holder and its supports (not shaded by the sample) will shade the detector and cause a loss of flux.

Atmospheric Absorption: The path lengths for incident and reflected energy will be different; hence, atmospheric absorption will introduce errors in the absolute measurement. These errors can be minimized in a comparison measurement.

Edge Losses: If the sample is not properly aligned in the first focal plane of the ellipsoid, some of the flux reflected by the specimen will miss the lower edge of the ellipsoidal mirror and be lost. Again, the amount depends on the geometric distribution of the reflected flux.

Detector Related Problems: A problem common to most previous reflectance measurement methods has been the need for large area detectors to accept the large images. Large area thermopiles, in particular, always have a non-uniform areal sensitivity (i.e., they do not sense flux equally well if the irradiated area of the detector is changed) and angular sensitivity (i.e., as the angle of the incidence gets farther from the normal, the detector is much less sensitive to the flux, due in part to shading by the housing of the thermopile, and because the absorbing blacks on the detector increase in reflectance at grazing incidence). The solution to this problem was established through the use of flux averaging devices discussed in Appendix C.

From the results reported in Appendix C, it can be stated that the use of an averaging sphere can be extended at least to 7 microns by use of sulfur as a sphere wall coating. Further, the inherent advantages of this approach are (1) the ability to accept images of varying size by use of a large extrance port and to measure accurately the total flux contained in the various images, (2) the ability to collect the aberrant portions of the image that would miss even large area detectors, and (3) a reduction in the required precision of optical alignment of the instrument. In addition, the use of this device will increase the accuracy of the ellipsoidal reflectometer. The major disadvantage is the reduction (by about 99 percent) of the flux that reaches the detector.

3.4 Analysis of an Ellipsoidal Mirror Reflectometer

The results reported in Appendix C indicate that the use of a sulfur coated averaging sphere with the detector will allow precise measurement of all the fluxes needed to accurately establish reflectance with the ellipsoidal mirror reflectometer. This section deals with the analysis of an ellipsoidal mirror reflectometer for both absolute and relative spectral reflectance measurements. The derivations of the reflectance equations in this section are, for the most part, applicable to any ellipsoidal or parabaloidal mirror reflectometer. A few of the simplifying assumptions are based on experimental measurements with the particular ellipsoidal mirror used in this work. However, these assumptions appear to be general in nature.

Two related analyses of the reflectometer are presented in this section: (1) The analysis of the absolute measurement of the reflectance $\rho(7^\circ, \varphi; 2\pi)$ by directly measuring the incident and reflected flux, and (2) the analysis of the relative (or comparison) reflectance measurement, where a calibrated

mirror is used as the reflectance standard.

In the derivations for both absolute and relative reflectances, two types of flux quantities are considered: (1) primary and (2) secondary. The primary fluxes comprise the major portion of the incident, or reflected flux, while the secondary fluxes are a very small fraction of the incident or reflected flux (usually less than 1 percent). The purpose of this distinction is to allow for very accurate correction of the large fluxes with the best possible techniques and to allow simplified (although only moderately accurate) corrections to be made to the secondary fluxes. This is based on the fact that corrections to terms comprising only 1 percent of the total flux can be in error by 50 percent and cause only a 1/2 percent error in the total flux, while corrections to the primary fluxes must be more accurate that the desired accuracy of the final answer. There are some intermediate fluxes lying between these two extremes which should be corrected on the basis of their maximum possible effect on the final answer. Throughout the following derivation only the secondary fluxes will be specifically denoted; all other fluxes are considered to be primary or intermediate. Furthermore, it should be noted that the approach outlined in this section is designed to obtain systematic information about the distribution of the flux in the reflectometer. Since the distribtuion obtained in this manner is dependent on tacit assumptions about the distribution of flux reflected from the sample, it is apparent that any analysis of errors will have to deal with the most probable maximum deviations from the assumptions used in these derivations.

3. 4. 1 <u>Absolute Measurement of Reflectance:</u> An absolute reflectance measurement is made by making two basic measurements: one of the incident flux F_I, and the other of the reflected flux F_R. Since neither of these measurements is as straight forward as would be desired, they will be discussed separately.

Incident flux (F_I): To measure the incident flux, the detector is placed at (or near) the first focal point of the ellipsoidal mirror (figure 5). A major problem with this measurement is that some flux is back-reflected out of the entrance port of the averaging sphere; some of this flux returns to the ellipsoidal mirror and is again reflected into the sphere, thus increasing the flux in the sphere that is read by the detector. This interchange was eliminated by placing a black shield 1 1/2 inches above the sphere port, with a hole just large enough to admit the incident beam. With this procedure the flux incident on the detector is

$$F_{I\,D} = F_I\,\eta \tag{14}$$

where η if the efficiency of the averaging sphere, which for a given sphere configuration is a function only of the reflectance of the sphere coating.

Reflected flux (F_R): Figure 6 illustrates the flux balance for the flux reflected by the sample. The flux absorbed by the mirror is denoted by F_α, the flux lost through the entrance hole is denoted by F_H. The flux scattered by the wire sample supports is $(\bar{\rho}_\epsilon)_W\,F_W$,[2] while the flux due to shading of the detector by the sample is $\bar{\rho}_\epsilon\,[F_{S\,P} - F_{S\,R}]$.[3] The flux crossing the first focal plane is $(\bar{\rho}_\epsilon)_S\,F_S$. Thus, the total flux reflected by the sample is:

$$F_R = F_S + F_W + [F_{S\,P} - F_{S\,R}] + F_H \tag{15}$$

where F_W and $F_{S\,R}$ are secondary fluxes. Depending on the distribution of the reflected radiation, the fluxes F_H and $F_{S\,P}$ may be secondary fluxes; however, they will be treated as intermediate fluxes, since, in general, they are considerably larger than fluxes F_W and $F_{S\,R}$. All the fluxes in equation (15) are defined on the basis of the flux leaving the sample.

To aid in establishing the quantities in equation (15), the following fluxes are defined (figure 7):

---

[2] $(\bar{\rho}_\epsilon)_X$ is the average effective reflectance of the ellipsoidal mirror for the given distribution of F_X on the mirror.

[3] $\bar{\rho}_\epsilon$ is the average effective reflectance of the central part of the ellipsoidal mirror, which varies by less than 0. 1 percent as given in Appendix D. The effective reflectance is defined in Appendix D.
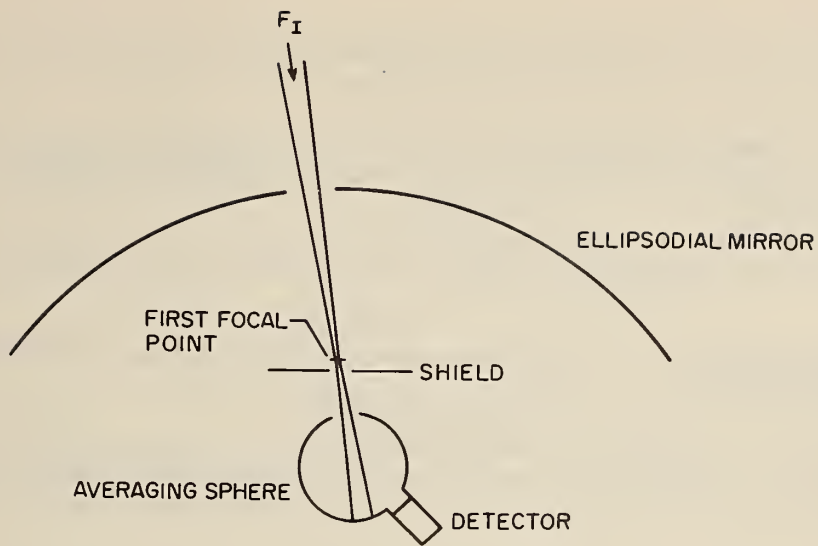
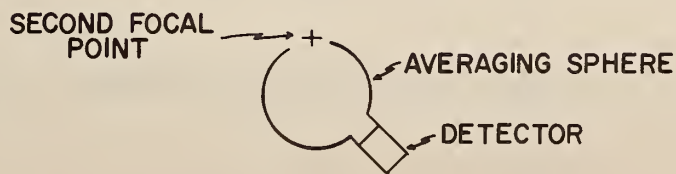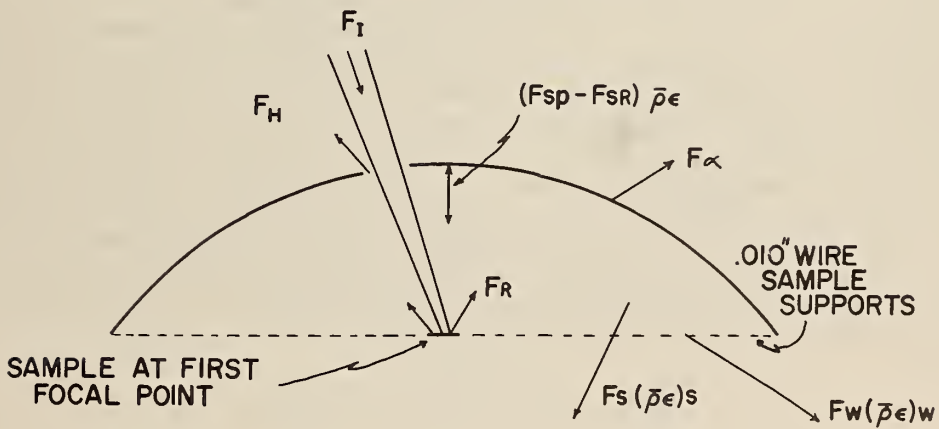Figure 5. Direct Measurement of the Incident Flux

Figure 6. Measurement of Reflected Flux and Definition
of the Four Basic Fluxes

13

F_s is defined as the flux crossing the first focal plane divided by the ellipsoidal mirror's average effective reflectance $(\bar{\rho}_\epsilon)_s$ for the particular distribution of F_s on the mirror.

F_{s1} is defined as the flux crossing the first focal plane divided by the mirror's average effective reflectance $(\bar{\rho}_\epsilon)_{s1}$ for the case when the A'_{sH} shield is placed in the first focal plane.

F_{s2} is defined as the flux crossing the first focal plane divided by the average effective reflectance $(\bar{\rho}_\epsilon)_{s2}$ of the outer edges of the ellipsoidal mirror for the case where shield A_{s2} is in the first focal plane.

F_D is defined as the flux crossing the first focal plane divided by the mirror's average effective reflectance $(\bar{\rho}_\epsilon)_D$ when shield A_D is in place.

It is possible to evaluate all of the defined fluxes one by one and then complete the flux balance for the reflected flux. After that it is then necessary to relate the defined fluxes (F_s, F_{s1}, F_{s2}, F_D) to those fluxes viewed by the detector (F_{sD}, F_{s1D}, F_{s2D}, and F_{DD}), which views a portion of the averaging sphere.

Mirror Loss (F_α): The ellipsoidal mirror will absorb some of the reflected Flux F_R. Further, if the ellipsoidal mirror has a poor surface finish and/or a partially transmitting mirror coating, the mirror may transmit some of F_R and/or scatter some of the reflected flux (i. e. , $F_R \rho_\epsilon$ where ρ_ϵ is the true reflectance of the coating) away from the second focal point. Thus, it is necessary to know the effective reflectance ρ'_ϵ of the ellipsoidal mirror. The effective reflectance of the ellipsoidal mirror is defined as the ratio of the flux that reaches a predefined area (i. e. , the entrance port to the averaging sphere) at the second focal plane to the flux incident on the ellipsoidal mirror from a defined area in the first focal plane (i. e. , the irradiated area of the specimen). By this definition, the absorptance $(1 - \rho'_\epsilon)$, includes losses by scattering of the ellipsoid, absorption by the ellipsoid, transmission by the ellipsoid, and any optical aberrations in the ellipsoidal mirror. This reflectance was measured for the particular ellipsoid used in this work, and the effective reflectance of the mirror as a function of position on the mirror is reported in Appendix D. These values indicate that the mirror reflects better (by about 1. 5 percent) near its edges than at the apex of the ellipsoid. Thus, the portion of flux reflected by this part of the mirror should be individually corrected for mirror reflectance. The use of the previously defined flux F_{s2} allows this individual correction to be made, since this is the flux that is incident on the higher reflecting edges of the ellipsoidal mirror. The average effective reflectance for each of the four defined fluxes is

$$(\bar{\rho}_\epsilon)_s = \frac{(F_s - F_{s2})\,\bar{\rho}_\epsilon + F_{s2}(1.015)\bar{\rho}_\epsilon}{F_s} \tag{16}$$

$$(\bar{\rho}_\epsilon)_s = \bar{\rho}_\epsilon \left[1 + \frac{F_{s2}}{F_s}\,(0.015)\right] \tag{17}$$

$$(\bar{\rho}_\epsilon)_{s1} = \frac{(F_{s1} - F_{s2})\,\bar{\rho}_\epsilon + F_{s2}(1.015)\bar{\rho}_\epsilon}{F_{s1}} \tag{18}$$

$$(\bar{\rho}_\epsilon)_{s1} = \bar{\rho}_\epsilon \left[1 + \frac{F_{s2}}{F_{s1}}\,(0.015)\right] \tag{19}$$

$$(\bar{\rho}_\epsilon)_D = \frac{(F_D - F_{s2})\,\bar{\rho}_\epsilon + F_{s2}(1.015)\,\bar{\rho}_\epsilon}{F_D} \tag{20}$$

$$(\bar{\rho}_\epsilon)_D = \bar{\rho}_\epsilon \left(1 + \frac{F_{s2}}{F_D}\,(0.015)\right) \tag{21}$$

and from the experimental data given in Appendix D

ELLIPSOIDAL MIRROR REFLECTOMETER

FIRST FOCAL PLANE

SAMPLE

$F_s(\bar{\rho}\epsilon)_s$

NO SHIELD

WIRE SUPPORTS

SAMPLE

SPECULAR COMPONENT

IMAGE OF ENTRANCE HOLE IN FIRST FOCAL PLANE (A'_H)

a) F_s

SHIELD A'_{SH}

$F_{s1}(\bar{\rho}e)_{s1}$

DETECTOR-SPHERE AT SECOND FOCAL POINT

b) F_{s1}

$F_{s2}(\bar{\rho}e)_{s2}$

SHIELD A_{s2}

c) F_{s2}
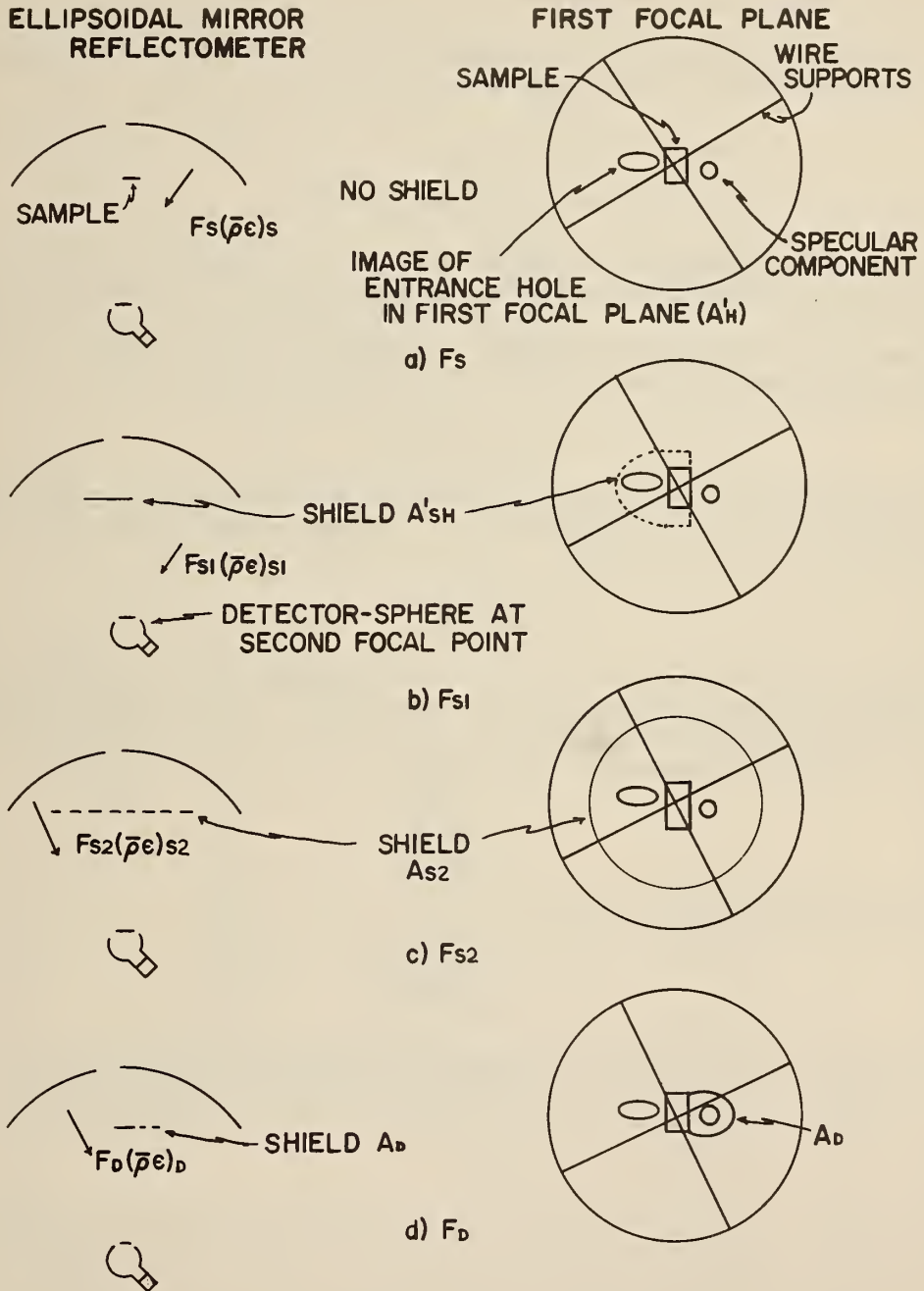
$F_D(\bar{\rho}e)_D$

SHIELD A_D

A_D

d) F_D

Figure 7. System Configuration for Definition of the Basic Fluxes F_s, F_{s1}, F_{s2} and F_D

$$(\bar{\rho}_\epsilon)_{s2} = 1.015\,\bar{\rho}_\epsilon \tag{22}$$

where $\bar{\rho}_\epsilon$ is the average effective reflectance of the central part of the ellipsoidal mirror.

Since F_{s2} is the only flux corrected for changes in the reflectance of the ellipsoidal mirror with positions of incidence on the mirror, the approximate magnitude of F_α is

$$F_\alpha = [F_s - F_{s2}](1 - \bar{\rho}_\epsilon) + F_{s2}[1 - \bar{\rho}_\epsilon(1.015)] \tag{23}$$

$$F_\alpha = F_s[1 - \bar{\rho}_\epsilon] - F_{s2}(0.015)\bar{\rho}_\epsilon$$

Note that the mirror actually absorbs slightly more flux than is indicated in equation (23), but these additional amounts are accounted for in the wire loss correction and the sample shading correction.

Hole Loss (F_H): The use of the defined fluxes F_s and F_{s1}, as shown in figure 8, allows the flux density around the entrance hole on the ellipsoidal mirror to be calculated, where

$$F_{SH} = F_s - F_{s1} \tag{25}$$

is the flux incident on the area A_{SH}, where A_{SH} is the area on the ellipsoidal mirror projected from the second focal point of $A_{SH}{}'$ in the first focal plane. Thus, the average flux density around the entrance hole is

$$\frac{F_{SH}}{A_{SH} - A_H} \tag{26}$$

A good assumption about the flux on the area $A_{SH} - A_H$ is that its distribution is sufficiently uniform that the correction for the flux lost through the entrance hole A_H, which is centered on the area A_{SH}, can be made on the basis that the average flux density over A_H is the same as the average flux density over $A_{SH} - A_H$. With this assumption, the hole loss is

$$F_H = \frac{A_H\,F_{SH}}{A_{SH} - A_H} \tag{27}$$

or in terms of the defined fluxes, the hole loss is

$$F_H = \frac{A_H\,(F_s - F_{s1})}{A_{SH} - A_H} \tag{28}$$

The assumption of uniform intensity over the small solid angle subtended by A_{SH} is more accurate and reasonable than the assumption of uniform intensity over the hemisphere used in most previous methods. A specific surface for which this correction F_H would be seriously in error is a diffraction grating with a reflection lobe directly out the hole.

Wire Loss (F_W): Some of the flux reflected by the sample and reimaged by the ellipsoidal mirror toward the second focal point is absorbed by the wire sample supports. The amount absorbed by the wire $[F_W(\bar{\rho}_\epsilon)_W]$ can be established in the following manner. First, it should be noted that the sample is oriented so that the specular component of reflection does not hit the wire support. That is, only a part of the nonspecular component of the reflected flux is blocked by the wires. Therefore, if a shield (of area A_D) were constructed to block out the flux about the specular component, then one could measure the nonspecularly reflected flux. This may be assumed to be uniformly distributed over the area (A_ϵ) of the first focal plane of the elliposidal mirror. Then a knowledge of the area A_ϵ over which the energy is distributed and the cross-sectional area of the wires allows the calculation of F_W.

$$(\bar{\rho}_\epsilon)\,F_W = F_D\,\frac{A_W}{A_\epsilon}\,(\bar{\rho}_\epsilon)_D \tag{29}$$

FIRST FOCAL PLANE

A's

WIRE SAMPLE SUPPORT

A'SH

AH

(b) FIRST FOCAL PLANE

PROJECTED AREA OF SAMPLE As

ELLIPSODIAL MIRROR

ENTRANCE HOLE-AH

A's AT FIRST FOCAL POINT

PROJECTION LINES FROM THE SECOND FOCAL POINT
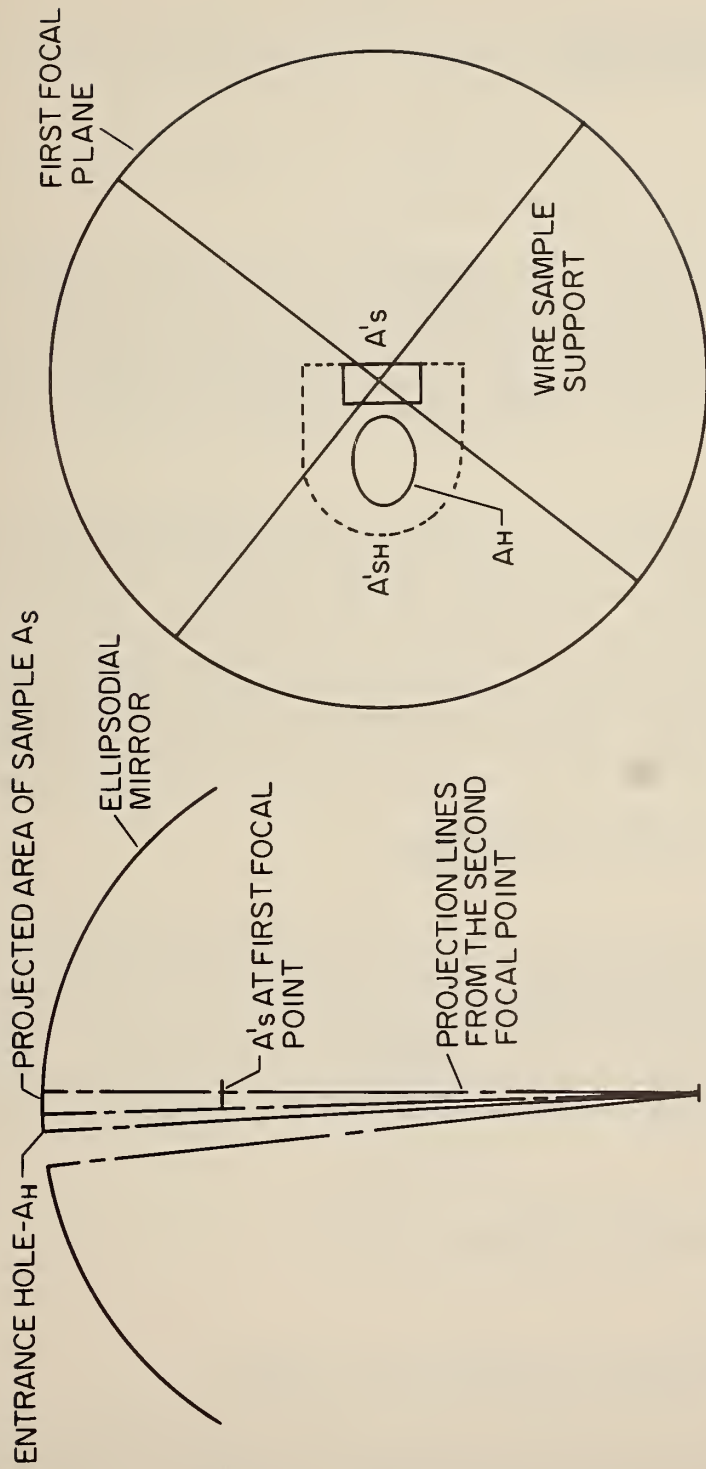
(a) SYSTEM CONFIGURATION

Figure 8. Illustration of Shields and Areas Involved in the Correction for the Hole Loss

17

where

$$A_\epsilon = \frac{\pi\, D_\epsilon{}^2}{4} - A_D \qquad (30)$$

where D_ϵ is the diameter of the opening of the ellipsoidal mirror in the first focal plane, and A_D is the area of the shield used to eliminate the specular component. This equation reduces to

$$F_W = F_D\, \frac{A_W}{A_\epsilon} \qquad (31)$$

since $(\bar{\rho}_\epsilon)_W = (\bar{\rho}_\epsilon)_D$ when F_D is evenly distributed over the area A.

It should be noted that the absorptance of the wire supports was not included in equation (31); this is because the wires are specular reflectors and any flux striking them is reflected out of the optical path between the first and second focal points and therefore is entirely lost to the system. Since F_W is a secondary correction, it is apparent that the assumption that average flux density over the first focal plane is intercepted by wire supports (except at the specular peak) is sufficiently accurate, especially since the wire supports comprise two diameters of the circle D_ϵ and the wire loss is distributed about the loss.

Sample Loss (F_{SP} and F_{SR}): Some of the reflected flux is shielded by the sample from the detector at the second focal point (figure 9); however, not all of this flux that strikes the sample is completely prevented from reaching the detector, since any of the reflected flux incident on the specimen in the area A_{S1} (the image on the first focal plane of the sphere entrance port at the second focal point) may be multiply reflected by the sample and ellipsoidal mirror to the second focal point and into the averaging sphere. To make the correction for these losses, the three defined fluxes F_D, F_s, and F_{S1} will be needed. The flux that is involved in these losses is that which strikes the ellipsoidal mirror on the projected area of the sample A_s. (This area is projected from the second focal point.) From figure 8 it is seen that A_s is partially surrounded by the shield A_{SH}, and will have approximately the same flux density as that on A_{SH}. Therefore, the total flux loss would be (from equation 16)

$$F_{SP} = \frac{A_S\, F_{SH}}{A_{SH} - A_H} \qquad (32)$$

if all of the flux within the area A_s on the ellipsoidal mirror were lost. However, of the flux F_{SP}, a portion A_{S1}/A_S (where A_{S1} is projected area on the ellipsoid of A_{S1}') is reflected from the sample so that it could reach the detector, since any flux leaving the sample from the area A_{S1}' can reach the detector. The question is how much of this reflected flux reaches the detector. It is reasonable to assume that the sample has the same non-specular component for flux incident from $7\,^\circ$ to the normal as for normally incident flux. Furthermore, it is this non-specular component of the flux reflected from the area A_{S1}' which will reach the detector; thus, it is apparent that of the flux striking the sample for the second time, the amount

$$\frac{A_S\, F_{SH}}{A_{SH} - A_H}\left[\frac{A_{S1}}{A_S}\right]\left[\frac{F_D}{F_S}\right]\rho_s\, \bar{\rho}_\epsilon{}^2\left[\frac{A_\epsilon - A_W}{A_\epsilon}\right]$$

reaches the detector. The amount

$$\left[\frac{A_S\, F_{SH}}{A_{SH} - A_H}\right]\left[\frac{F_S - F_D}{F_S}\right]\rho_s\, \bar{\rho}_\epsilon$$

is reflected back into the area A_s on the ellipsoidal mirror. This flux if then reflected back to the sample, where again part of the flux $[A_{S1}/A_S]$ is reflected toward the detector. The amount that reaches the detector on the third reflection from the sample is

$$\left[\frac{F_{SH}\,(A_S)}{A_{SH} - A_H}\right]\left[\frac{A_{S1}}{A_S}\right]\left[\frac{A_\epsilon - A_W}{A_\epsilon}\right]\left[\frac{F_S - F_D}{F_S}\right]\left[\rho_s{}^2\, \bar{\rho}_\epsilon{}^3\right]\left[\frac{F_D}{F_S}\right]$$

18

As

TOP PORTION OF
ELLIPSOIDAL MIRROR

$(F_{SP} - F_{SR})$

A's

SAMPLE SHIELDING

INCIDENT IMAGE

WIRE SUPPORTS

A's (SAMPLE)

A'si (IMAGE OF SPHERE ENTRANCE)
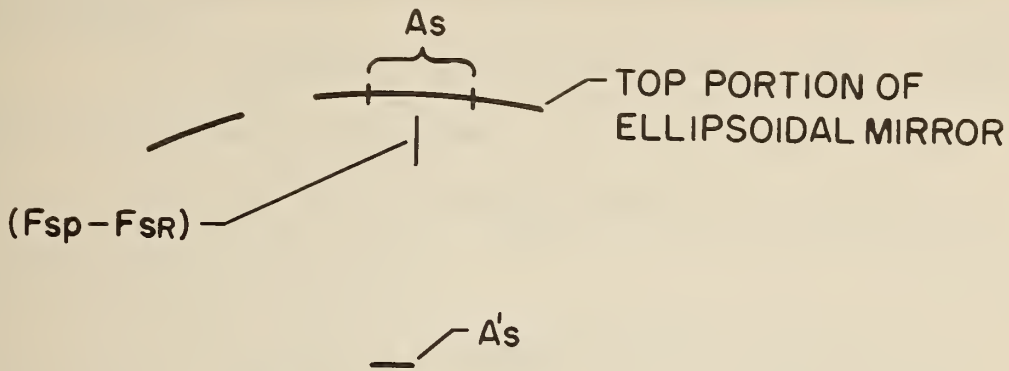
IMAGE IN FIRST FOCAL PLANE

Figure 9. Illustration of Sample Loss Terminology

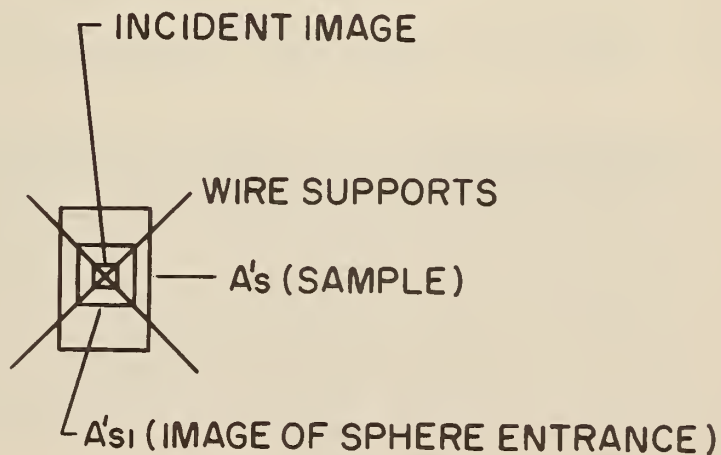Further, the amount of flux reaching the detector after the "nth" reflection from the sample is

$$[\frac{(A_s)\, F_{SH}}{A_{SH} - A_H}]\, [\frac{A_{S1}}{A_S}]\, [\frac{F_D}{F_S}\, \rho_s\, \bar{\rho}_\epsilon{}^2]\, [\frac{A_\epsilon - A_W}{A_\epsilon}]\, [\rho_s\, \bar{\rho}_\epsilon\, (\frac{F_s - F_D}{F_s})]^{n-1}$$

Therefore, F_{SR} of the flux F_{SP} in equation (32) reaches the sphere port where

$$F_{SR} = \sum_{n=1}^{\infty} [\frac{F_{SH}\, (A_{S1})}{A_{SH} - A_H}]\, [\frac{F_D}{F_s}\, \rho_s\, \bar{\rho}_\epsilon^2]\, [\frac{A_\epsilon - A_W}{A_\epsilon}]\, [\rho_s\, \bar{\rho}_\epsilon\, (\frac{F_s - F_D}{F_s})]^{n-1} \qquad (33)$$

which sums to

$$F_{SR} = [\frac{F_{SH}\, (A_{S1})}{A_{SH} - A_H}]\, [\frac{F_D}{F_s}\, \rho_s\, \bar{\rho}_\epsilon^2\, (\frac{A_\epsilon - A_W}{A_\epsilon})]\, \frac{1}{1 - \rho_s\, \bar{\rho}_\epsilon\, (\frac{F_s - F_D}{F_s})} \qquad (34)$$

Thus, the total effect of the sample shielding the detector is

$$F_{SP} - F_{SR} = \frac{F_s - F_{S1}}{A_{SH} - A_H}\, [A_s - A_{S1}\, (\frac{F_D}{F_s}\, \rho_s\, \bar{\rho}_\epsilon^2)\, (\frac{A_\epsilon - A}{A_\epsilon})\, (\frac{1}{1 - \rho_s\, \bar{\rho}_\epsilon\, (\frac{F_s - F_D}{F_s})})] \qquad (35)$$

This completes the calculation of the individual losses. The foregoing provide a basis for calculating F_R as given in equation (15).

$$F_R = F_s + F_H + F_W + (F_{SP} - F_{SR}) \qquad (36)$$

Upon substitution of equations (23), (28), (31) and (35) into equation (36), F_R, in terms of the defined fluxes, sample reflectance and system constants, is given by

$$FR = F_s + (\frac{F_s - F_{S1}}{A_{SH} - A_H})\, AH + \frac{F_D\, A_W}{A_\epsilon} + \frac{F_s - F_{S1}}{A_{SH} - A_H}\, \{A_s - A_{S1}\, (\frac{F_D}{F_s}\, \rho_s\, \bar{\rho}_\epsilon^2\, [\frac{A_\epsilon - A_W}{A_\epsilon}]\, [\frac{1}{1 - \rho_s\, \rho_\epsilon(\frac{F_s - F_D}{F_s})}])\} \qquad (37)$$

3.4.2 <u>Measurement of Fluxes</u>: Now the defined fluxes F_s, F_{S1}, F_{S2}, and F_s must be evaluated in terms of the flux that the detector views. First F_s will be considered. The measurement of these quantities is complicated because the "detector" is not black: that is, flux is reflected back out the sphere entrance port into the optical path, and some of it gets back into the sphere and increases the flux sensed by the detector. Specifically, for the F_s measurement, the flux $(\rho_\epsilon)_s\, F_s$ is the desired quantity entering the sphere port. However, some η' of this flux is reflected out of the sphere entrance port where η' is the ratio of F_1 (the back-reflected flux) to $(\bar{\rho}_\epsilon)_s\, F_s$. This flux is reflected nearly diffusely so that $f_{s-\epsilon}\, \eta'\, F_s\, (\bar{\rho}_\epsilon)_s$ is intercepted by the ellipsoidal mirror and refocused on the sample at the first focal point.[4] The sample then reflects this flux back to the ellipsoidal mirror, which then refocuses it onto the sphere entrance. Thus, an amount of F_s' is added to the flux $F_s\, (\bar{\rho}_\epsilon)_s$ that was originally incident on the sphere port.

$$F_s' = \rho_{HS}\, (\bar{\rho}_{\epsilon D})^2\, \eta'\, f_{s-\epsilon}\, [F_s\, (\bar{\rho}_\epsilon)_s] \qquad (38)$$

where $\bar{\rho}_{\epsilon D}$ is the average effective reflectance of the ellipsoidal mirror for flux coming diffusely from the sphere entrance at the second focal point and ρ_{HS} is the bi-hemispherical reflectance of the sample. Further, of the flux F_s' that reaches the sphere entrance on the second pass, the amount

$$F_s'' = \rho_{HS}\, (\bar{\rho}_{\epsilon D})^2\, \eta'\, f_{s-\epsilon}\, F_s' \qquad (39)$$

---
[4] $f_{s-\epsilon}$ is standard diffuse configuration factor as defined in reference 4.

is added to the flux in the sphere in the same manner as $F_s{}'$ was added. This continues until the total flux in the sphere is

$$F_{SS} = (\bar{\rho}_\epsilon)_s \, F_s \, [1 + \rho_{HS} \, (\bar{\rho}_{\epsilon D})^2 \, \eta' \, f_{s-\epsilon} + [\rho_{HS} \, (\bar{\rho}_{\epsilon D})^2 \, \eta' \, f_{s-\epsilon}]^2 \ldots \ldots] \qquad (40)$$

which, since $\rho_{HS} \, (\bar{\rho}_{\epsilon D})^2 \, \eta' \, f_{s-\epsilon} < 1$, sums to

$$F_{SS} = (\bar{\rho}_\epsilon)_s \, F_s \, \left[\frac{1}{1 - \rho_{HS} \, (\bar{\rho}_{\epsilon D})^2 \, \eta' \, f_{s-\epsilon}} \right] \qquad (41)$$

Thus the flux viewed by the detector is

$$F_{SD} = \eta \, (\bar{\rho}_\epsilon)_s \, FS \, \left[\frac{1}{1 - \rho_{HS} \, (\bar{\rho}_{\epsilon D})^2 \, \eta' \, f_{s-\epsilon}} \right] \qquad (42)$$

Several simplifying assumptions are made in the foregoing discussion:

(1) $\bar{\rho}_{\epsilon D}$ is the same for the flux leaving the second focal point and going to the first focal point as for the flux leaving the first focal point and going to the second focal point. Furthermore, it is logical to assume that $\bar{\rho}_{\epsilon D} = (\bar{\rho}_\epsilon)_D$.

(2) The loss of flux due to the shading of the ellipsoidal mirror by the sample and sample holder is accounted for in the calculation of $f_{s-\epsilon}$. Furthermore, the loss due to the entrance hole is included in $f_{s-\epsilon}$.

(3) After the energy is re-reflected by the sample back to the ellipsoid, the losses due to (1) shading of the sphere port by the sample, and sample holder, and (2) the entrance hole, are neglected.

Assumption (2) involves no error, since it just specifies the method of calculation for $f_{s-\epsilon}$. Assumptions (1) and (3) yield only extremely small errors, since they involve small corrections to a quantity which is very small compared to F_s.

Thus, F_s is related to the flux striking the detector in the following manner

$$\frac{F_{SD} \, [1 - \rho_{Hs} \, (\bar{\rho}_{\epsilon D})^2 \, \eta' \, (f_{s-\epsilon})]}{\eta \, (\bar{\rho}_\epsilon)_s} = F_s \qquad (43)$$

The effect on the F_s measurement given by equation (43) is also present in the measurement of F_{s1}, F_{s2} and F_D. The major changes arise in the calculation of $f_{s-\epsilon}$ and in the reflectance of the sample. The changes in $f_{s-\epsilon}$ are caused by the shields (S1 and S2) shading the ellipsoid from the detector. The calculation of $f_{s-\epsilon}$ can easily be corrected for this shading. However, the effect of the change in reflectance (due to the types of reflectances involved) is not so easily established. The best assumption for F_s, F_{s1}, and F_D is to assume that the hemispherical reflectance of the specimen remains the same for these measurements. This is a very good approximation, since the introduction of the small shields A_{s1} and A_D into the first focal plane does not markedly change the condition of hemispherical illumination and hemispherical viewing. However, the F_{s2} measurement presents an entirely different problem, since the A_{s2} shield does not allow either hemispherical irradiation or hemispherical viewing. An approximation to the differences between ρ_{HS} and ρ_{HS2} could be

$$\rho_{HS2} = \rho_{HS} \, \left[\frac{F_s - F_{s2}}{F_s} \right] \qquad (44)$$

No effort is made to defend this approximation, except to say that for a specular sample, equation (44) results in $\rho_{HS2} = \rho_{HS}$, which is approximately true (except for the effects of Fresnels's law); and for the diffuse reflector, equation (44) results in the sample reflecting the same amount of flux onto the lower edge of the ellipsoidal mirror for illumination conditions of $7°$ to normal as for near grazing illumination conditions. This yields a low value for ρ_{HS2} since most surfaces tend to become specular at grazing incidence. It is felt that equation (44), although a guess at best, is better than no correction at all.

From these assumptions, then, the flux that the detector views for measurement of the remaining fluxes F_{s1}, F_{s2}, and F_D is

$$F_{s1D} = \eta \, F_{s1} \, (\bar{\rho}_\epsilon)_{s1} \left[\frac{1}{1 - \rho_{HS} \, (\bar{\rho}_{\epsilon D})^2 \, \eta' \, (f_s - \epsilon) \, S1} \right] \tag{45}$$

$$F_{s2D} = \eta \, F_{s2} \, (\bar{\rho}_\epsilon)_{s2} \left[\frac{1}{1 - \left(\dfrac{F_s - F_{s2}}{F_s} \right) \rho_{HS} \, (\bar{\rho}_{\epsilon D})^2 \, \eta' \, (f_s - \epsilon) \, S2} \right] \tag{46}$$

$$F_{DD} = \eta \, F_D \, (\bar{\rho}_\epsilon)_D \left[\frac{1}{1 - \rho_{HS} \, (\bar{\rho}_{\epsilon D})^2 \, \eta' \, (f_s - \epsilon) \, D} \right] \tag{47}$$

Equations 45 through 47 can be rewritten to give F_{s1}, F_{s2}, and F_D as functions of the system and the flux that the detector views.

$$F_{s1} = \frac{F_{s1D} \, [1 - \rho_{HS} \, (\bar{\rho}_{\epsilon D})^2 \, \eta' \, (f_s - \epsilon) \, S1]}{\eta \, (\bar{\rho}_\epsilon)_{s1}} \tag{48}$$

$$F_{s2} = \frac{F_{s2D} \left[1 - \dfrac{F_{SD} - F_{s2D}}{F_{SD}} \rho_{HS} \, (\bar{\rho}_{\epsilon D})^2 \, \eta' \, (f_s - \epsilon) \, S2 \right]}{\eta \, (\bar{\rho}_\epsilon) \, S1} \tag{49}$$

$$F_D = \frac{F_{DD} \, [1 - \rho_{HS} \, (\bar{\rho}_{\epsilon D})^2 \, \eta' \, (f_s - \epsilon) \, D]}{\eta \, (\bar{\rho}_\epsilon)_D} \tag{50}$$

In equation (46) the term $(F_s - F_{s2})/F_s$ occurs, which, as shown later, is closely approximated by $(F_{SD} - F_{s2D})/F_{SD}$, which has been substituted in equation (49).

It is now possible to find F_R in terms of measured quantities and system parameters by use of equation (37) with equations (43), (48), (49) and (50). First, however, some simplifying assumptions will be made about the terms composed of ratios of fluxes in the last term of equation (37). The ratios F_D/F_s and $(F_s - F_D)/F_s$ both appear. The ratios are equal to

$$\frac{F_D}{F_s} = \frac{F_{DD} \, [\, 1 - \rho_{HS} \, (\bar{\rho}_{\epsilon D})^2 \, \eta' \, (f_s - \epsilon)_D \,] \, \eta \, (\bar{\rho}_\epsilon)_s}{F_{SD} \, [\, 1 - \rho_{HS} \, (\bar{\rho}_{\epsilon D})^2 \, \eta' \, (f_s - \epsilon)_s \,] \, \eta \, (\bar{\rho}_\epsilon)_D} \tag{51}$$

and

$$\frac{F_s - F_D}{F_s} = 1 - \frac{F_{DD} \, [\, 1 - \rho_{HS} \, (\bar{\rho}_{\epsilon D})^2 \, \eta' \, (f_s - \epsilon)_D \,] \, \eta \, (\bar{\rho}_\epsilon)_s}{F_{SD} \, [\, 1 - \rho_{HS} \, (\bar{\rho}_{\epsilon D})^2 \, \eta' \, (f_s - \epsilon)_s \,] \, \eta \, (\bar{\rho}_\epsilon)_D} \tag{52}$$

In equations (51) and (52), all corresponding terms are equal or have been previously assumed equal without introducing significant errors. Thus,

$$\frac{F_D}{F_s} = \frac{F_{DD}}{F_{SD}} \quad \text{and} \quad \frac{F_s - F_D}{F_s} = \frac{F_{SD} - F_{DD}}{F_{SD}} \tag{53}$$

Further, equations (17), (19) and (21) can be converted to functions of F_{s2D}, F_{SD}, and F_{s1D} in the same manner.

Substituting equations (43), (48), (49), (50) and (53) into equation (37), and combining terms, yields

$$F_R = \frac{F_{SD}\left[1 - \rho_{HS}\,(\bar{\rho}_{\epsilon D})^2\,\eta'\,(f_{s-\epsilon})_s\right]}{\eta(\bar{\rho}_\epsilon)\left[1 + \dfrac{F_{S2D}}{F_{SD}}(0.015)\right]}\left[1 + \frac{A_H + A_S}{A_{SH} - A_H} - \frac{A_{S1}}{A_{SH} - A_H}\left[\frac{F_{DD}}{F_{SD}}\,\rho_S\,(\bar{\rho}_{\epsilon D})^2\left(\frac{A_\epsilon - A_H}{A_\epsilon}\right)\text{X}\,\frac{1}{1 - \rho_S\bar{\rho}_\epsilon\dfrac{F_{SD} - F_{DD}}{F_{SD}}}\right)\right]$$

$$+\frac{F_{S1D}\left[1 - \rho_{HS}(\bar{\rho}_{\epsilon D})^2\eta'(f_{s-\epsilon})_{s1}\right]}{\eta\,\bar{\rho}_\epsilon\left[1 + \dfrac{F_{S2D}}{F_{S1D}}(0.015)\right]}\left[-\frac{A_H + A_S}{A_{SH} - A_H} + \frac{A_{S1}}{A_{SH} - A_H}\left[\frac{F_{DD}}{F_{SD}}\,\rho_S\bar{\rho}_\epsilon^2\left(\frac{A_\epsilon - A_H}{A_\epsilon}\right)\frac{1}{1 - \rho_S\bar{\rho}_\epsilon\dfrac{F_{SD} - F_{DD}}{F_{SD}}}\right]\right] + \frac{F_{DD}\left[1 - \rho_{HS}(\bar{\rho}_{\epsilon D})^2\eta'(f_{s-\epsilon})_0\right]A_H}{\eta\,\bar{\rho}_\epsilon\left[1 + \dfrac{F_{S2D}}{F_{DD}}(0.0015)\right]A_\epsilon}$$

$$\tag{54}$$

There are three major unknowns in equation (54). They are as follows:

(1) The efficiencies of the averaging sphere η and η'.

(2) The hemispherical reflectance ρ_{HS} of the sample for the correction to the various terms for the detector-ellipsoid interchange.

(3) The reflectance of the sample, ρ_S. A good approximation to this is $\rho_S = F_{SD}/F_{1D}$.

The remaining terms of equation (54) are either fixed system parameters, or are obtained from measurements of F_{DD}, F_{SD}, F_{S1D} and F_{S2D}.

For the absolute measurement of $\rho(7°, \varphi; 2\pi)$, the reflectance of the sample (from equations 14 and 54) is equal to

$$\rho_S\ (7°, \varphi; 2\pi) = \frac{F_R}{F_1} \tag{55}$$

Thus, to establish absolute reflectance with the ellipsoidal mirror reflectometer, one needs to have good estimates for η, η', and the various values of ρ_{HS}. It will become clear that the comparison measurement, when a calibrated mirror is used for the reference standard, eliminates the need for an accurate knowledge of these terms.

3.4.3 <u>Relative Measurement of Reflectance:</u> As in the case of the absolute reflectance measurement, a value for the incident flux is needed so that the reflected flux F_R of equation (54) can be compared to the incident flux to calculate reflectance.

Incident flux (F_1): In this case a value of flux related to the incident flux is obtained by using a calibrated specular mirror as the reference sample. The flux F_1 that is incident is reflected by the sample so that

$$F_{RM} = F_1\,\rho_M \tag{56}$$

Of the flux F_{RM} that leaves the sample, an amount $F_{RM}\,\bar{\rho}_\epsilon$ reaches the entrance port of the detector, where again there is an interchange between the averaging sphere and the ellipsoidal mirror which increases the flux in the averaging sphere so that the flux which the detector views is

$$F_{1D} = F_1\,\rho_M\,\bar{\rho}_\epsilon\,\frac{\eta}{\left[1 - \rho_{HM}\,(\bar{\rho}_{\epsilon D})^2\,\eta'\,(f_{s-\epsilon})_1\right]} \tag{57}$$

where $f_{(s-\epsilon)_1}$ is equal to $f_{(s-\epsilon)_s}$.

From equation (57)

$$F_1 = \frac{F_{1D}\,\left(1 - \rho_{HM}(\bar{\rho}_{\epsilon D})^2\eta'(f_{s-\epsilon})_1\right)}{\rho_M\,\rho_\epsilon\,\eta} \tag{58}$$

Therefore, the reflectance $\rho(7°, \varphi; 2\pi)$ is equal to F_R, equation (54), divided by F_1, equation (58). Further, the simplifying assumption that all the $[1 - \rho_{HS}\,\bar{\rho}_\epsilon^2\,\eta\,f_{(s-\epsilon)}]$ terms for F_{1D}, F_{SD}, F_{S1D}, and F_{DD} are equal, and the fact that η' and η are identical throughout equations (54) and (58) yields

$$\rho(7°, \varphi; 2\pi) = \frac{\rho_M}{F_{ID}} \left\{ \left[\frac{F_{SD}}{\left[1 + \frac{F_{S2D}}{F_{SD}}(0.015)\right]} \left\{ 1 + \frac{A_H + A_S}{A_{SH} - A_H} - \frac{A_{S1}}{A_{SH} - A_H} \times \right. \right. \right.$$

$$\left. \left. \left[\frac{F_{DD}}{F_{SD}} \rho_S (\bar{\rho}_{\epsilon D})^2 \left(\frac{A_\epsilon - A_W}{A_\epsilon}\right) \frac{1}{1 - \rho_S \bar{\rho}_\epsilon \frac{F_{SD} - F_{DD}}{F_{SD}}} \right] \right\} \right] + \frac{F_{DD}}{1 + \frac{F_{S2D}}{F_{DD}}(0.015)} \left[\frac{A_W}{A_\epsilon} \right]$$

$$+ \frac{F_{S1D}}{\left[1 + \frac{F_{S2D}}{F_{SD}}(0.015)\right]} \left[-\frac{A_H + A_S}{A_{SH} - A_H} + \frac{A_{S1}}{A_{SH} - A_H} \left\{ \frac{F_{DD}}{F_{SD}} \rho_S \bar{\rho}_\epsilon^2 \left[\frac{A_\epsilon - A_W}{A_\epsilon} \right] \frac{1}{1 - \rho_S \bar{\rho}_\epsilon \frac{F_{SD} - F_{DD}}{F_{SD}}} \right\} \right] \right\} \quad (59)$$

where the only remaining unknown is ρ_s, which is the same as $\rho(7°, \varphi; 2\pi)$. A very good approximation to ρ_s, as previously stated, is

$$\rho_s = \frac{F_{SD}}{F_{ID}} \quad (60)$$

Even if ρ_s of equation (59) was wrong by five percent, this would have little effect on $\rho(7°, \varphi; 2\pi)$, since ρ_s is only found in secondary flux terms. Further, if the need and capability for more accuracy were justified by the other corrections, one could, of course, iterate this process by calculating successively better ρ_s by using $\rho(7°, \varphi; 2\pi)$ calculated from ρ_s of equation (60) and then, successively, the $\rho(7°, \varphi; 2\pi)$ calculated from equation (59).

This section has presented the general analyses for an ellipsoidal mirror reflectometer, which are based on the supposed ability to measure accurately four defined fluxes. Through the use of the four defined fluxes and an accurate knowledge of system parameters, it is possible to make corrections for system losses based on tacit assumptions about the arbitrary geometric distribution of the flux from the general engineering surface. The lack of knowledge concerning the distribution of reflected flux from common materials has seriously handicapped previous attempts to measure reflectance accurately; however, with the ellipsoidal mirror reflectometer, one is able to establish the important features of the reflected flux's distribution that is, the required average flux density is established for each correction and the assumptions concerning these corrections appear more realistic than those previously used with other reflectometers. Further, many of the assumptions leading up to equation (59) can be made more accurate at the cost of further complication of equation (57). With present source-detector limitations, it was felt that more accurate corrections to the system losses were not justified. However, with the advent of infrared continuous-wave, many-wavelength lasers and more sensitive supercooled solid state detectors, the ability to account for the system losses will increase and thus the assumptions leading up to equation (59) should be reviewed and revised as necessary.

It is also apparent from the analyses presented that the relative reflectance measurement requires less knowledge about the system losses than the absolute reflectance measurement. Further, the use of a calibrated mirror as the only reference reflectance standard is very desirable, since such mirrors are available and can be individually calibrated by an investigator. All other reflectometers using mirrors to collect hemispherically the reflected flux from the sample require the use of a non-existent diffuse reflectance standard; and even if it did exist, corrections for the hole loss based on the diffuse standard are questionable, due to differences in geometric distribution of the flux reflected by the diffuse standard and that reflected by the sample.

In fact, many investigators would denote both the absolute and relative methods discussed here as absolute, since the final answer is given in absolute reflectance units and not relative to some standard (such as Mg0). The difference implied in this work between relative and absolute reflectance measurement has to do with how the incident flux is measured and not with how the data are reported.

Several losses which were not discussed in this section are:
(a) Atmospheric absorption.

(b) Edge loss, due to improper sample leveling in the first focal plane.

(c) The possibility that the detector does not read all fluxes the same.

However, these are losses that can be largely eliminated by careful attention to experimental technique.

Table II   Flux Terminology[5]

F_I = The flux incident on the sample at the first focal point.

F_R = The total flux reflected by the sample (not including interreflections).

F_α = The flux effectively absorbed by the ellipsoidal mirror.

F_W = The flux absorbed by the wire divided by $(\bar{\rho}_\epsilon)_W$. (i. e., F_W is the flux leaving the sample headed in the direction of the wires.)

F_{SP} = The flux that is initially shaded from the detector by the sample, divided by $\bar{\rho}_\epsilon$.

F_{SR} = The flux that reaches the detector after multiple reflections with the sample, divided by $\bar{\rho}_\epsilon$.

F_H = The flux lost out the entrance hole.

F_s = The total flux crossing the first focal plane (excluding detector ellipsoid interchanges) divided by $(\bar{\rho}_\epsilon)_s$.

F_{s1} = The total flux crossing the first focal plane when shield A_{SH} is used divided by $(\bar{\rho}_\epsilon)_{s1}$.

F_{s2} = The total flux crossing the first focal plane when shield A_{s2} is used divided by $(\bar{\rho}_\epsilon)_{s2}$.

F_D = The total flux crossing the first focal plane when shield A_D is used divided by $(\bar{\rho}_\epsilon)_D$.

Table II   Reflectance Terminology

ρ_ϵ' = Effective reflectance of a point on the ellipsoidal mirror.

$\bar{\rho}_\epsilon$ = Effective reflectance of the central area of the ellipsoidal mirror.

$(\bar{\rho}_\epsilon)_s$ = Effective reflectance of the ellipsoidal mirror to the flux F_s.

$(\bar{\rho}_\epsilon)_{s1}$ = Effective reflectance of the ellipsoidal mirror to the flux F_{s1}.

$(\bar{\rho}_\epsilon)_{s2}$ = Effective reflectance of the ellipsoidal mirror to the flux F_{s2}.

---

[5] The subscript D added to the subscript of any of the above fluxes implies the flux actually viewed by the detector when the defined flux is measured by the detector.

$(\bar{\rho}_\epsilon)_D$ = Effective reflectance of the ellipsoidal mirror to the flux F_D.

ρ_{HS} = The hemispherical reflectance of the sample.

ρ_{HM} = The hemispherical reflectance of the reference mirror.

ρ_M = The reflectance of the specular reference standard.

ρ_S = The normal hemispherical reflectance, and is approximately equal to $\rho(7^\circ, \varphi; 2\pi)$

$(\bar{\rho}_\epsilon)_W$ = The effective reflectance of the ellipsoidal mirror to the flux F_W.

$\rho_{\epsilon D}$ = Effective reflectance of the ellipsoidal mirror to diffuse flux from the second focal point.

Table II Area Terminology

A_H = Area of the entrance hole.

A_ϵ = Area of the opening of the ellipsoidal mirror in the first focal plane minus the area of the shield A_D.

A'_{SH} = Area of the shield A_{SH} in the first focal plane.

A'_S = Area of the sample in the first focal plane.

A'_{S1} = First focal plane area of the image of the sphere entrance port at the second focal point.

A_D = Area of the shield used to block the specular component.

A_{S2} = Area of the shield used to establish the flux distribution for mirror loss corrections.

A_{SH} = Projection of A'_{SH} from the second focal point onto the ellipsoidal mirror.

A_S = Projection of A'_S from the second focal point onto the ellipsoidal mirror.

A_{S1} = Projection of A'_{S1} from the second focal point onto the ellipsoidal mirror.

Table II Miscellaneous Terminology

η = Efficiency of the averaging sphere (i. e. , the ratio of the flux viewed by the detector to that entering the sphere).

η' = The ratio of flux leaving the entrance port of the sphere to that incident on the entrance port.

$f_{S-\epsilon}$ = Diffuse configuration factor from the sphere entrance port to the ellipsoidal mirror (corrected for shading effects of the sample and sample support and for the effect of the entrance hole).

3.5 Calibration of the Ellipsoidal Mirror Reflectometer

This section deals with estimating the errors involved in the various corrections discussed earlier which are required to establish $\rho(7°,\varphi;2\pi)$.[6] The estimated error is used because most of the corrections depend on an unknown quantity, the geometric distribution of the reflected flux. Thus the error analysis is based on an estimate of the effects of various changes in the geometric distribtuion of the fluxes on the individual losses. In this section the various parameters will be considered to vary over ranges that are larger than the expected ranges for engineering surfaces, in order to arrive at a conservative estimate of the accuracy of an ellipsoidal reflectometer measurement. The analysis does not distinguish between the errors caused by imprecision and the errors caused by uncertainties in measured parameters (random error and bias).

The error analysis will concern equation (60), which is the equation used to determine the absolute reflectance of the sample. The additional errors present in the direct measurement of absolute reflectances are discussed later. In the error analysis of the relative reflectance measurement, the following types of errors are considered.

(a) Errors due to the flux interchange between the ellipsoidal mirror and the averaging sphere.
(b) Errors due to incomplete knowledge of system parameters.
(c) Errors due to uncertainty in the measurement of F_{SD}, F_{S1D}, F_{S2D} and F_{DD}.
(d) Errors due to faulty assumptions concerning the geometric distribution of the reflected flux.
(e) Errors caused by the uncertainty in the reflectance of the specular reflectance standard.
(f) Other sources of error.

First, the errors associated with the flux interchange between the averaging sphere and the ellipsoidal mirror are discussed, then the effect of the uncertainty in the reflectance of the specular reflectance standard and the effect of the uncertainty of reading the various fluxes. Next, the effect of variation in the reflectance of the ellipsoidal mirror is analyzed. The remaining errors are discussed in connection with the specific corrections for the hole loss, wire loss, mirror loss, and the sample shading effect. A set of assumptions is made concerning the distribution of the reflected flux in order to establish an over-all estimate of accuracy. Since the magnitudes and interdependence of the various fluxes used in equation (59) are unknown, standard error propagation formulas are not used. It is felt that continued use of this instrument will provide the massive amount of data needed to justify a more accurate error analysis.

3.5.1 <u>Sphere-Ellipsoid Interchange</u>: The error associated with the interchange of flux between the averaging sphere and the ellipsoidal mirror is caused by the assumptions that (in derivation of equation 59)

$$\frac{[1 - \rho_{HS}\ (\bar{\rho}\epsilon_D)^2\ \eta'\ (f_{s}-\epsilon)_s]}{[1 - \rho_{HM}\ (\bar{\rho}\epsilon_D)^2\ \eta'\ (f_{s}-\epsilon)_l]} \equiv 1 \tag{61}$$

$$\frac{[1 - \rho_{HS}\ (\bar{\rho}\epsilon_D)^2\ \eta'\ (f_{s}-\epsilon)_{s1}]}{[1 - \rho_{HM}\ (\bar{\rho}\epsilon_D)^2\ \eta'\ (f_{s}-\epsilon)_l]} \equiv 1 \tag{62}$$

$$\frac{[1 - \rho_{HS}\ (\bar{\rho}\epsilon_D)^2\ \eta'\ (f_{s}-\epsilon)_D]}{[1 - \rho_{HM}\ (\bar{\rho}\epsilon_D)^2\ \eta'\ (f_{s}-\epsilon)_l]} \equiv 1 \tag{63}$$

and

$$\frac{[1 - \rho_{HM}\ (\bar{\rho}\epsilon_D)^2\ \eta'\ (\frac{F_{SD} - F_{S2D}}{F_{S2D}})(f_{s}-\epsilon)_{s2}]}{[1 - \rho_{HM}\ (\bar{\rho}\epsilon_D)^2\ \eta'\ (f_{s}-\epsilon)_l]} \equiv 1 \tag{64}$$

The error arises from the fact that $\rho_{HS} \neq \rho_{HM}$ and the various $f_{s}-\epsilon$ terms are not equal. However, in equations (61), (62) and (63) the differences among these three configuration factors are insignifi-

---

[6] Throughout this section ρ_s and $\rho(7°,\varphi;2\pi)$ are used interchangeably.

cant since the use of small shields in the first focal plane (17 in. from the sphere entrance port) does not appreciably change the flux reflected back to the ellipsoidal mirror by the averaging sphere. Further, the left hand side of equation 64 is a term that is used only to establish the mirror absorption F_α; therefore, it is possible to simply factor out a single term from the entire equation (59) and study the effect of setting this term equal to one. The resulting equation is

$$\rho_s = \frac{[1 - \rho_{HS}\ (\bar{\rho}_{ED})^2\ \eta'(f_{s-\epsilon})]}{[1 - \rho_{HM}\ (\bar{\rho}_{ED})^2\ \eta'(f_{s-\epsilon})]}\ \rho_s{}' \tag{65}$$

where ρ_s is the true reflectance and $\rho_s{}'$ is the reflectance for the assumption that the multiplying term is one. Thus the error in ρ_s caused by the assumptions of equation (61), (62), (63) and (64) is

$$\frac{\rho_s - \rho_s{}'}{\rho_s} = \frac{[\rho_{HM} - \rho_{HS}]\ (\bar{\rho}_{ED})^2\ \eta'\ f_{s-\epsilon}}{1 - \rho_{HS}\ (\bar{\rho}_{ED})^2\ \eta'\ f_{s-\epsilon}} \tag{66}$$

Experimental measurements indicate that the term $(\bar{\rho}_{ED})^2\ \eta'\ f_{s-\epsilon}$ has a maximum value of 0.04. These measurements were made with a specular mirror sample with and without a shield in the first focal plane that completely eliminated this interchange. Thus equation (66) becomes

$$\frac{\rho_s - \rho_s{}'}{\rho_s} = \frac{[\rho_{HM} - \rho_{HS}]\ (0.04)}{1 - \rho_{HS}\ (0.04)} \tag{67}$$

It remains then to establish the values for ρ_{HS} and ρ_{HM}. Jakob [6] indicates that for conductors $(1 - \rho_N)/(1 - \rho_H)$ lies between 1.00 and 1.33, while for insulators he indicates the limiting values to lie between approximately 0.935 and 1.05, where ρ_N is essentially the $\rho(7^\circ, \varphi; 2\pi)$ measured by the ellipsoidal mirror reflectometer. Thus, by letting $\rho_{HM} = \rho_M$ and $\rho_{HS} = \rho_S$, the error caused by this term can be graphed as a function of ρ_S with ρ_M as a parameter. Figure 10 illustrates such a graph and indicates that accurate reflectance measurements are possible either (1) when $\rho_{HM} \approx \rho_{HS}$ or (2) when the terms in equations 61 through 64 can be accurately evaluated and the appropriate corrections made to the terms in equation (59).

3.5.2 Reflectance Standard: The error caused by the uncertainty in the reflectance of the specular reflectance standard is $\pm 0.0015/\rho_M$ which, for the case of the aluminum and gold standards, is (on the average) ± 0.0017. Since ρ_M is multiplied by all the terms of equation (59), the uncertainty of ρ_M carries over directly as an uncertainty in ρ_s.

3.5.3 Flux Measurement: The uncertainty in the measurement of the various fluxes F_{SD}, F_{S1D}, F_{S2D}, F_{DD}, and F_{1D} will affect $\rho(7^\circ, \varphi; 2\pi)$. Examination of equation (59) indicates that the flux ratios F_{SD}/F_{1D}, F_{DD}/F_{1D}, F_{S2D}/F_{1D}, and F_{S1D}/F_{1D} are the only terms involving measured fluxes that could appreciably affect $\rho(7^\circ, \varphi; 2\pi)$. Furthermore, it is apparent that the measurement of each of these fluxes involves about the same uncertainty, so that in effect the uncertainty of measurement of the fluxes can be converted (as a first order approximation) to the uncertainty in F_R/F_I where

$$\rho_s = \frac{F_R}{F_I} \tag{68}$$

All other flux ratios in equation (59) are in secondary terms so that no significant error is caused by uncertainty in measurement of these ratios. The uncertainty of measurements in this case involves several variables, (1) the actual mechanics of reading signals from a 10 in. strip chart recorder, (2) the lack of linearity of the detector-electronics system, (3) the instability of the entire system between measurements and (4) the effects of spatial variations in the sensitivity of the detector.

The strip chart recorder has an accuracy of ± 0.2 percent of full scale. The linearity of the system is accounted for by an independent check on the linearity of the complete system. The effects due to variations in sensitivity are minimized in the relative measurement by careful placement of all

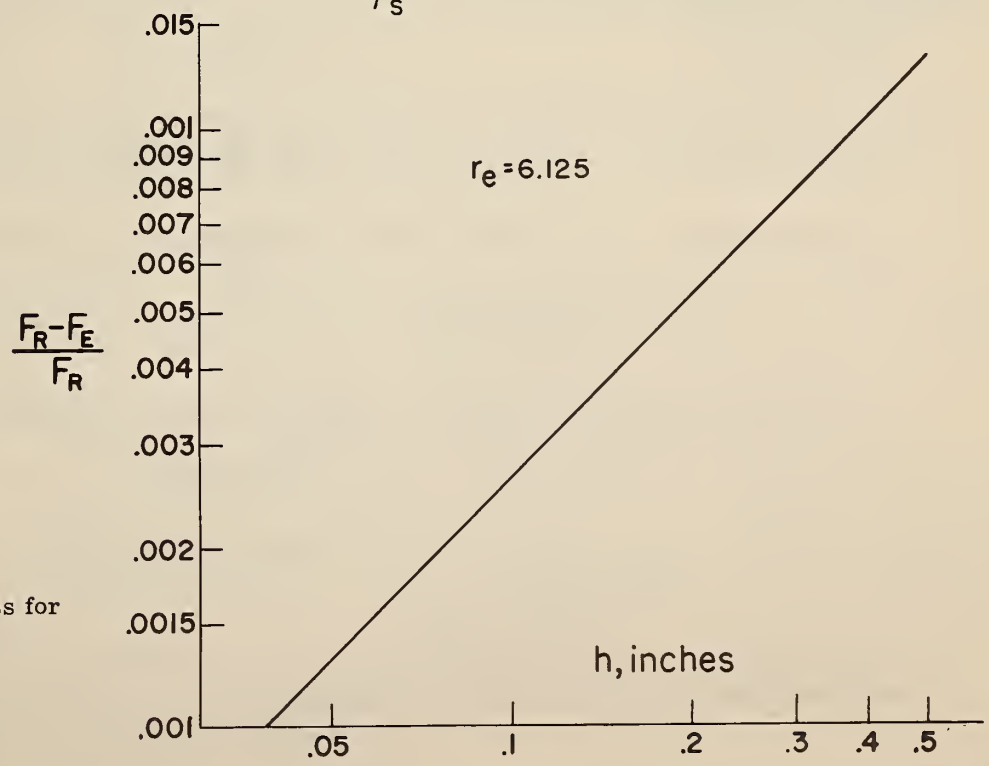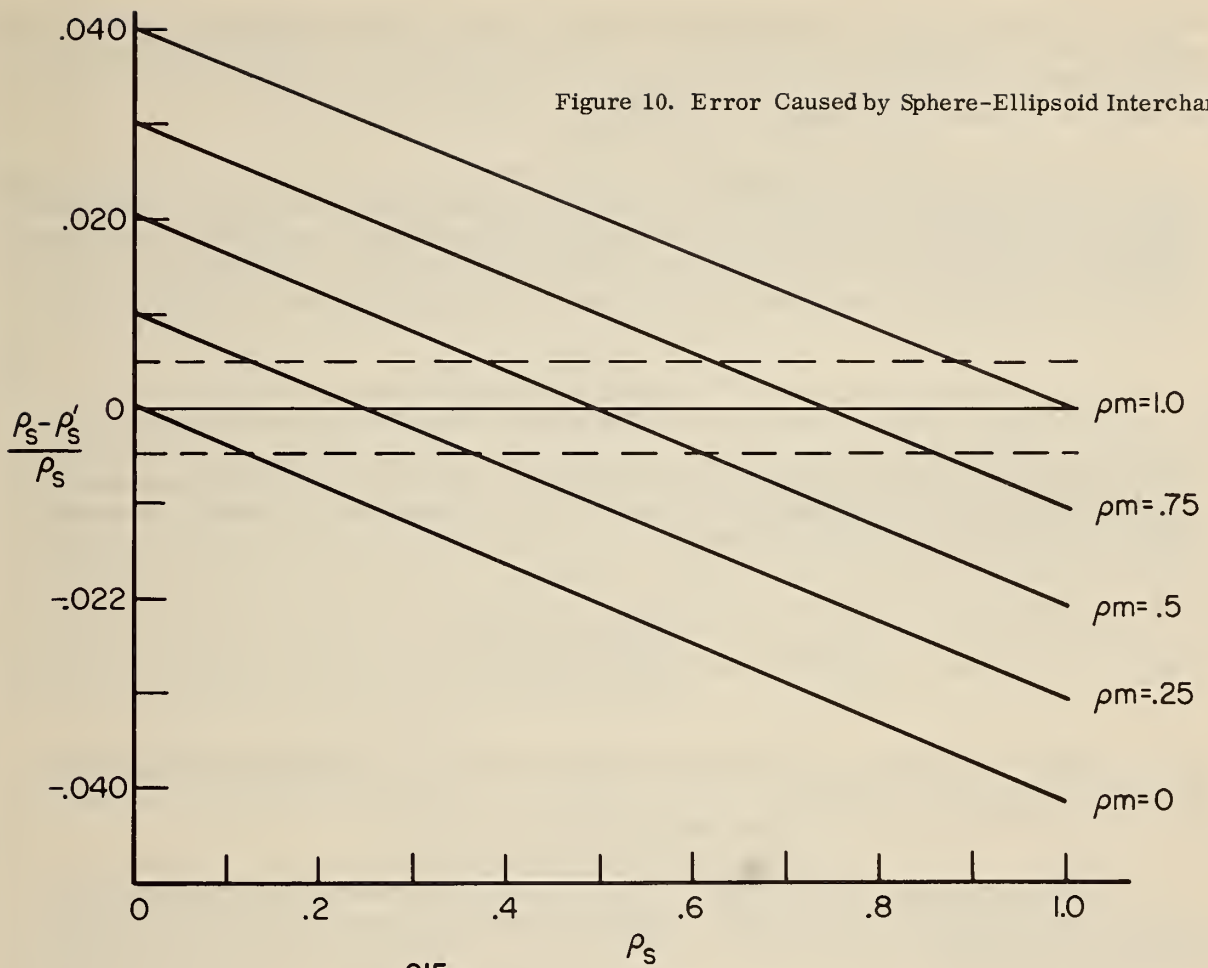Figure 10. Error Caused by Sphere-Ellipsoid Interchange

Figure 11. Edge Loss for Perfect Diffuser

29

beams on the same part of the averaging sphere's wall. Thus the total uncertainty of careful measurements of fluxes is estimated to be less than ±0.5 percent. This precision could be increased by the use of a mechanical digital voltmeter, which gives one additional significant figure, and by a statistical analysis of repeated readings of these fluxes.

3.5.4 <u>Variation in Mirror's Reflectance:</u> The edges of the ellipsoidal mirror were found to reflect about 1.5 percent more of the incident flux than did the central portions of the mirror. Previously, a correction for the effect was established. In equation (59) each term is multiplied by this correction and since the corrections to the different terms are very nearly equal, the total effect of the correction can be studied by assuming this term to factor out of equation (59) so that

$$\rho_s = \frac{1}{1 + \frac{F_{S2D}}{F_{SD}}(0.015)} [F_{59}] \tag{69}$$

where F_{59} represents the remaining terms in equation (59). The factor (0.015) is the increased reflectance of the edges of the ellipsoidal mirror and is estimated to have uncertainty of less than ±0.003. The effect of this uncertainty on ρ_s is

$$\frac{\rho_s - \rho_s{}'}{\rho_s} = 1 - \frac{1 + \frac{F_{S2D}}{F_{SD}}(0.015 \pm 0.003)}{1 + \frac{F_{S2D}}{F_{SD}}(0.015)} \tag{70}$$

where $F_{S2D}/F_{SD} = 0.20$ for the case of the perfect diffuser. This yields an uncertainty in ρ_s of less than ±0.0009. It is also apparent that, since the value for F_{S2D}/F_{SD} will in general be less than 0.2 this uncertainty will generally be smaller than ±0.0009.

3.5.5 <u>Flux and System Assumptions:</u> In order to establish the effects of the remaining factors involved in an estimate of the uncertainty, the following assumptions are made about the geometric distribution of the flux.

(1) $\dfrac{F_{SD}}{F_{ID}} = 0.95 \, \rho_s$ (4) $\dfrac{F_{DD}}{F_{ID}} = 0.90 \, \rho_s$

(2) $\dfrac{F_{S1D}}{F_{ID}} = 0.7 \, \rho_s$ (5) $\dfrac{F_{S2D}}{F_{SD}} = 0.16$

(3) $\dfrac{F_{S2D}}{F_{ID}} = 0.15 \, \rho_s$ (6) $\dfrac{F_{S2D}}{F_{S1D}} = 0.21$

(7) $\dfrac{F_{S2D}}{F_{DD}} = 0.17$

The following values for system constants are approximately those used in this work.

(1) $\bar{\rho}_\epsilon = 0.97$ (3) $\dfrac{A_H}{A_{SH} - A_H} = \frac{1}{3}$

(2) $\rho_M = 0.98$ (4) $\dfrac{A_{S1}}{A_{SH} - A_H} = \frac{1}{12}$

(5) $\dfrac{A_\epsilon}{A_W} = 0.0021$

The above values for the flux ratios and the system parameters are used in the following analyses.

3.5.6 <u>Hole Correction:</u> From a previous section the hole correction is given as

$$\frac{F_H}{F_R} = \frac{A_H}{A_{SH} - A_H} \left(\frac{\rho_M}{\rho_S \, F_{1D}}\right) \left(\frac{F_{SD}}{1 + \dfrac{F_{S2D}}{F_{SD}}(0.015)} - \frac{F_{S1D}}{1 + \dfrac{F_{S2D}}{F_{S1D}}(0.015)} \right) \qquad (71)$$

The value for F_H/F_R under the previous assumptions is 0.0816. There remain two sources of error in this correction which have not yet been discussed; these are the uncertainty in area ratios and in the average flux density assumption of equation (28). The area ratio was measured with an accuracy of ±0.01 square inch, which generates by calculation similar to equation (70) an uncertainty in equation (71) of ±0.0015.

In equation (28), it was assumed that $(F_S - F_{S1})/(A_{SH} - A_H)$ was the flux density on the area of the ellipsoidal mirror immediately surrounding the entrance hole in the mirror. A very large error[7] for this correction would occur if, instead of being distributed evenly about the shield A_{SH}, the flux was distributed such that no flux left through the entrance hole while 25 percent of the reflected flux was absorbed by the shield. In this case there would be no hole correction, but equation (28) would indicate that 8.33 percent of the flux was lost out the hole. This is a very large error, but no known engineering surface has a distribution of this nature; further, experimental techniques are available that will enable the investigator to check for such a distribution, such as tilting the sample with respect to the first focal plane and observing the variation in F_{S1D}. On the whole, an uncertainty of less than ±0.003 is expected from this correction. As more goniometric reflectance data become available, this loss can be more accurately evaluated.

3.5.7 <u>Wire Correction:</u> The wire correction is given by

$$\frac{F_W}{F_R} = \frac{A_W}{A_\epsilon} \frac{\rho_M}{\rho_S \, F_{1D}} \left[\frac{F_{DD}}{1 + \dfrac{F_{S2D}}{F_{DD}}(0.0015)} \right] \qquad (72)$$

which under the previous assumptions is equal to 0.0018. The uncertainty of the area ratio is ±0.005 when the uncertainty in A_W is ±0.005 and the uncertainty in A_ϵ is ±0.05. This affects the value of ρ_S by less than ±0.0005.

The assumption that the flux density over A_W is the same as the flux density over A_ϵ is probably the most accurate assumption of all, for the case where the specular component is not incident on the wires; as such, no uncertainty is attributed to this assumption.

3.5.8 <u>Sample Shading Correction:</u> The two sample shading correction terms are

$$\frac{F_{SP}}{F_R} = \frac{\rho_M}{\rho_S \, F_{1D}} \left[\frac{F_{SD}}{1 + \dfrac{F_{S2D}}{F_{SD}}(0.015)} - \frac{F_{S1D}}{1 + \dfrac{F_{S2D}}{F_{S1D}}(0.015)} \right] \frac{A_S}{A_{SH} - A_H} \qquad (73)$$

and

$$\frac{F_{SR}}{F_R} = \frac{\rho_M}{\rho_S \, F_{1D}} \left[\frac{F_{SD}}{1 + \dfrac{F_{S2D}}{F_{SD}}(0.015)} - \frac{F_{S1D}}{1 + \dfrac{F_{S2D}}{F_{S1D}}(0.015)} \right] \times$$

$$\left[\frac{A_{S1}}{A_{SH} - A_H} \right] \left[\frac{F_{DD}}{F_{SD}} \rho_S \, \bar{\rho}_\epsilon^{\,2} \left(\frac{A_\epsilon - A_W}{A_\epsilon} \right) \frac{1}{1 - \rho_S \, \bar{\rho}_\epsilon \left(\dfrac{F_S - F_{DD}}{F_{SD}} \right)} \right] \qquad (74)$$

First F_{SP} is analyzed for the remaining unaccounted for uncertainty due to the uncertainty in

_____
[7] Again excluding the case of a diffraction grating.

$A_S/(A_{SH} - A_H)$. The value of F_{SP}/F_R under the original assumptions is 0.020 and the uncertainty in $A_S/(A_{SH} - A_H)$ is ±0.001 which yields an uncertainty in F_{SP}/F_R that is less than ±0.0002.

In equation (74) the value of F_{SR}/F_R is 0.0008 (for $\rho_s = 1.0$) and the effect of the uncertainty in $A_{S1}/(A_{SH} - A_H)$ and $(A_\epsilon - A_W)/A_\epsilon$ is negligible, for even if these terms were 50 percent in error they would influence ρ_s by only ±.0003, thus no uncertainty is attached to this term, in fact it will almost always be neglected; it is included in the analysis so that its magnitude can be checked for each sample and used whenever it is significant.

3.5.9 <u>Edge Loss:</u> If the sample is placed slightly below the first focal plane, the ellipsoidal mirror no longer collects flux over the entire hemisphere, because the edge of the ellipsoidal mirror is in the first focal plane. In the experimental measurements care was exercised to insure that the sample was at or above the first focal plane. The effect of the sample being below the first focal plane is easily studied for the case of the perfect diffuser. In this case

$$F_R = \pi L \tag{75}$$

where L is the outgoing radiance and is constant over the hemisphere. If the sample is slightly below the focal plane then the flux collected by the ellipsoid is

$$F_E = \int_0^{2\pi} \int_0^{\theta^*} \cos\theta' \, \sin\varphi' \, d\varphi' \, d\theta' \tag{76}$$

where θ^* is the angle from the normal to the specimen to the edge of the ellipsoidal mirror.

The fraction of the total reflected flux lost is

$$\frac{F_R - F_E}{F_R} = 1 - \frac{2\pi \left[1 - \cos^2 \theta^*\right]}{(2)\pi} = \cos^2 \theta^* \tag{77}$$

where the $\cos\theta^*$ is (as function of the distance (h) below the first focal plane and radius (r_e) of the opening of the ellipsoidal mirror).

$$\cos\theta^* = \left[\frac{h^2}{h^2 + r_e^2}\right]^{\frac{1}{2}} \tag{78}$$

or

$$\frac{F_R - F_E}{F_R} = \frac{h^2}{h^2 + r_e^2} \tag{79}$$

The quantity expressed in equation (79) is graphically illustrated in figure 11. Further, if the instrument were deliberately operated with the sample a fixed distance below the first focal plane, the S2 shield could be used to establish the average flux density on the edges of the mirror, then a correction, similar to the entrance hole correction, could be used.

3.5.10 <u>Absolute Measurement:</u> The major additional uncertainty in the absolute measurement arises from the fact that the sphere-ellipsoid interchange is present only in the reflected flux measurement, thus the error caused by this interchange is essentially shown by the $\rho_M = 0$ curve in figure 10. That means that a good knowledge of this interchange is needed to provide accurate data with the absolute measurement technique. In addition, a better knowledge of the ellipsoidal mirror's reflectance is needed, since for the absolute measurement the reflectance $\bar{\rho}_\epsilon$ doesn't cancel out, as it does in the relative measurement.

3.5.11 <u>Summary:</u> Since only fragmentary data are presently available for use in an error analysis, no effort was made to establish accurately the relation between the various uncertainties calculated in this section. Table III lists the percentage undertainties. It should be noted that most of

32

the uncertainties will also depend on the difference between the reflectances of the standard and the sample.

From Table III it appears that the ellipsoidal mirror reflectometer is capable of accuracies of better than two percent. However, only continued reevaluation can establish unequivocally the overall accuracy of this instrument. Furthermore, figures 10 and 11 indicate specific non-random errors which must be corrected for or eliminated if highly accurate measurements of reflectance are desired.

Table III Expected Uncertainties

Uncertainty Due to	Term Involved	Expected Uncertainty in ρ_s*
Reflectance Standard	ρ_s *	±0. 17%
Flux Measurement	ρ_s	±0. 50%
Variation in Mirror Reflectance	ρ_s	±0. 09%
Area Ratio	F_H/F_R	±0. 15%
Average Flux Density	F_H/F_R	±0. 30%
Area Ratio	F_W/F_R	±0. 05%
Area Ratio	F_{SP}/F_R	±0. 02%
Area Ratio	F_{SR}/F_R	±0. 01%

*$\rho_s = \rho(7°, \varphi; 2\pi)$

3. 6 Experimental Data

This section presents preliminary experimental data taken with an ellipsoidal mirror reflecto-meter. There are four main parts to this section: (1) system parameters and alignment, (2) directional hemispherical reflectance, (3) specular component of reflectance, and (4) directional annular cone reflectance.

3. 6. 1 <u>System Parameters and Alignment:</u> Alignment: Optical alignment of the ellipsoidal mirror reflectometer was accomplished by setting the monochromator so that the visible light was focused on the exit slits. The image of the exit slit [8] was visually focused (by the 49-inch radius of curvature spherical mirror) through the entrance hole in the ellipsoidal mirror onto the center of a diffuse sample. The sample holder and mirror holder were adjusted to give an image of minimum size and maximum sharpness at the second focal point. To ascertain that all of the beam of reflected flux was passing through the entrance port of the averaging sphere at the second focal point, a film holder [9]

---

[8] The exit slits were masked to a height of 2mm.

[9] The film was Polaroid type 47 – a 3000 speed film.

33

was placed in the second focal plane centered on the second focal point. Two different samples were used at the first focal point, (1) an aluminum mirror and (2) a diffuse porcelain enamel reflectance standard. Figure 12 shows the images formed at the second focal point for the two different samples and for different exposure times. The black area around each image outlines the approximate size and shape of the entrance port of the averaging sphere.

The image formed when the aluminum mirror was used in the first focal plane is quite clear and well defined. The image formed when the mirror was inclined 25° with respect to the first focal plane shows light grey areas surrounding the white image, which indicate that the scatter and aberration of the ellipsoidal mirror increase with distance from the apex. The image formed at the second focal point when the porcelain enamel (a fairly good diffuser) was placed at the first focal point is enlarged and indicated that careful positioning of the image on the sphere entrance port is required if one expects to collect all of the flux represented by these images. The increased image size for the diffuser is indicative of the total scatter and aberrations for this particular ellipsoidal mirror. In all cases, increased time of exposure yielded slightly enlarged images, indicating that a small amount of flux surrounds the visual image. The conclusion drawn from the results displayed in figure 12 is that flux at the second focal point does pass through the sphere entrance when care is taken to center the visual image on the entrance to the sphere.

Linearity: A set of five sector discs was constructed to provide an independent check of the linearity of the entire detector electronics system. These discs were made by machining out equally spaced radial sections of an aluminum disc, leaving a multiple bladed disc. The transmittance of these rotating discs is equal to the ratio of the open area on the disc to the total area of the disc. These areas were very accurately measured by the Engineering Metrology Section of the National Bureau of Standards.

Reference 7 contains a more complete description of these sector discs. The discs (rotating at about 1300 rpm) were used to attenuate the incident flux when an aluminum mirror was at the first focal point and the averaging sphere-detector at the second focal point. The output of the amplifier was read on a 10 inch strip chart recorder. The unattenuated signal was then divided into the five attenuated signals to give the ratios that the system yields for the five separate known transmittances. These results, along with the measured working ratios for each disc, are presented in Table IV. The values are reported for each of the wavelengths used in this work.

Table IV Linearity Check

Disc	Calculated Transmittance	Standard Deviation of Calculated Transmittance	Signal Attenuation (average of 4 tests)							
			1. 5μm	2. 0μm	2. 5μm	3. 5μm	4. 5μm	5. 5μm	6. 5μm	7. 5μm
A	0. 7510	±0. 002	0. 748	0. 749	0. 749	0. 748	0. 751	0. 752	0. 751	0. 746
B	. 5000	±. 0002	. 498	. 497	. 499	. 500	. 503	. 500	. 502	. 496
C	. 2528	±. 0014	. 252	. 250	. 254	. 253	. 250	. 254	. 251	. 251
D	. 1273	±. 001	. 126	. 126	. 127	. 127	. 130	. 126	. 125	. 124
E	. 0507	±. 0003	. 050	. 049	. 046	. 049	. 049	. 047	. 050	. 046

From Table IV it is apparent that, within the precision of reading a 10-inch strip chart recorder, no corrections for non-linearity are necessary.

Sphere-ellipsoidal interchange: The interchange of flux between the averaging sphere and the ellipsoidal mirror was measured by using the aluminum mirror and a shield just below the first focal plane that only passed the specularly reflected beam from the mirror. By comparing the detector

Aluminum Mirror
0° Sample Holder
2-Second Exposure

Enamel
0° Sample Holder
2-Second Exposure

Aluminum Mirror
0° Sample Holder
1-Minute Exposure

Enamel
0° Sample Holder
15-Second Exposure

Aluminum Mirror
25° Sample Holder
5-Second Exposure

Enamel
0° Sample Holder
45-Second Exposure

Aluminum Mirror
25° Sample Holder
1.5-Minute Exposure

Enamel
0° Sample Holder
2-Minute Exposure

Figure 12. Image Configurations at the Second Focal Plane

signal when the shield was in the system and when it was not in the system it was possible to calculate $(\bar{\rho}_{\epsilon D})^2 \ \eta' \ f_{s-\epsilon}$ from equations in earlier sections of this report. The values for this term are given in Table V.

<p align="center">Table V Measured Values of $(\bar{\rho}_{\epsilon D})^2 \ \eta' \ f_{s-\epsilon}$</p>

λ	$(\bar{\rho}_{\epsilon D})^2 \ \eta' \ f_{s-\epsilon}$
1. 5	0. 039
2. 0	. 039
2. 5	. 040
3. 5	. 036
4. 5	. 031
5. 5	. 026
6. 5	. 018
7. 0	. 013

Shields: To enable measurement of F_{s1D}, F_{DD} and F_{s2D} two shields were constructed. (1) a small shield shaped as depicted in figure 8 and (2) a circular disc which only allows flux from the central part of the ellipsoidal mirror to reach the second focal point.

The same small shield was used for both the F_{s1D} and F_{DD} measurements. The shield was placed on opposite sides of the sample for the two measurements. No effort was made to design a specific shield to block out only the specular component, since this is a study in itself. The area of this shield projected onto the ellipsoidal mirror is 1.905 square inches. The other shield (for F_{s2D}) was constructed so that it blocked the flux from the outer 2 inches of the mirror. Then to get the flux on this area of the mirror the signal read with the shield in the system is subtracted from the signal for the system with no shield (F_{sD}).

The area of the entrance hole was measured to be 0. 339 square inches and the projected area of the sample is 0. 146 square inches. Thus

$$\frac{A_s + A_H}{A_{sH} - A_H} = 0.310$$

Area A_{s1} is 0. 05 ± 0. 01 so that

$$\frac{A_{s1}}{A_{sH} - A_H} = 0.032$$

The platinum-13% rhodium sample was a 1/2 inch diameter disc which yields (after correcting for the overlap of the image of the hole and the sample).

$$\frac{A_s + A_H}{A_{sH} - A_H} = 0.331$$

3. 6. 2 <u>Directional Hemispherical Reflectance</u> Several samples were chosen for reflectance measurement with the ellipsoidal mirror reflectometer (1) platinum-13% rhodium, (2) gold mesh, (3) a porcelain enamel, (4) oxidized Kanthal, and (5) Crystex brand sulfur. Samples (1) and (4) are high temperature emittance standards provided by the National Bureau of Standards and described by Richmond, et. al [7]. Sample (2) was provided by Bernd Linder of the Missile and Space Division, General Electric Co., Philadelphia, Pa., and is 2 mil stainless steel wire screen (135 mesh) backed by 0. 15 mil mylar with vapor deposited gold coating. Sample (3) is a standard of luminous daylight reflectance of the type formerly issued by the National Bureau of Standards. Sample (5) is the same sulfur that has been used throughout this work.
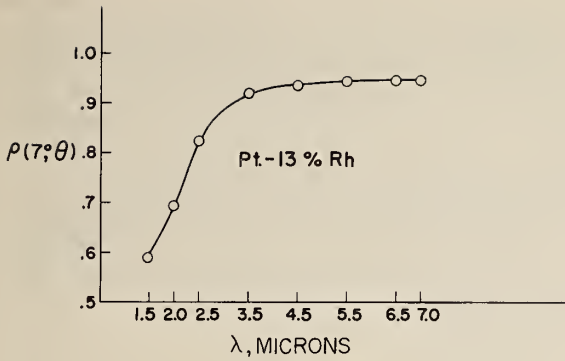
$\rho(7;\theta)$

1.0
.9
.8
.7
.6
.5

1.5 2.0 2.5 3.5 4.5 5.5 6.5 7.0

Pt.-13 % Rh

λ, MICRONS

Figure 13. Reflectance of Platinum-13% Rhodium

λ	Specular Component
1.5µ	13%
2.0	13%
2.5	13%
3.5	13%
4.5	13%
5.5	13%
6.5	13%
7.0	13%

$\rho(7;\theta)$

1.00
.90
.80
.70
.60

1.5 2.0 2.5 3.5 4.5 5.5 6.5 7.0

λ, MICRONS

Figure 14. Reflectance of Gold Mesh

$\rho(7;\theta)$

.7
.6
.5
.4
.3
.2
.1
0

1.0 1.5 2.0 2.5 3.5 4.5 5.5 6.5 7.0

λ	Specular Component
1.5µ	12%
2.0	13%
2.5	13%
3.5	21%
4.5	34%

λ, MICRONS
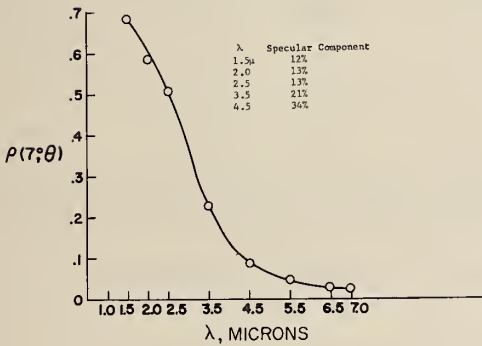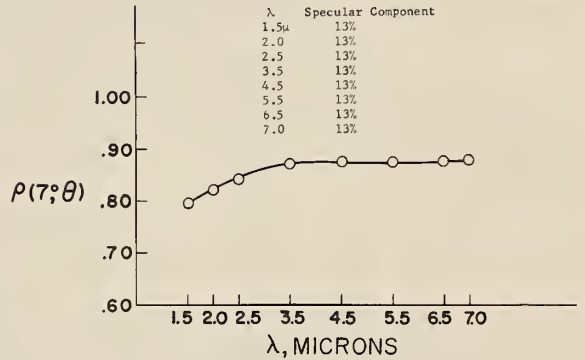
Figure 15. Reflectance of Porcelain Enamel

Figure 16. Reflectance of Oxidized Kanthal

$\rho(7;\theta)$

.50
40
.30
.20
.10
0

1.5 2.0 2.5 3.5 4.5 5.5 6.5 7.0

λ	Specular Component
1.5µ	6%
2.0	7%
2.5	8%
3.5	8%
4.5	8%
5.5	8%
6.5	8%
7.0	8%

λ, MICRONS

Figure 17. Reflectance of Mu Sulfur

$\rho(7;\theta)$

1.00
.80
.60

1.5 2.0 2.5 3.5 4.5 5.5 6.5 7.0

λ (IN MICRONS)

37

Platinum-13% rhodium: the average value of six determinations of the reflectance of two samples is shown in figure 13. Table VI gives the individual reflectances and the standard deviations of th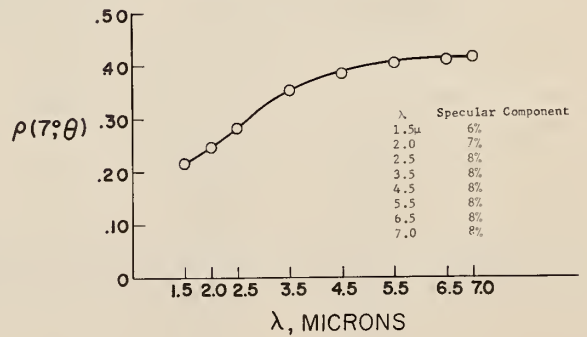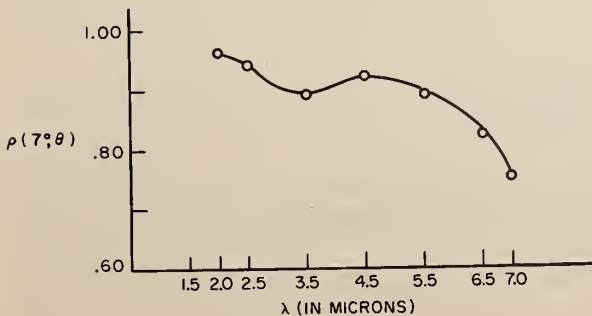eir average. The six reflectances reported in Table VI were measured by two different operators over a period of one week. Further, determinations 1a and 2a were made on samples tilted 10° to the first focal plane to eliminate the hole and sample corrections. This is possible because, as the specular component in Table VI indicates, the reflected flux is concentrated around the specular peak and tilting the sample does not result in an edge loss. The data for the case where the samples were tilted show no significant difference from the data for the samples in the first focal plane, thus the hole and sample corrections apparently were correct. Further examination of the values given in Table VI indicates that there may be a slight difference in reflectance between the two samples. The specular component presented in Table VI will be discussed later.

Table VI Reflectance of Platinum – 13% Rhodium**

Wave-length	1a	1b	1c	2a	2b	2c	Average	Standard Deviation	Specular Component*
1.5	0.610	0.597	0.591	0.566	0.574	0.603	0.596	±0.005	69%
2.0	.701	.691	.692	.694	.686	.696	.693	.002	82%
2.5	.823	.813	.821	.826	.827	.820	.822	.002	83%
3.5	.919	.905	.921	.924	.930	.913	.919	.005	86%
4.5	.933	.926	.937	.935	.940	.929	.933	.004	87%
5.5	.942	.936	.940	.946	.947	.932	.941	.005	88%
6.5	.945	.938	.940	.947	.949	.942	.944	.005	90%
7.0	.947	.940	.942	.946	.953	.943	.945	.005	92%

*This is an approximation of the specular component, computed as $[(F_{SD} - F_{DD}) / F_{SD}] \times 100$, and includes the diffuse component of flux in the solid angle about the specular direction.

**Two samples are represented in this table, sample 1 and sample 2. 1a and 2a were made with the sample tilted 10° to the first focal plane.

NBS Reflectance for Pt. 13% Rh. reference 7 (various sample temperatures)

λ	800 °K	1100 °K	1300° K
1.5μ	74.8%	78.7%	77.4%
2.0	80.8	81.5	80.3
2.5	83.5	83.2	82.0
3.5	87.4	85.7	84.5
4.5	89.1	87.4	86.5
5.5	90.4	88.9	87.3
6.5	91.4	89.9	88.7
7.0	91.6	90.4	89.2

Gold mesh: the data for the gold mesh are presented in figure 14 where each data point is the average of three determinations. The data are self-explanatory.

Enamel: the data for the procelain enamel reflectance standards are presented in figure 15. No effort was made to correct the low reflectances for the sphere-ellipsoid interchange.

Oxidized Kanthal: The data for the oxidized Kanthal[10] are graphed in figure 16. These data were taken by attenuating the flux for the reference measurement by 50 percent, by use of one of the previously described sector discs. No attenuation was used for the sample measurement. In addition, the data were corrected for the sphere-ellipsoid interchange through use of equation (66).

Sulfur: The directional hemispherical reflectance for mu sulfur is presented in figure 17. The dip in reflectance at about 3.5μ indicates an absorption band that could be caused by an organic contaminant in the sulfur. It is not known whether this absorption occurs in the sulfur-coated averaging sphere.

3.7 Specular Component of Reflectance

The data in Table VI, and figures 14, 15, 16 and 17 include the specular component of the reflected flux. No effort was made to study the size of shield that would yield the most useful component; instead a convenient shield (the A_{SH} shield) was used. The specular components reported were calculated as follows:

$$\% \text{ specular component} = \frac{F_{SD} - F_{DD}}{F_{SD}} (100) \tag{80}$$

Thus the experimental specular component for the diffuser (assuming sulfur to be a near perfect diffuser) is 9 percent. The specular component defined by equation (80) minus the specular component for sulfur is the "true" specular component and is shown in Table VII for the samples reported in this work.

Table VII "True" Specular Component

λ	Pt–13% Rh	Gold Mesh	Porcelain Enamel	Oxidized Kanthal	Mu Sulfur
1.5	60.%	4.%	3%	− 3.%	0.0%
2.0	73.%	4.%	4%	− 2.%	0.0
2.5	74.%	4.%	4%	− 1.%	0.0
3.5	77.%	4.%	12%	− 1.%	0.0
4.5	78.%	4.%	25%	− 1.%	0.0
5.5	79.%	4.%	--	− 1.%	0.0
6.5	81.%	4.%	--		0.0

3.7.1 Directional – Annular Cone Reflectance: Various directional annular cone reflectances of three samples were measured and compared to the values expected for the "perfect" diffuser. The reflectance measured for this section was

$$\rho(\text{directional annular cone}) = \frac{\int_0^{2\pi} \int_{\theta*}^{\pi/2} L'(\theta', \varphi') \cos\theta' \sin\varphi' \, d\varphi' \, d\theta'}{L(7°, \varphi) \cos 7° (\Delta \omega)} \tag{81}$$

where the flux reaching the detector was restricted to the annular solid angle between $\theta*$ and $\pi/2$ by use of a circular disc centered on the sample and placed just below the first focal plane. Five shields providing different $\theta*$s were used. Then the detector signals for each of the five shields were divided by F_R and compared to resulting values calculated for the perfect diffuser, which is

---

[10] Kanthal is an iron-chromium-aluminum alloy.

$$\frac{\rho(\text{directional annular cone})}{\rho(\text{directional hemispherical})} = \cos^2 \theta* \qquad (82)$$

The angle $\theta*$ was measured for each of the shields and Table VIII illustrates the data for three samples at 2.5µm. They are sulfur, $BaSO_4$, and the gold mesh.

Table VIII Ratio of Directional Annular Cone Reflectance
to the Directional Hemispherical Reflectance for Suspected Diffusers*

$\theta*$	Perfect Diffuser	Mu Sulfur	$BaSO_4$	Gold Mesh
79.5	0.033	0.035	0.035	0.033
62.8	.210	.207	.207	.194
43.7	.522	.523	.520	.480
34.3	.683	.692	.680	.641
14.5	.936	.935	.934	.917

*data taken at 2.5µ

3.8 Present Conclusions Regarding Ellipsoidal Mirror Reflectometer

From the foregoing discussion it is evident that the use of an ellipsoidal mirror, sulfur coated averaging sphere over the detector, and a specular reference standard have allowed the development of a very versatile reflectometer. This versatility includes the ability to measure accurately $\rho(\theta, \varphi; 2\pi)$, $\rho(\theta, \varphi; \theta', \varphi')$ $\rho(\text{specular})$, $\rho(\text{non-specular})$, and $\rho(\text{directional annular cone})$. High accuracy is possible due to the following factors: (1) variations in the areal and angular sensitivity of the detector have been laregely eliminated by use of the sulfur coated averaging sphere; (2) an accurate technique for correcting for the entrance and/or exit hole loss has been utilized; (3) the use of the ellipsoidal mirror reduces aberrations in the system and reduces the size of the solid angle of flux incident on the detector; (4) the effective reflectance of the ellipsoidal mirror was measured as a function of position, providing an accurate correction for variations in the mirror's reflectance with position; (5) the reflectometer needs only a specular reference standard which is easy to calibrate; (6) the system losses can be evaluated by establishing the flux involved in each loss through the use of shields placed in the first focal plane.

The actual accuracy (errors) of this type of instrument is estimated to be not more than two percent and probably less than one percent; however, the present lack of comprehensive data on the geometric distribution of reflected flux from common engineering materials precludes a positive general statement of accuracy at this time. This reflectometer provides more information concerning the reflectance of engineering samples than have previous instruments. Further, the separation of the detector and sample permits heating and/or cooling of the sample.

During the development of the ellipsoidal mirror reflectometer, the following results were obtained:
(a) The use of the sulfur coated averaging sphere permitted the construction of a simple and accurate infrared specular reflectometer.
(b) A method of applying sulfur to a sphere wall was developed. The resulting coating appeared to be more durable than standard sphere coatings (i.e., MgO or $BaSO_4$).
(c) A simple bech test was proposed for studying sphere coatings for use in the infrared.
(d) The directional annular cone reflectance was used to study the diffuseness of several samples.

During the course of the development of the ellipsoidal mirror reflectometer several ideas for redesign and/or use of this instrument were generated. They are:

(a) Care should be used in the design of an ellipsoidal mirror reflectometer to keep the specular component of the reflected flux, after reflection by the mirror, as far away from the sample as is practical.

(b) It is recommended that a more complete ellipsoid, such as shown in figure 18, be used as the mirror. This will allow tilting of the sample without flux losses around the edges of the mirror. (It may also be necessary to tilt the detector in some cases.)

(c) It is suggested that the continuous-wave laser would be a superb source, since it has a high intensity collimated beam. Further, the use of the laser would allow the smallest possible entrance hole and reduce the hole loss to nearly zero. However, only a few wavelengths are available.

(d) To use this instrument at its best accuracy, a set of at least 5 specular standards, whose reflectances are evenly distributed between zero and one, should be developed.

(e) Figure 19 illustrates a proposed design for a recording spectrometer using a chopped double beam source.

(f) Additional work on controlling the first, second and third reflections inside a gold-roughened averaging sphere may make this device suitable for use with the reflectometer and extend its range to 10μm.

(g) The instrument is easily convertible to the 0.4 to 2.0μm range by changing the source, detector, and sphere coating.

(h) Figure 20 illustrates the use of the ellipsoidal mirror optics for transmittance and scattering measurements.

(i) Figure 21 illustrates one method of varying the angle of incidence on the sample. However, the construction of this device is not simple, since the flat mirror's angle with respect to the source must change as the mirror is moved in and out, so that the source always appears to be at the second focal point.

(j) In order to extend the useful wavelength range to cover the entire spectrum of interest, it is suggested that an interferometer spectrometer be developed for use as a spectral sorting detector in combination with a gold roughened averaging device and an ellipsoidal mirror reflectometer. The next section discusses the use of the interferometer spectrometer and various measurements recently taken with the instrument to indicate its capability.

4. Interferometer Spectrometer

This section attempts to present the basic concept and advantages of interferometer techniques as applied to relative radiometric measurements. For the sake of clarity several prominent references in the field of interferometry will be quoted extensively. Those wishing a more detailed and complete analysis are referred to the references at the end of the report. The Michelson interferometer will be used for this purpose; however, it should be noted that there are many other interferometric approaches to providing the same kind of data. The following passages have been reprinted, with permission, from reference 8.

The interferometer spectrometer differs from the more well known prism and grating spectrometers in the manner in which the incident radiation is separated into component wavelengths.

Both prism and grating spectrometers contain three basic elements: a slit; a dispersing device (prism or diffraction grating) which separates radiation according to wavelength; and a suitable optical system to produce the spectrum lines, which are monochromatic images of the slit.

Interference spectroscopy, on the other hand, uses the principle of constructive and destructive interference of light waves, [9]. Further, the interferometer spectrometer is basically a pointing radiosity detector. That is, the instrument, in its present usage, is a dc system which measures all the energy incident upon it, whether directly emitted into its optical path or reflected into its
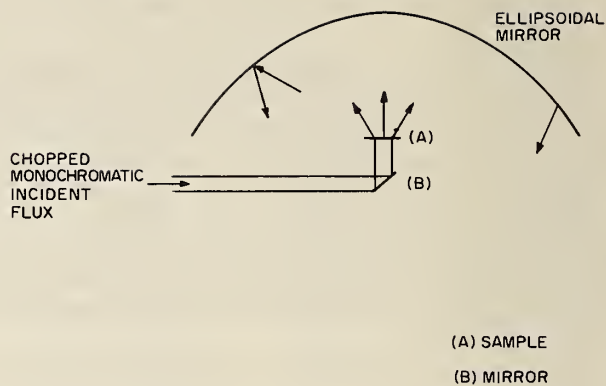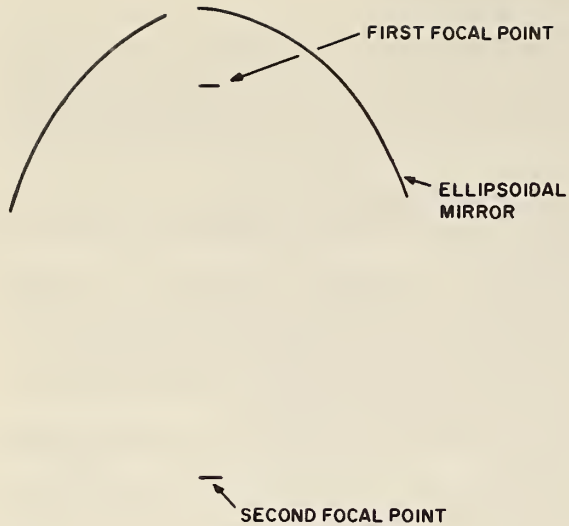
Figure 18. Enlarged Ellipsoidal Mirror

Figure 20. Transmittance and Scatter Optics
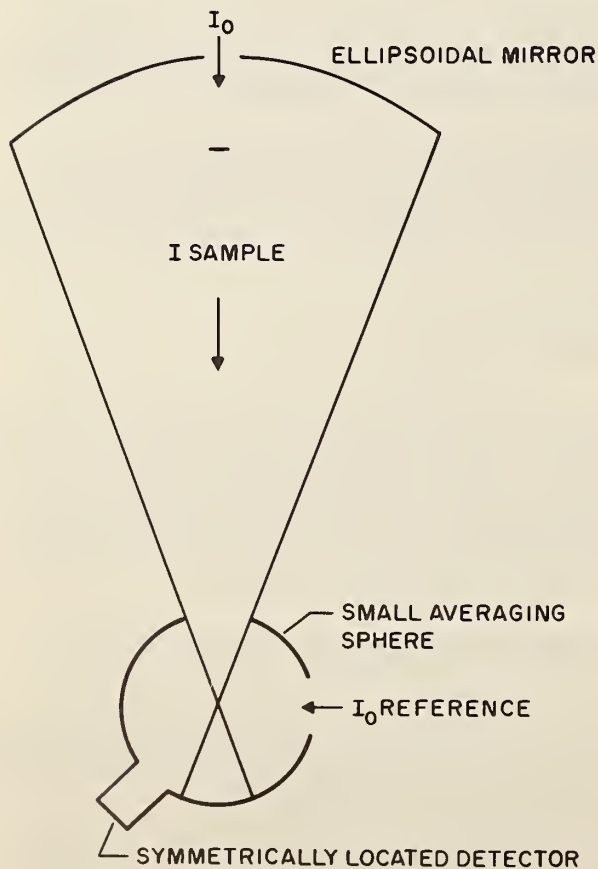Using an Ellipsoidal Mirror

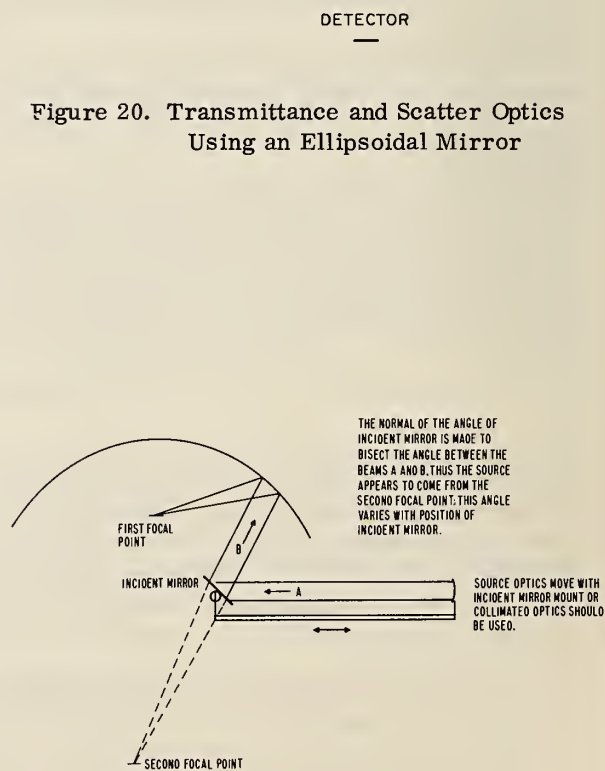
Figure 19. Double Beam Ellipsoidal Reflectometer

Figure 21. Varying Angle of Incidence for
Ellipsoidal Mirror Reflectometer

optical path.

Figure 22 is a block diagram of the electronic chassis and optical head of a commercial interfer-ometer spectrometer [8]. The electronics can be divided into three sub-groups: the input regulator and plus and minus 12 volt regulator; the transducer sweep generator and drive amplifier; and the post amplifier. The optical head consists of the optical cube with its associated lenses, mirrors, beamsplitter, and detector, together with the preamplifier and detector bias supply.

The function of the optical cube is to heterodyne the extremely high electromagnetic frequencies of the infrared radiation down to audio frequencies on the detector, yielding an exact analog of the original light frequencies, since the frequency transformation interferogram or audio frquency spec-trum may be tape recorded for later play back into a narrow-band variable-frequency bandpass filter which is slowly tuned over the appropriate audio frequency range. The result would then be a record of the amount of energy at each frequency. This data reduction process in effect accomplishes the Fourier transform of the original light spectrum into the amplitude-frequency domain. Alternatively, the inverse Fourier transform may be computed on a digital computer.

The interferometer spectrometer under discussion utilizes the Michelson optical system. Optical ray traces are shown in Figure 23. S is a semi-reflective mirror (called a beamsplitter) which reflects half of the light which strikes it and permits the other half to pass. M_1 and M_2 are mirrors which reflect essentially all the light which reaches them; they are identical except that M_1 can be displaced a distance Δx normal to its surface.

Assuming that perfect (non absorbing) mirrors and a perfect beamsplitter (a non-absorbing, partially transmitting mirror that always transmits half and reflects half of any beam incident upon it, regardless of its wavelength or polarization) are used, a beam of radiant flux entering the interfero-meter as shown in Figure 23 will be split into two equal parts, one transmitted to mirror M_1, and one reflected to mirror M_2. The part transmitted to mirror M_1 will be reflected back to the beamsplitter and again split into two equal parts, one reflected to the detector, and the other passing out the entrance port. The part reflected to mirror M_2 will be reflected back to the beamsplitter and again split into two equal parts, one transmitted to the detector and the other reflected out the entrance port.

Thus, two equal beams, each comprising one fourth of the initial beam, reach the detector. If the initial beam is monochromatic, the two beams will form an interference pattern that will consist of a series of alternately light and dark circular rings, surrounding a light or dark area at the center. The width of the fringes, and hence the diameter of the first distinct ring, is a function of the relative pathlengths of the two beams, the dimensions of the interferometer, and the degree of collimation of the incident beam. The optical path length is measured in units of the wavelength, λ, of the radiant flux involved, and includes the effects of phase changes on reflection at the mirrors and on reflection and transmission by the beamsplitter. If the incident monochromatic beam is perfectly collimated, which can never be achieved in practice, or if the optical path lengths of the two beams are identical, the central area will occupy the entire field, and there will be no fringe pattern. When the path lengths are equal, the image of mirror M_2 reflected in the beamsplitter will exactly coincide with Mirror M_1. As mirror M_1 is moved away from this position in a direction normal to its reflecting surface, circu-lar fringes will appear at the outer edges of the field, and the fringe patterns will move radially toward the center of the field as mirror M_1 is moved farther from the image of mirror M_2, and the number of fringes in the pattern will increase. As the mirror is moved through the distance $\lambda/2$, the difference in path lengths of the two beams will be changed by one wavelength, λ, and each fringe will go through a complete cycle from bright to dark to bright. The effect of this cyclic change is to cause the fringes to appear to move radially from the center to the edge of the field, while the whole pattern moves inward. In effect, for each distance of $\lambda/2$ that the mirror moves, a new fringe originates at the center of the pattern, and as the mirror movement continues, the fringe moves radially outward, but never disappears from the field. As more fringes appear they become more crowded and the diameter of the first distinct ring becomes smaller.

In a properly designed optical system, the degree of collimation of the incident flux, the dimensions
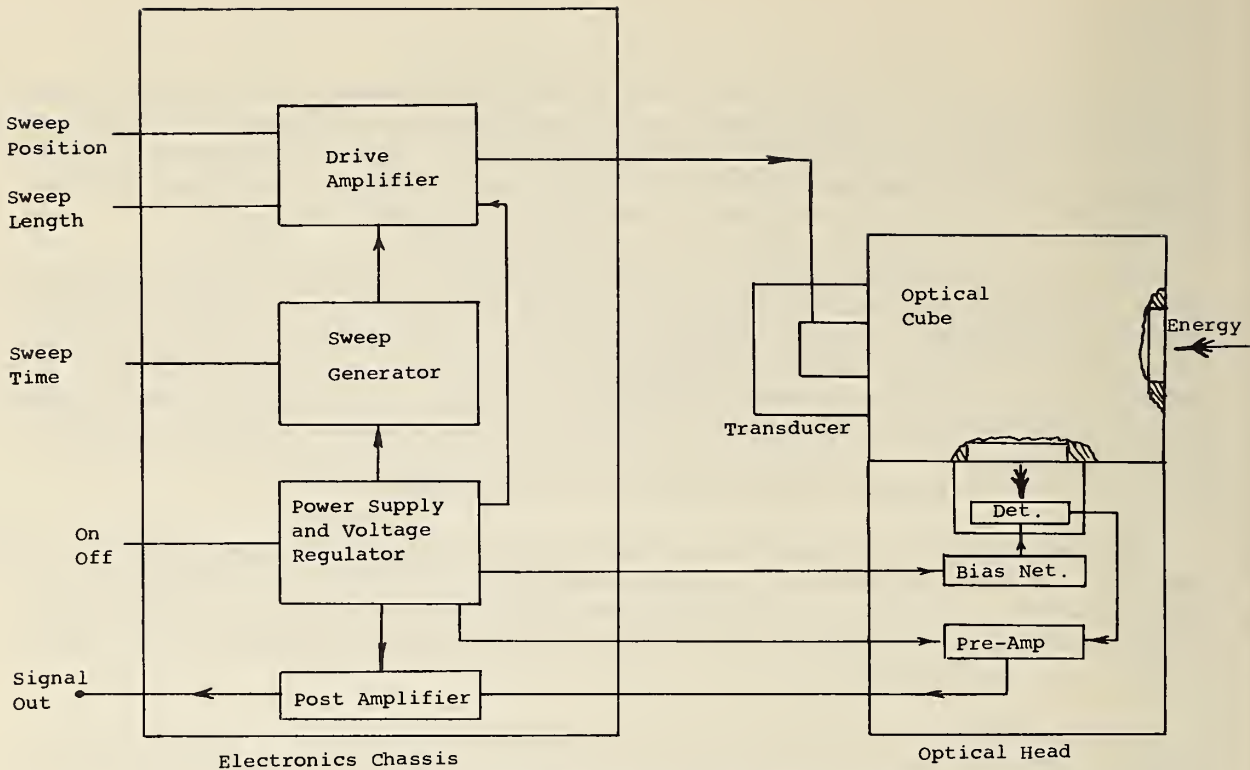
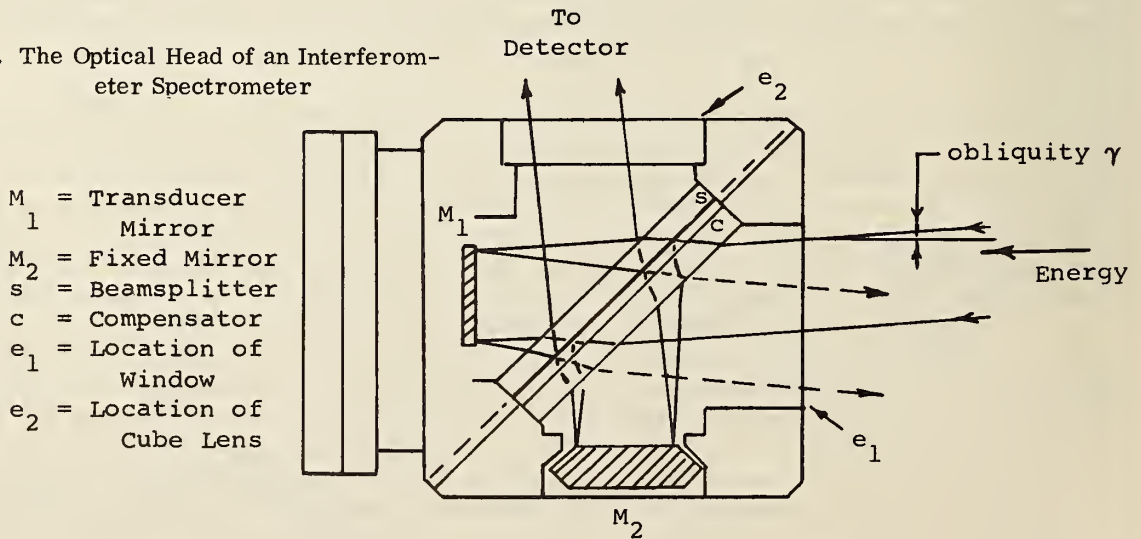Figure 22. Block Diagram of Interferometer Spectrometer Electronics

Figure 23. The Optical Head of an Interferometer Spectrometer

M$_1$ = Transducer Mirror
M$_2$ = Fixed Mirror
s = Beamsplitter
c = Compensator
e$_1$ = Location of Window
e$_2$ = Location of Cube Lens

T = Sweep Time

F = Flyback Time
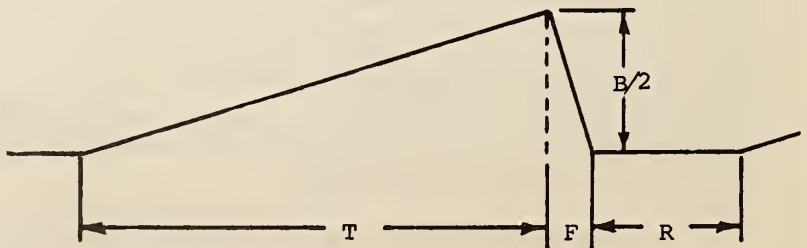
R = Recovery Time

B = Excursion

Figure 24. Mirror Motion

44

of the system and the distance over which mirror M_1 moves are controlled so that only the flux in the central portion of the area inside the first distinct ring reaches the detector. Under these conditions there will be complete destructive interference, and no signal from the detector, whenever the difference in the two path lengths is $\lambda/2$ or an odd multiple of $\lambda/2$ ($\pm \lambda/2$, $\pm 3\lambda/2$, $\pm 5\lambda/2$, etc.), and complete constructive interference, and a maximum signal from the detector each time the difference in the two path lengths is zero or an integral multiple of λ ($\pm\lambda$, $\pm2\lambda$, $\pm3\lambda$ etc.).

As mirror M_1 is moved away from the image of mirror M_2, the signal from the detector will vary sinusoidally as the difference in path lengths increases by integral wavelengths, according to the equation

$$L = 0.5 \, L_0 \; (1 + \cos 2\pi \, \upsilon \, Bt/T) \tag{83}$$

where L is the radiance at the center of the fringe pattern, L_0 is the radiance on the entrance port of the interferometer, υ is the wavenumber of the incident flux ($\upsilon = 1/\lambda$) in cm^{-1}, $B/2$ is the displacement of the movable mirror in the time interval T, or sweep time, and t is the time elapsed from the beginning of a sweep (see figure 25). $Bt/2T$ is the displacement, x, of the mirror at time t. Equation (83) shows that the frequency of the signal from the detector is related to the wavenumber, υ, of the incident flux and the mirror velocity, $B/2T$.

Since the difference in path length is twice the mirror displacement, we can write

$$F_\upsilon = 2 \cdot \upsilon \cdot B/2T = \upsilon B/T \tag{84}$$

where F_υ is the frequency of the signal from the detector. Thus for flux of any given wavelength λ, the frequency F_υ of the signal from the detector is directly related to mirror velocity.

Equations (83) and (84) can be derived also by considering the doppler shift of the frequency of the incident flux at mirror M_1, which will then beat with the flux from the stationary mirror when the two beams are combined. The two explanations of the effect are completely compatible, and lead to the same results.

The explanation given above is somewhat simplified, since perfect mirrors and perfect beamsplitters do not exist, and polarization effects cannot be neglected. However, the explanation is qualitatively correct, and equation (84) is rigorously correct. With real materials it is generally not possible to make the two beams reaching the detector exactly equal. The result is that there is uniform radiance, equal to the difference in the radiance from the two beams, superimposed on the fringe pattern. Since ac amplification of the signal from the detector is employed, the signal from this non-varying flux is not amplified and is essentially lost. The result is that there is an instrument calibration factor, η, that must be inserted into equation (83) when dealing with real materials.

$$L = \eta \, 0.5 \, L_0 \; (1 + \cos 2\pi \, \upsilon Bt/T) \tag{85}$$

This instrument calibration factor is wavelength dependent, and includes corrections for absorption along the optical path as well as the flux lost due to failure of the beamsplitter to divide the incident beam into two equal parts, and effects due to polarization within the interferometer head.

When polychormatic flux is incident on the interferometer entrance port, the detector signal is not a single audio-frequency sine wave, but is made up of sinusoidal audio frequencies corresponding to the optical frequencies present in the incident polychromatic beam. If an ideal interferometer were used, the amplitude of the signal at each audio frequency F_υ would be related to the spectral radiance, L_λ, of the incident flux at the corresponding wave number, as indicated in equation (83). However, since a non-ideal interferometer is used, equation (85) applies, and η_λ must be evaluated for the interferometer for all wavelengths of interest. The output of the detector, plotted as a function of time, is what is known as an interferogram, or the Fourier transform of the radiant spectrum of the flux incident on the entrance port of the spectrometer, and can be reduced as explained earlier in this section.

In the interferometer spectrometer being discussed, the movable mirror, M_1, is mounted on the armature of an electromagnet, and is displaced by changing the dc current through the solenoid. Figure 24 is a diagram of the variation in mirror position with time.

The audio frequency range to which the incident radiation is heterodyned can be changed by varying the sweep velocity. For instance, if T is halved while B is kept the same, the resulting audio frequency (for a given monochromatic input) will double.

The capability of a practical instrument to resolve two neighboring frequencies is specified in terms of the smallest increment of wavelength, $\Delta\lambda$, which can be distinguished at the output (or alternatively, in terms of wavenumber, $\Delta\nu$). It can be shown that the upper limit of spectral resolution is a constant dependent only on the maximum internal retardation, B, according to $\Delta\nu = K/B$ where K is determined by the amount of refraction at the entrance aperture. For this interferometer, K = 1, approximately, so that $\Delta\nu = 1/B$. This limit is never realized in practice.

Since the interferometer looks at all component frequencies of the spectrum of interest all the time, instead of one small wavelength bandpass at a time as with conventional monochromators, it is apparent that the interferometer offers an advantage in its more efficient use of the scan time interval. This is called Fellgett's advantage [10].

Reference 11 discusses this advantage as follows: "A simple argument allows one to predict the order of magnitude of gain that can be expected. If with an exploring dispersive spectrometer it is desired to measure M spectral elements during time T, each element is observed during time T/M; with a spectrograph or a multiplex method, each element is observed during the whole time T. In the case where the fluctuations have a spectrum of uniform frequency and where the background noise is not increased by the simultaneous arrival of all spectral elements, the precision varies as the square root of the exploration time. The gain in sensitivity is therefore of the order of $\sqrt{M}$. Hence, in the infrared where photon noise is negligible compared with receiver noise, the spectroscopic method using Fourier transformations is the most powerful, no matter what may be the desired resolution, and is all the more interesting because the spectrum studied contains more spectral elements. This gain in sensitivity can be expressed in several ways:
    --the signal/noise ratio, s/n, can be multiplied by $\sqrt{M}$ if the duration of the measurement is the same as in the classical method:
    --for equal s/n, the duration of the measurement is divided by M;
    --finally, for a given s/n and measurement time, one can obtain an increase in resolution and thus treat some problems inaccessible by any other method."

In general, interferometer spectrometers are run as dc systems: that is, the input is not chopped and rectified, but rather, the modulation of the signal onto the detector by the interferometer itself produces the frequency variation of the signal. The response time constant of the detector sets an upper bound to the rate T^{-1} at which the instrument may be scanned for any given maximum according to $F_\nu = \nu B/T$. Problems of detector drift and of time variation of the target radiation set a lower bound. In general, it is found that optimum scan rates fall within the range of 0.5 to 8 sec.$^{-1}$.

On the other hand, one classical method of achieving increased sensitivity is to scan more slowly, i.e. to increase the system's time integration. Since this is impractical with this interferometer spectrometer, a special purpose time averaging computer has been designed (called a "Coadder") which samples the input interferogram repeatedly, at a rate which, for meaningful results, should be more than twice the maximum frequency present in the signal. The samples are sequentially digitized and stored in the core memory. Each series of samples is initiated by a triggering pulse supplied by the interferometer at the beginning of each interferogram. Therefore, the samples from successive interferograms correspond precisely in time and their levels are digitally added in the memory, so that the coherent signal increases linearly in amplitude with the number of interferograms accumulated. On the other hand, due to the random character of the noise present at the input, it accumulates with the square root of the number of scans. The resultant gain in signal to noise is thus $\sqrt{N}$ where N is the number of times the same signal is sampled. For example, if the Coadder accumulates as

few as 16 interferograms, the s/n will be increased by a factor of four.

The Coadder memory contains 1024 words, so that a maximum of 1024 samples may be stored. Each sample is digitized by an 8 bit analog to digital converter that is set to accept a maximum signal of 9 volts peak to peak. Since the capacity of each word in the memory is 16 bits, it is possible to co-add up to 256 interferograms with a 9 volt peak to peak component. Smaller amplitude interferograms, of course, may be co-added many more times.

In addition to improving the signal quality of interferograms, the Coadder lends a greater dimension of versatility to the basic interferometer spectrometer system. For example, the SUBTRACT function makes it possible to effectively eliminate unwanted background information whenever circumstances allow the background to be sampled in the absence of the desired source.

The interferometer has a size advantage over comparably sensitive dispersive instruments.

Due to the use of a large aperture hole rather than of flux-limiting slits it intercepts more spectral power from the target. In particular, if the target fills the field of view, the collected spectral power P is independent of the distance of the source and is a function only of the aperture stop and focal ratio of the optical system. This function is called throughput (θ) and is equal to the product of acceptance solid angle (Ω) and the aperture stop area (A), $\theta = A\Omega$.

In the interferometer spectrometer the aperture stop is typically about 200mm^2 whereas the aperture stop (slit area) of a comparable dispersive instrument would be on the order 2mm^2. Moreover, the interferometer's focal ratio is f/3.8, rather fast for a dispersive instrument, which would be typically f/6, a factor in solid angle of about 3. Together, these give the interferometer an advantage in throughput (and hence in signal to noise ratio) of from 100 to 1000. This, added to the above discussed advantage (in the instrument noise limited case) of $\sqrt{M}$ where M is the number of resolution elements, usually on the order of 100, will yield an overall advantage of 10^3 to 10^4 in signal to noise ratio in one scan over a comparable dispersive instrument. When the Coadder is used, further increase in signal to noise ratio of $\sqrt{N}$ where N is the number of scans co-added, and may be greater than 10^3 itself in some instances, will yield total advantage of 10^4 to 10^6.

The interferometer spectrometer appears to have many advantages for use in relative radiometric measurements.

(a) A markedly increased signal/noise ratio allowing either (1) better resolution at a given wavelength or (2) measurements at longer wavelengths (compared to conventional spectrometers) or (3) shorter total measurement time for the same signal to noise ratio.

(b) Small, compact, and portable optical head.

(c) The facility in the Coadder (which is a small computer) to subtract the background for the desired signal. For instance, the interferometer has the capability of taking the following readings over the 4-40 micron region at a rate of four per <u>second.</u> (1) Radiance Spectra of the source (L_s), (2) background Spectra of the source (L_{bs}), (3) radiance Spectra of the reflected flux from a sample (L_R), (4) background Spectra of the reflected flux (L_{bR}).

These readings can then be stored as $L_I = L_s - L_{bs}$ and $L = L_R - L_{bR}$ in the memory of the Coadder. These numbers could then be divided and the ratio could be plotted after the data were analyzed by a wave analyzer or by taking the inverse transform of the Fourier spectrum on the computer. When using the wave analyzer the total measurement time, including data reduction, would be on the order of 15 minutes for the 4-40 micron region. Similar time advantages would be gained for the 40 to 500 micron region. The short time between measurement of the incident signal and reflected signal would eliminate essentially all effects of source and background instability.

(d) The ability to use many optical heads with one Coadder-analyzer setup will greatly reduce the per unit cost in laboratories with the need for more than one spectrometer.

In view of the above it is possible to foresee an ellipsoidal mirror reflectometer capable of the

following:

   (a) Absolute reflectance (1) directional hemispherical, (2) bi-directional, (3) specular component, (4) diffuse component and (5) directional annular cone.

   (b) Absolute transmittance; same adjectives as applied for reflectance.

   (c) Absolute reflectance and absolute transmittance over the 0.25 to 500-micron range.

   (d) The angle of incidence for the reflectance measurements would cover the range from 6° off normal out to 80° off normal.

   (e) Absolute reflectance and absolute transmittance of a sample as a function of sample temperature from $5\,^\circ$K to $1400\,^\circ$K.

   (f) The instrument would be essentially a double-beam ratio-recording system. The entire data reduction would be done in the instrument and the chart would plot absolute reflectance or transmittance as a function of wavelength.

   (g) The reference specular standard could be directly calibrated on a multiple reflection specular reflectometer incorporated in an optional optical path of the system. This would enable the measurement of specular reflection to at least a tenth of one percent.

   (h) The instrument could directly calculate α/ϵ from the spectral data, given the necessary parameters, and give α/ϵ as a numerical output.

   (i) The instrument data reduction program can take into account all the relevent system corrections outlined previously.

   (j) The reflectance-transmittance optics could be housed in a vacuum chamber so that data could be taken in a vacuum or a controlled atmosphere.

   (k) The effect of UV degradation of spectral reflectance of common NASA materials could be measured. This measurement could be made while the degradation was occurring; and in any case, the sample would remain in vacuum between the time of degradation and the time of reflectance or transmittance measurements.

   (l) The effect of roughness on the directional hemispherical reflectance and on the distribution of the reflected flux could be studied.

4.1 Test of the Interferometer Spectrometer

   In order to establish the problems involved in adapting the interferometer for accurate radiometric measurements, personnel from NBS performed the following tests on the equipment at Block Engineering, Inc.:

   (a) The areal and angular sensitivity of the optical head was measured.

   (b) A check of the linearity of the system was performed.

   (c) The system was used with a multiple reflection specular reflectometer to measure reflectance of rhodium, gold, and aluminum mirrors.

   (d) The sulfur coated averaging device was tested in an effort to eliminate the areal and angular sensitivity of the optical head.

   The main results of these tests are presented in figure 25 and 26. Part A of figure 25 represents the Fourier transform of the 4-40 micron spectrum as printed by a digital computer. The upper curve in figure 26 Part A was reduced from this particular transform. Each data spectrum taken has an associated transform, such as this one. The large peak in the center corresponds to zero retardation, where all wavelengths are in phase at the detector. The vertical axis corresponds to relative energy at the detector, while the horizontal axis is the displacement of the mirror or time (which are exactly related).

   Part B of figure 25 illustrates the experimental setup for making the remaining measurements. Path A of Part B illustrates the instrumentation for the angular and areal sensitivity measurements. This arrangement is much the same as that used in the study of averaging devices. The optical head of the interferometer was mounted on a milling head which moved $8''$ in the x and y directions and was free to rotate in the x-y plane. Part C gives the results of the angular sensitivity test at 5 microns, which indicates a marked angular sensitivity, much the same as that of the detectors
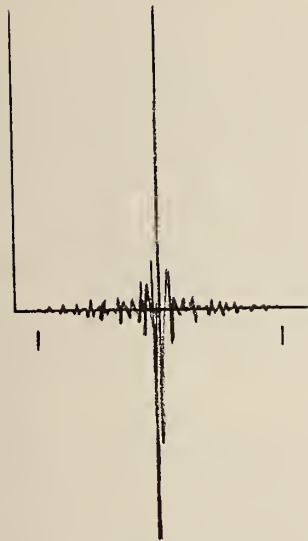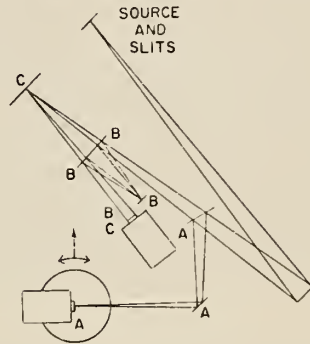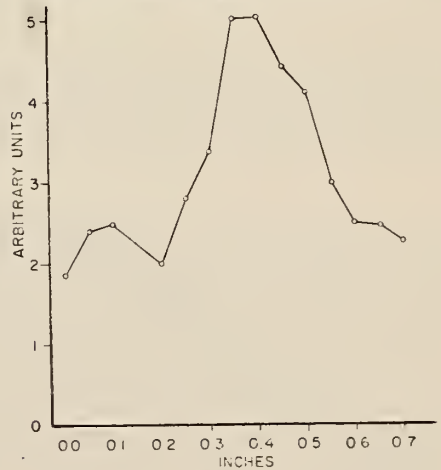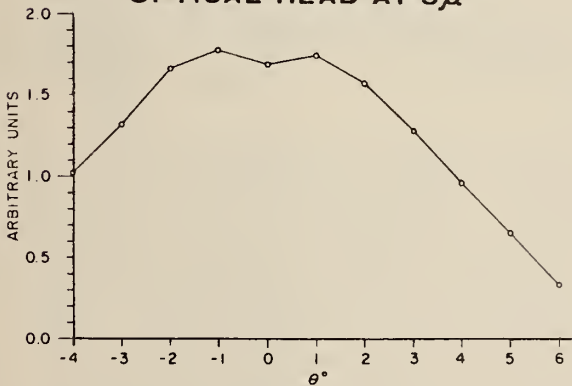
Figure 25. A. Interferogram. B. Optical Arrangement for tests of Interferometer Spectrometer and Reflectance of Gold. C. Angular Sensitivity of Interferometer Spectrometer. D. Areal Sensitivity of Interferometer Spectrometer

Figure 26. Reflectance of Gold. A. Spectra of Incident and
Reflected flux. B. Reflectance of Gold

50

illustrated earlier in this report (of course the variations in the sensitivity are caused by different effects). Further data at several other wavelengths demonstrated equivalent angular sensitivity.

Part D of figure 25 illustrates the areal sensitivity at 5μ and was representative of areal sensitivity at other wavelengths.

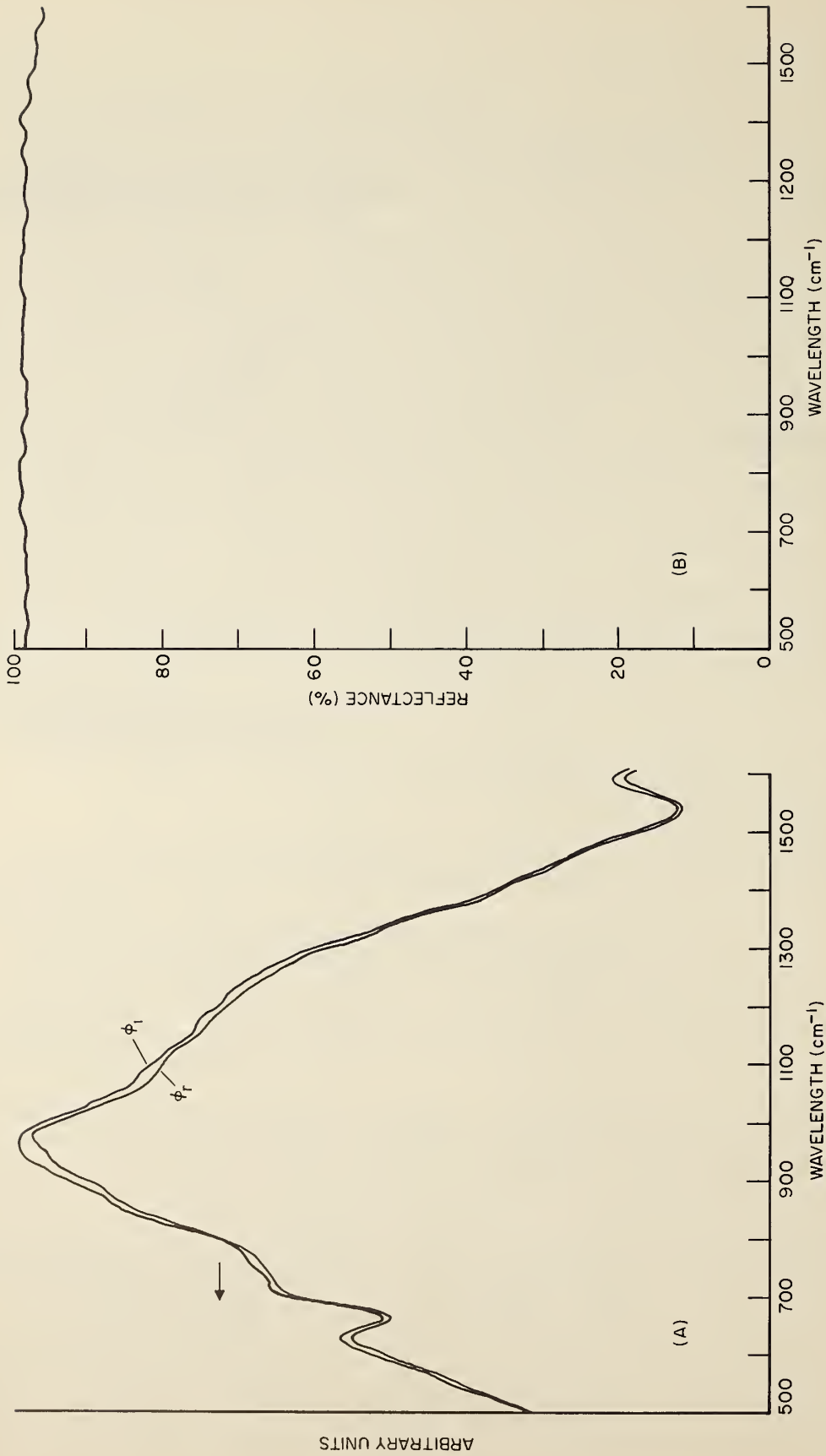In view of the demonstrated angular and areal sensitivity of the interferometer it was decided to use an averaging device over the entrance port to the sphere. However, since the interferometer is a dc system, the background radiation (collected by the sphere from 2π sr of the room and due to its own emission) was not separable from that received from the small area, small solid angle source. Thus the background completely masked the signal. There are two approaches to eliminating this problem (a) chopping the source and synchronously amplifying the signal and (b) cooling the sphere and directing it only at the source (i. e. with cold baffles). The second approach is not very feasible from a practical standpoint and furthermore, unless the detector is cooled to the same temperature, no significant advantage will be gained. This method was tried with only marginal results. Synchronous amplification techniques are therefore recommended. These cause problems (however, they are solvable) since the interferogram is essentially a chopped signal, with a different chopping rate for each wavelength.

The use of an averaging sphere could give rise to another problem, due to interreflections between the sphere and interferometer. The flux that is reflected from the fixed mirror M_1 back into the averaging sphere will be scattered in the sphere and will be indistinguishable from the flux intially incident on the entrance aperture of the sphere. The net effect will be to add a small increment, $\Delta\Phi_0$, to the initially incident flux, $\Phi_0 H$, reaching the detector, where H is the efficiency of the sphere. The size of this increment, again assuming an interferometer with a perfect beamsplitter and non-absorbing mirrors will be

$$\Delta\Phi = (\Phi_0 \, \frac{HH'}{4}) \, / \, (1 + \frac{H'}{2}) \tag{86}$$

where H' is the back reflection efficiency of the sphere. It should be noted that $H'>H$ in every case, because the detector aperture of the sphere will always view all of the area of the sphere wall directly illuminated by the back reflected beam, but none of the area illuminated by the beam incident through the entrance aperture.

The portion $\Phi_0 H/4$ of the flux that is reflected by the moving mirror M_2 back into the averaging sphere will have undergone a doppler shift in frequency of $4\pi V/\lambda$, where V is the velocity of the moving mirror (B/2T in equation 84). A fraction H' of this flux will return to the interferometer and one fourth of it will reach the detector by way of the fixed mirror M_1, where it will beat with the unshifted flux to produce a signal of frequency F_v, that will add an increment $\Delta'\Phi_0$ to the primary signal. The fourth of the back reflected flux by way of the moving mirror M_2 will undergo a second doppler shift in frequency of $4\pi V/\lambda$, and hence will beat with the flux that has undergone one doppler shift to produce a signal of frequency F_v, which will add an increment $\Delta''\Phi_0$ to the primary signal. It will also beat with the flux that has undergone no doppler shift to produce a signal of frequency $2F_v$, which will appear to be caused by flux Φ' of wavelength $\lambda/2$. The sizes of these various increments are given by the following equations.

$$\Delta'\Phi_0 = \Phi_0 \, HH'/16 \tag{87}$$

$$\Delta''\Phi_0 = \Phi_0 \, HH'/32 \tag{88}$$

$$\Phi' = \Phi_0 \, HH'/32 \tag{89}$$

The phase relationships of the increments $\Delta'\Phi_0$ and $\Delta''\Phi_0$ to the primary signal are not known, hence they may either increase or decrease it. In any case H' will probably be less than 0.1, and these errors are not serious. They can be evaluated experimentally.

Figure 26 illustrates the reflectance of gold mirror in the 7 to 20 micron range. The wavelength range of the measurement was limited because of atmospheric absorption, poor throughput from the source, a mistake in printing out the data, and low signal to noise at the longest wavelengths (i. e. 40 microns). All of these deficiencies can be corrected in future measurements. The measurement of the specular reflectance was accomplished with a Strong reflectometer, with signals received for 1 and 3 reflections, see Path B, figure 25, part B. No averaging device was used to eliminate the angular and areal sensitivity previously illustrated. Instead, the entrance optics of the interferometer head were placed in the field of the flux, thus hoping to eliminate areal sensitivity and reduce the angular sensitivity. Each measurement scanned the 6-40 micron spectrum in 1/4 of a second. Spectral scans were taken and coherently added and accumulated in the co-adder until the signal to noise ratio allowed recording of decent spectra. This took around 150 scans or about 45 seconds for each set of usable 6-40μm spectra.

The two resulting signals for each measurement are shown in part A of figure 26, with the characteristic CO_2 absorption band showing up as a dip on the curves around 15 microns. The ratio of these two curves is the square of the reflectance of the two mirrors, if the two mirrors have equal reflectance. Our earlier work showed that the reflectance of the two mirrors was the same. Further, it should be noted that no effort was made to substract the background from the signals in part A of figure 26. However, it was established that the background was the same for both signals and on the order of 1% of the signal. Thus the background does not cause significant errors in this measurement.

Part B of figure 26 illustrates the reflectance of the gold mirror as reduced from the spectra in part A of the same figure. This reduction was carried out on a digital computer. It is also obvious that it would be impossible to reduce these data by hand, since in many cases, the computer plotted lines of part A appear to lie on top of each other. Table IX is the digital readout used by the computer to plot part B of figure 26. It illustrates the spread in the data. Further from Table IX and figure 26, part B, it can be seen that a straight line fit to the data (assuming the randomness in the data is caused by noise) falls about 0.3% below the data in reference 12. Furthermore, these mirrors were prepared in a 10^{-6} or 10^{-6} torr atmosphere, and reference 12 indicates that such mirrors should be about 0.3% lower than the reflectance of the high-vacuum gold mirrors described in reference 12. Thus it is apparent that additional co-adding and/or a least squares fit to the data would yield very high accuracy data (on the order of that reported in reference 12).

4.2 Conclusions Drawn from Preliminary Tests

The results of experimental tests and analysis of the scanning interferometric spectrometer indicate that this technique is well adaptable to the relative measurement of flux in the 4-40 micron range, and furthermore the experimental results imply the usefulness of various interferometric techniques from 0.25μm to 500μm. In addition, these tests imply that the measurement accuracy can be 2 in the third significant figure and possibly with some additional design efforts, better than 5 in the fourth significant figure. One other advantage of the instrument is its extremely short measurement time; i. e., it takes 3 minutes to measure and reduce the specular reflectance data for the 4-40μm region. This could provide an immense saving to all NASA data measuring programs; in fact, it should cut data taking costs per sample by a factor of about 25. In addition, it may allow the taking of 25 times as much data per instrument facility with double the wavelength range of present instrumentation.

Furthermore, the existing experimental concepts (i. e., integrating sphere, heated cavity, ellipsoid, and paraboloid reflectometer) appear to be compatible with this instrument when modified as proposed. This technique appears uniquely applicable to measurement of spectral intensity of solar simulators, emittance, and in situ reflectance and emittance measurement, to mention only a few of the other applications.

5 Roughness Summary

Recent publications in the literature have tended to cast doubt upon the validity of the assumption that the flux reflected from a roughened surface (under directional irradiation) can be described as a combination of diffusely and specularly reflected flux. Thus it is necessary to establish a new model of reflectance from roughened metals for those heat transfer calculations where the directional properties do not average out because of multiple reflections in a system. Such cases occur most often in thermal control of spacecraft with louvers, fins, and grooves. From the literature data and a paper published under this contract it appears (a) that the specular–diffuse assumption may be utilized for $\sigma/\lambda \leq 1/4\pi \cos\theta_s$ and (b) that it may be possible to empirically describe the directional characteristics of $\rho(\theta,\varphi;2\pi)$ for rough metallic surfaces for which $\sigma/\lambda \gg 1/4\pi \cos\theta_s$. However, this empirical description awaits literature data on the bi-directional reflectance for high angles of incidence both in and out of the plane of incidence. Thus, it appears possible to describe the directional characteristics of a sample by measuring a minimum of three data points for each sample at each wavelength of interest, (a) the ratio of the flux reflected normal to the surface to that reflected in the specular direction, $\Phi(0)/\Phi(\theta_s)$, (b) the directional hemispherical reflectance, $\rho(\theta,\varphi;2\pi)$, and (c) the reflection function for specular reflectance, $f(\theta,\pi;\theta_s,0)$. The ratio $\Phi(0)/\Phi(\theta_s)$ can be expressed in terms of the radiance ratio, $L(0)/L(\theta_s)$, as follows:

$$\frac{\Phi(0)}{\Phi(\theta_s)} = \frac{L(0)\ d\omega'}{L(\theta_s)\ \cos\theta_s\ d\omega_s} \tag{90}$$

where ω_s and θ_s refer to the solid angle of collection at the specular peak, and ω' refers to the solid angle of collection for the normally reflected flux.

Better correlation was shown between experimental and theoretical data on the total specular reflectance of roughened metals when using the proposed method of data reduction than when using conventional methods.

6 Appendix A

This section lists the publications and talks resulting from work on this contract.

1. Dunn, S. Thomas,   Application of sulfur coatings to integrating spheres, Applied Optics 4, 877, (July 1965).

2. Clark, H. E., On avoiding errors from stray radiation in measuring the spectral emittance of diffusely reflecting specimens, Applied Optics 4, 1356, (October 1965).

3. Dunn, S. Thomas, Flux averaging devices for the infrared, NBS Technical Note 279.

4. Dunn, S. Thomas, Richmond, J. C., and Wiebelt, J. A., Ellipsoidal mirror reflectometer, NBS Journal of Research C, Engineering and Instrumentation 70C, No. 2, 75-88, (April–June 1966).

5. Clark, Howard E. and Moore, Dwight G., A rotating cylinder method for measuring normal spectral emittance of ceramic oxide specimens from 1200° to $1600\ ^\circ K$, NBS Journal of Research A, Chemistry and Physics 70A, 393, (Sept. –Oct. 1966).

6. Dunn, S. Thomas., Design and analysis of an ellipsoidal mirror reflectometer, May 1965 Ph. D. Thesis, Oklahoma State University. This work was done at NBS under the sponsorship of first the Air Force and then NASA. It is available from University Microfilms, Inc.

7. Dunn, S. Thomas, Parmer, J. F., and Richmond, J. C., Survey of infrared measurement techniques and computational methods in radiant heat transfer, Journal of Spacecraft and Rockets, 961-975, (July 1966).

8. Accurate reflectance measurements: an ellipsoidal mirror reflectometer, NBS Technical News Bulletin, STR-3186 (June 1965).

9. Geist, J., Coleman, T., and Dunn, S. Thomas, Use of the Interferometer Spectrometer for Radiometric Measurements, presented at the Philadelphia meeting of the Optical Society of America, (October 6-8, 1965).

10. Kelly, F. J. and Moore, D. G., A test of analytical expressions for the thermal emissivity of shallow cylindrical cavities, Applied Optics $\underline{4}$, 31-40, (1965). Work done under Marshall Center Contract.

11. Dunn, S. Thomas, A possible approach to evaluation of flux scattered by roughened surfaces, AIAA Paper No. 66-20.

12. Dunn, S. Thomas, Some Methods Used for Thermal Radiation Properties Measurement at the National Bureau of Standards, presented at a Colloquium at West Virginia University, (May 17, 1965).

13. Dunn, S. Thomas, Ellipsoidal Mirror Reflectometer, Southern California Thermal Radiation Group, (August 3, 1965).

14. Dunn, S. Thomas, Ellipsoidal Mirror Reflectometer, San Francisco Section of O.S.A., (July 27, 1965).

7 Appendix B

7.1 Specular Reference Samples for the Ellipsoidal Reflectometer

This section describes a simple, but accurate, infrared specular reflectometer. In previous infrared specular reflectometers, very precise alignment of the optics was necessary to insure that the detector viewed different reflected signals indentically [13, 14]. The specular reflectometer used in this work to measure the reflectance of the calibration mirrors is illustrated in figure 27. The sulfur-coated diffusing sphere described in Appendix C was used to average the monochromatic flux from the Globar for two different signals, one being the flux that is reflected once by each of the sample mirros, and the other being the unreflected incident flux. The use of the sulfur-coated diffusing sphere reduces the required precision of optical alignment, since the "images" of the two signals need not be the same size, nor on exactly the same area of the sphere wall.

In the reflectometer, the path length for the two measurements is different, so that it is necessary either to operate in a non-absorbing atmosphere, or at wavelengths where atmospheric absorption can be neglected. In this case, the reflectance was measured at the same wavelengths and with the same band passes as were used with the ellipsoidal mirror reflectometer. Due to the longer path length (approximately 1 1/2 inches longer), the signal reflected by the two sample mirrors has an image area on the sphere wall about 2.1 times that of the unreflected signal. For each measurement, the small unreflected image of the incident flux was visually centered on the large image of the double reflected flux. This insured accurate measurement of both signals.

The ratio of the twice reflected flux to the incident flux is equal to the product of the reflectances of the two sample mirrors. If the reflectances of the two mirrors can be considered equal, then the ratio is equal to the square of the reflectance of the mirrors. This procedure increases the accuracy of the reflectance measurement, since the expected error in the measured ratio is the same whether one or two reflections are involved (i. e., with two reflections the final error is approximately the square root of the error in the measurement of the ratio).

The two sets of calibration mirrors were selected as follows: (a) Aluminum mirrors: a set of 12 optically polished 1/2 inch by 1/4 inch glass samples were prepared. The aluminum coating was then vacuum deposited on all of the samples at the same time, to an opaque thickness, in a time of

Table IX Reflectance Gold Mirror Digital Readout

X*	ρ	X*	ρ	X*	ρ	X*	ρ
4140	0.9877	4217	0.9907	4276	0.9844	4355	0.9882
4141	.9884	4220	.9928	4277	.9859	4356	.9887
4142	.9887	4221	.9945	4300	.9881	4357	.9896
4143	.9887	4222	.9955	4301	.9905	4360	.9905
4144	.9888	4223	.9954	4302	.9924	4361	.9909
4145	.9889	4224	.9946	4303	.9935	4362	.9905
4146	.9892	4225	.9933	4304	.9936	4363	.9894
4147	.9893	4226	.9919	4305	.9929	4364	.9877
4150	.9890	4227	.9909	4306	.9917	4365	.9860
4151	.9881	4230	.9906	4307	.9907	4366	.9845
4152	.9869	4231	.9910	4310	.9901	4367	.9837
4153	.9855	4232	.9919	4311	.9900	4370	.9836
4154	.9844	4233	.9931	4312	.9903	4371	.9841
4155	.9838	4234	.9941	4313	.9908	4372	.9851
4156	.9840	4235	.9949	4314	.9912	4373	.9862
4157	.9851	4236	.9953	4315	.9912	4374	.9872
4160	.9866	4237	.9954	4316	.9908	4375	.9878
4161	.9881	4240	.9953	4317	.9903	4376	.9880
4162	.9891	4241	.9950	4320	.9899	4377	.9879
4163	.9893	4242	.9946	4321	.9897	4400	.9875
4164	.9888	4243	.9939	4322	.9897	4401	.9870
4165	.9877	4244	.9928	4323	.9899	4402	.9864
4166	.9864	4245	.9913	4324	.9900	4403	.9857
4167	.9853	4246	.9897	4325	.9898	4404	.9850
4170	.9847	4247	.9881	4326	.9892	4405	.9845
4171	.9848	4250	.9869	4327	.9884	4406	.9842
4172	.9854	4251	.9865	4330	.9877	4407	.9844
4173	.9863	4252	.9870	4331	.9874	4410	.9852
4174	.9873	4253	.9883	4332	.9877	4411	.9866
4175	.9879	4254	.9901	4333	.9887	4412	.9883
4176	.9882	4255	.9917	4334	.9901	4413	.9900
4177	.9882	4256	.9926	4335	.9917	4414	.9913
4200	.9880	4257	.9926	4336	.9929	4415	.9919
4201	.9878	4260	.9914	4337	.9937	4416	.9915
4202	.9877	4261	.9894	4340	.9939	4417	.9902
4203	.9880	4262	.9873	4341	.9937	4420	.9883
4204	.9886	4263	.9856	4342	.9934	4421	.9862
4205	.9892	4264	.9848	4343	.9932	4422	.9845
4206	.9895	4265	.9849	4344	.9934	4423	.9839
4207	.9892	4266	.9857	4345	.9936	4424	.9844
4210	.9885	4267	.9867	4346	.9939	4425	.9863
4211	.9875	4270	.9874	4347	.9937	4426	.9890
4212	.9865	4271	.9874	4350	.9931	4427	.9920
4213	.9859	4272	.9867	4351	.9919	4430	.9943
4214	.9861	4273	.9855	4352	.9905	4431	.9952
4215	.9870	4274	.9844	4353	.9892	4432	.9944
4216	.9886	4275	.9839	4354	.9884	4433	.9918
						4434	.9881

*X is inversely related to wavelength, with 4140 being about 22 microns and 4434 about 7 microns.

one second. This should give essentially the same values for the reflectance that Bennett, et al. [15] report for their ultra-high-vacuum coatings of aluminum. Hass [16] indicates that the fast evaporation times at normal vacuums yield the same reflectance values as those measured for the ultra-high vacuum coatings. The aluminum used for the coatings was 99.999% pure. (b) Gold mirrors: a set of 12 optically polished 1/2 inch by 1/4 inch glass samples were prepared. The gold was vapor-plated on all of the samples at the same time, over a chromium substate (to increase its mechanical durability), in accordance with standard procedures. At the time the specimens were coated, it was not known that the infrared reflectance of gold (like that of aluminum) varies significantly with evaporation techniques [12]; hence no effort was made to control the evaporation time to ensure a coating of the highest possible reflectance.

Four mirrors were visually selected from each set of 12 to form the two sets of calibration mirrors, as follows:
(1) They were examined with an 8-power microscope with grazing illumination for surface irregularities, and
(2) They were examined for opacity and scatter when illuminated by the 0.632μm line of a helium-neon laser.

The aluminum and gold mirrors both exhibited no visible surface irregularities under examination with the microscope, and they were both opaque to the 0.632μm laser line. Qualitatively, the aluminum and gold mirrors both seemed to scatter the 0.632μm laser beam about the same. No quantitative value of scatter was obtained.

The reflectance of the two sets of calibration mirrors was then measured in the following manner:

Six reflectance measurements were made; 2 each of three combinations of pairs from each set of the mirrors. This does not exhaust the six unique pairs from a set of four, but does allow intercomparison of all of the mirrors to establish that their reflectances are indeed equal, as would be expected for samples prepared at the same time.

Table X gives the results for aluminum. Each reflectance value is the square root of the ratio of the two signals. Further, each of the six readings represents a completely separate measurement, taken on different days and after realignment of the optics and repositioning of the samples; therefore, these measurements should be independent and errors should be random. The results for reflectance of the different pairs of mirrors indicate that, within the precision of measurement, there is no variation in reflectance among the samples in this set. The arithmetic average and the standard deviation of the measurements are reported in Table X and are compared to the data (accurate to ±.001 reflectance units) reported by Bennett, et al. [15]. The agreement is excellent beyond three microns; the tendency of the measured reflectance to be lower than Bennett's values at the shorter wavelengths is attributed to differences in optical finish and oxide formation on or in the coating. The reflectance values reported in this work are higher than the reflectance values reported for standard aluminum coatings throughout the 1.5 to 7.0 micron range [16]. Furthermore, when these values are compared to other values in the literature, the band width accepted for measurement at 1.5 microns is very important, since aluminum's reflectance is changing quite rapidly below 2.0 microns. Due to this, the wide band (about 0.18 microns in width) values reported for 1.5 microns in this work will be lower than narrow band literature values for a coating with the same spectral reflectance.

The results for the gold mirrors shown in Table XI are qualitatively similar to the results for aluminum mirrors. That is, the reflectances of all four gold mirrors are equal, and the reported reflectances tend to be lower than the best lieterature values at the shorter wavelengths. Since the gold mirrors were prepared without special attention being paid to the evaporation time or the level of vacuum, exact agreement with the literature was not expected. The recent work of J. Bennett[12] indicates that ultra-high vacuum techniques increase the reflectance of gold by 1 percent in the infrared.

Table XII gives the average value of reflectance for a set of four rhodium mirrors purchased from Evaporated Metal Films Corp., Ithaca, New York, These mirrors are also 1/2 inch by 1/4 inch, and

Table X Reflectance of Aluminum

λ	ρ_{1-2}*	ρ_{1-2}	ρ_{1-3}	ρ_{1-3}	ρ_{2-4}	ρ_{2-4}	Average	Standard Deviation	Best Literature Values[15]
1.5	0.961+	0.961−	0.962	0.960−	0.962	0.959	0.9608	0.0012	0.9742
2.0	.975	.975+	.972	.975−	.976	.972	.9742	.0017	.9779
2.5	.977−	.976+	.974	.976	.975	.976	.9757	.0010	.9794
3.5	.985+	.983	.984	.981	.982	.982	.9828	.0005	.9816
4.5	.985	.985+	.982	.984−	.984−	.984	.9840	.0011	.9835
5.5	.985	.986	.983	.985+	.986−	.986+	.9852	.0012	.9850
6.5	.985	.985	.983	.985	.986	.987+	.9852	.0013	.9861
7.0	.988	.988−	.984	.985+	.986	.987+	.9863	.0017	.9866

*The subscripts on the symbol "ρ" for reflectance indicate the particular mirrors used for the measurement.

$$\text{Average} = \frac{1}{n} \sum_1^N \rho$$

$$\text{Standard deviation} = \left[\frac{1}{(n-1)} \sum_1^N (\rho - \bar{\rho})^2 \right]^{\frac{1}{2}}$$

exhibit reflectances very close to literature values at the longer wavelengths and much lower at the shorter wavelengths. Visual examination of these samples with the 0.632μm laser beam qualitatively indicated considerably more scatter than for the aluminum or gold mirrors.

The lower reflectance values at the short wavelengths reported in this work do not represent an instrumental error, since there is every reason to expect an increase in accuracy at the shorter wavelengths, where more energy is available for detection and the required precision of optical alignment is a minimum.

Since in the calibration of the ellipsoidal reflectometer these mirrors are used with several different angles of incidence (from $0°$ from the normal to $52°$ from the normal), the effect of changing the angle of incidence was studied. Within the accuracy of the measurements, no change of reflectance with angle of incidence was observed for the gold and aluminum mirrors (for incident angles up to $50°$).

7.2 Summary

The mirrors used for calibrating the ellipsoidal reflectometer, and later to be used as reference reflectance standards, have a reflectance that is known to ±0.0015 reflectance units, and do not vary in reflectance by more than −0.000 and +0.003 reflectance units with angle of incidence up to incident angles of $50°$.

The design of a very simple and accurate infrared specular reflectometer, with an accuracy of at least ±0.0015 reflectance units has been described. The use of the sulfur-coated diffusing sphere in
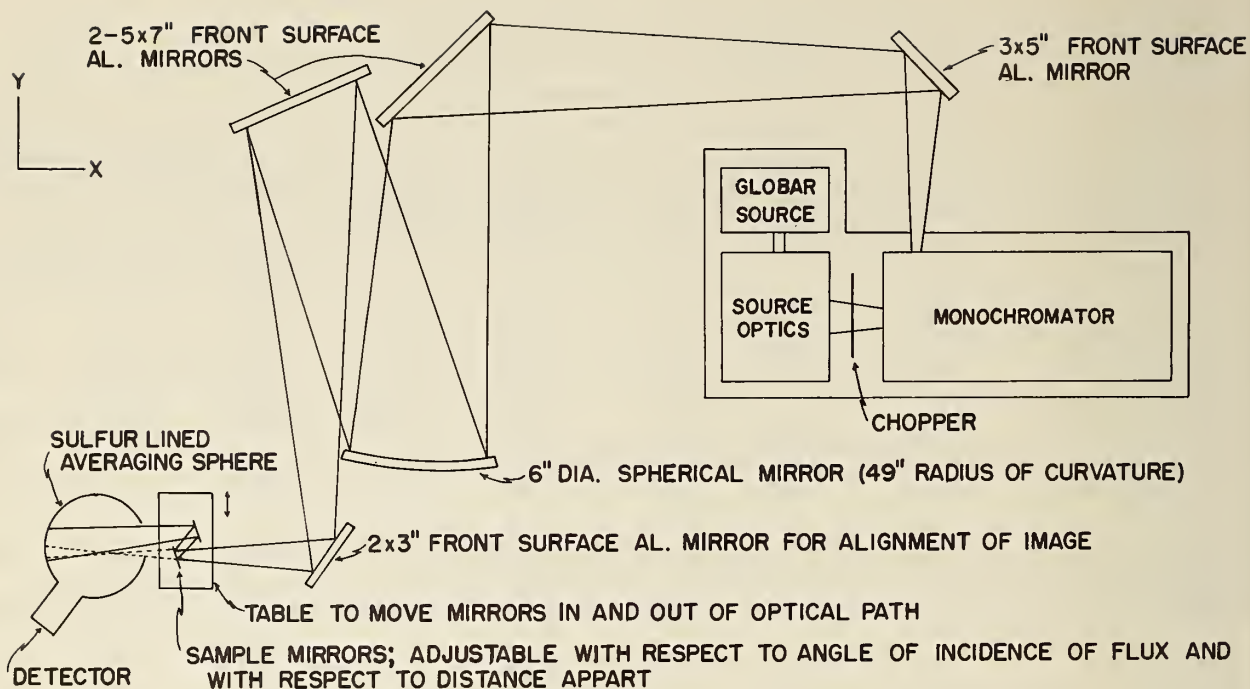
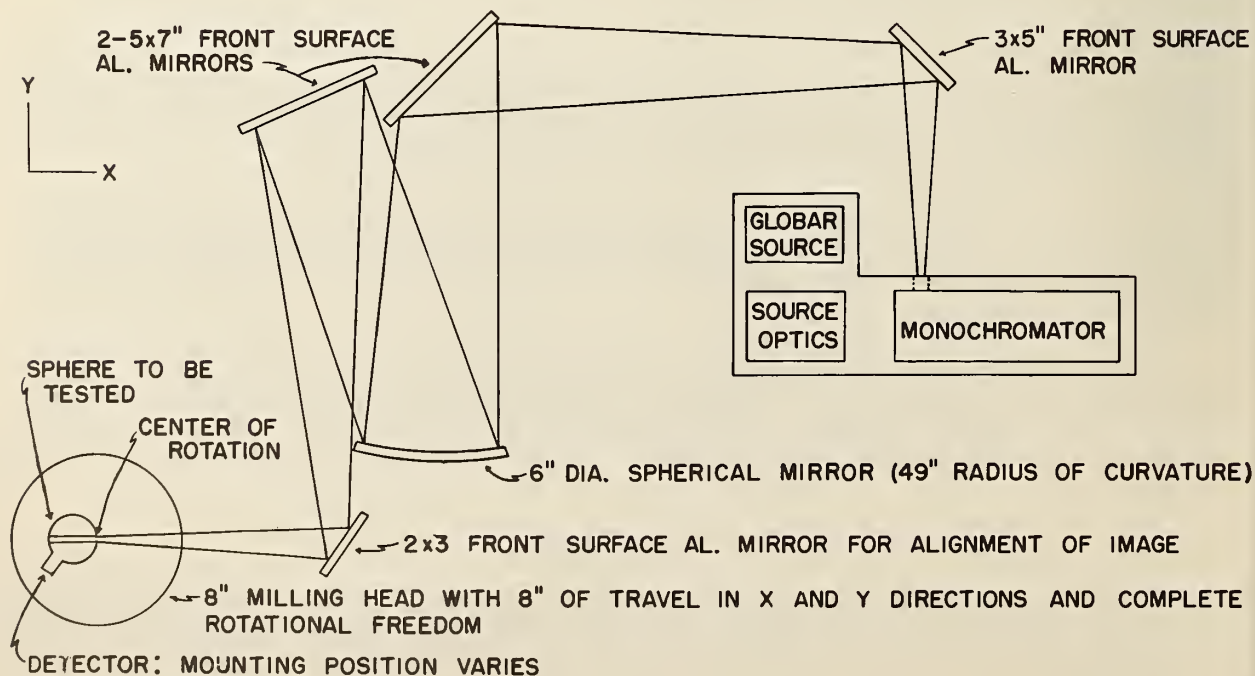Figure 27. Specular Reflectometer

Figure 28. Areal and Angular Sensitivity Test Equipment

Table XI Reflectance of Gold

λ	ρ_{1-2}*	ρ_{1-2}	ρ_{2-3}	ρ_{2-3}	ρ_{3-4}	ρ_{3-4}	ρ_{3-4}	Average	Standard Deviation	Literature Values [16]	Best Literature Values [12]
1.5	0.980	0.981	0.980	0.981	0.982	0.983	0.979	0.9809	0.0014	0.982	0.9806
2.0	.984	.984+	.984	.983	.983	.983+	.981	.9831	.0010	.983	.9914
2.5	.984	.986+	.986	.982	.984	.984	.984+	.9843	.0014	.983	.9922
3.5	.987	.987	.988	.987	.986	.987	.988	.9872	.0005	.983	.9934
4.5	.986+	.988	.987+	.988	.987	.986+	.987+	.9870	.0008	.983	.9938
5.5	.987	.989	.988+	.986	.985	.986−	.988	.9873	.0014	.983	.9938
6.5	.988−	.987+	.988	.987	.988+	.988		.9877	.0005	.983	.9939
7.0	.988	.987+	.988	.992	.989	.989		.9888	.0017	.984	.9939

*The subscripts on the symbol "ρ" for reflectance indicate the particular mirrors used for the measurements.

59

Table XII Reflectance of Rhodium

λ	Average	Literature Values [17]
1. 5	0. 8383	0. 882
2. 0	. 8850	. 905
2. 5	. 9104	. 915
3. 5	. 9339	. 932
4. 5	. 9428	. 942
5. 5	. 9470	. 946
6. 5	. 9474	. 950
7. 0	. 9510	. 953

front of the detector considerably reduces the inherent problems of optical alignment, and detector areal sensitivity. The design illustrated in figure 27 is not the best design, but was the most convenient for this work. It would be a better instrument if an odd number of reflections were used and the path length kept constant. The sulfur sphere (with a thermocouple detector and SiC source) should easily extend the use of the Bennett and Koehler [14] specular reflectometer to 8 microns. A 1, 3, 5 reflection specular reflectometer which will utilize the sulfur coated averaging device discussed in the next section, is now being designed.

8. Appendix C Flux Averaging Devices for the Infrared

8. 1 Introduction

From the turn of the century, large area thermopiles have been used as infrared radiation detectors for large area beams. It is astounding that for all this time the general practice has been to use these detectors as though they were areally insensitive.[11]

Only recently have experimental measurements been reported that confirm the fallacy of this assumption [18, 19 and 20]. These data show tremendous variations in angular[12] and areal sensitivity.

The data obtained on the angular and areal sensitivity of detectors indicate that a flux-averaging device would be required for use with any of the available large-area infrared detectors. The function of such a device is to distribute the available flux uniformly over the sensitive area of the detector, regardless of image size, shape, or intensity distribution. Any averaging device will, of course, reduce the efficiency of a detector system, because some of the incident flux is absorbed by the diffuser, and some is scattered away from the sensitive area and is lost. In general, the losses in a diffuser tend to increase with an increase in its effectiveness as a diffuser.

The literature provides several references to flux-averaging devices. One is the work of Bennett and Koehler [14], who used a small integrating sphere to average the incident radiation over a photo-

---

[11] Areal sensitivity is defined as variation in response of the detector with change in the irradiated area of the sensitive area.

[12] Angular sensitivity is defined as the variation in response of the detector with angle of incidence (with respect to the sensitive area of the detector) of the measured flux.

multiplier detector. Another is the work of Ronzhin [21], who tried light ducts and integrating spheres to average radiation over the sensitive area of photomultiplier. However, these references offer solutions only in the ultraviolet, visible, and near infrared portions of the spectrum, where good integrating sphere coatings are available. In the infrared, no one has yet shown that satisfactory integrating sphere coatings exist for use beyond 4 microns. Reference 19 also illustrates the use of several similar averaging devices.

Three different types of diffusing devices were investigated. They are listed in estimated order of increasing degree of diffusion as: (1) a diffusing screen placed directly over the detector, (2) a light duct with diffusing walls or a diffusing surface in the system, and (3) an averaging sphere[13] coated with a material having high reflectance in the infrared and sufficient diffusion to permit it to be used as an averaging device. This last device was the only one that proved successful.

To establish the usefulness of the various averaging devices, three tests were devised, as follows:

Test A – Areal Sensitivity: this test was designed to illustrate the required precision of incident image placement for comparing beams of nearly the same image area. The general optical system for this and the following tests is shown schematically in figure 28. A 6 inch diameter spherical mirror of 49 inch radius was used to form an image of the monochromatic source on the entrance port of the averaging device. The averaging device, with the detector, was mounted in a milling head, so that it could be moved 8 inches in the x and y directions, and rotated 360° in the x-y plane. The x direction was aligned with the optical axis.

In the areal sensitivity test, the averaging device was mounted at the center of the milling head, with its plane of entrance perpendicular to the incident beam from the spherical mirror. The entrance port of the device was then moved across the incident beam (the size of this beam was 3mm by 3mm) and the detector response was recorded as a function of beam position.

Test B – Size Sensitivity: this test was designed to evaluate the variation in detector response with the size of the irradiated area on the entrance to the averaging device, when the total flux is held constant. The detector and averaging device was mounted on the milling head (figure 28) with the axial ray of the incident beam (3mm by 3mm) centered on and normal to the entrance port of the averaging device. The port was moved along the axial ray of the incident beam, and the detector response was recorded as a function of the entrance port position. Since the incident beam is diverging from an image, the size of the irradiated area could be varied from a minimum when the beam was imaged on the entrance port, to a maximum when the marginal rays fell just inside the port.
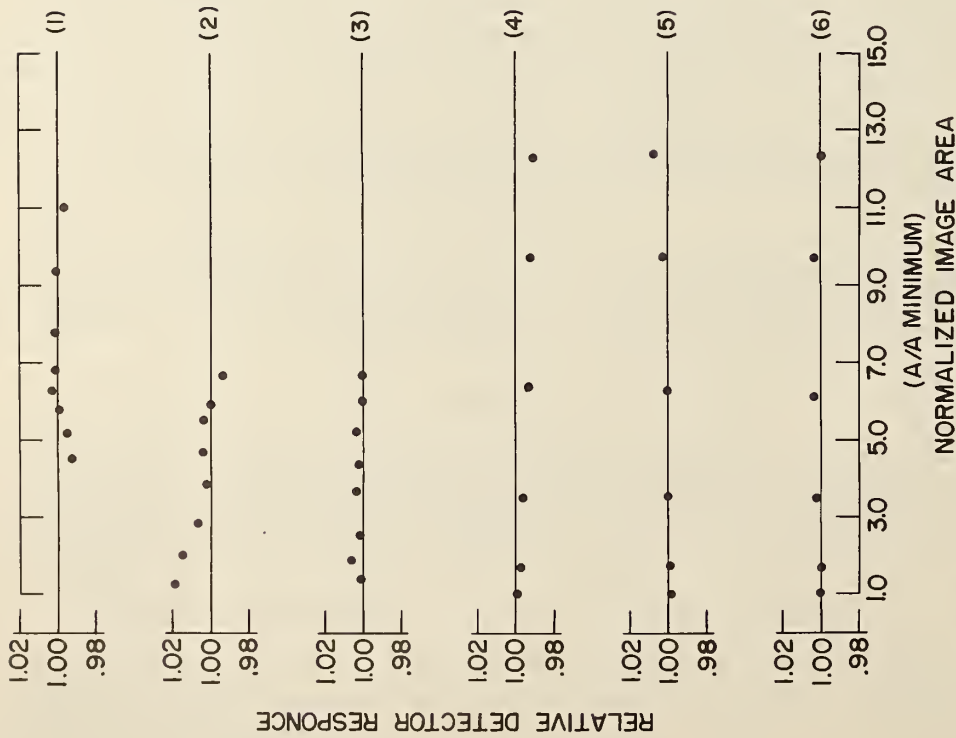
Test C – Angular Sensitivity: in this test, the averaging device was placed on the milling head and the image from the 49 inch radius of curvature mirror was placed on the entrance to the averaging device. The output of the detector was recorded as a function of incident angle as the milling head was rotated. The recorded data were then normalized to a specified direction.
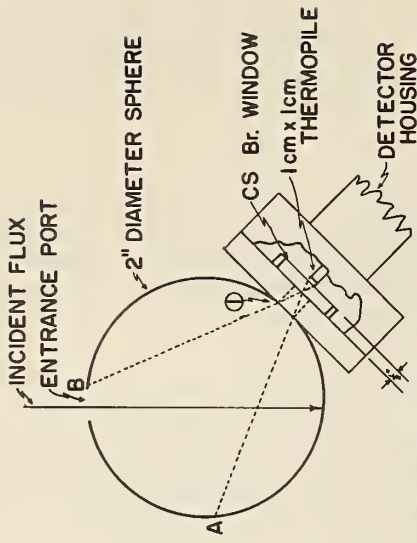
8.2 Averaging Spheres

Preliminary results, using a 2-inch-diameter sphere mounted over the detector, with a white velvet diffusing paint coating (MMM), indicated that this approach seemed feasible, at least at short wavelengths where known diffusers are available [22]. It is known from the theory of integrating spheres [23] that for sphere efficiency to be high, it is necessary for (1) the wall reflectance to be close to unity, (2) the diameter of the sphere to be a minimum, and (3) the area of the entrance and exit ports to be a minimum. In addition the detector should also view the entire sphere. Further, it is

---

[13] A distinction is made between an integrating and an averaging sphere. In the case of the averaging sphere, the main requirement is that the distribution and fraction of the incident flux on the detector must be independent of the area of the sphere wall irradiated for a certain specified area on the sphere, while the integrating sphere assumes uniform diffusion of flux over the entire sphere wall (with the exception of the directly irradiated portion).
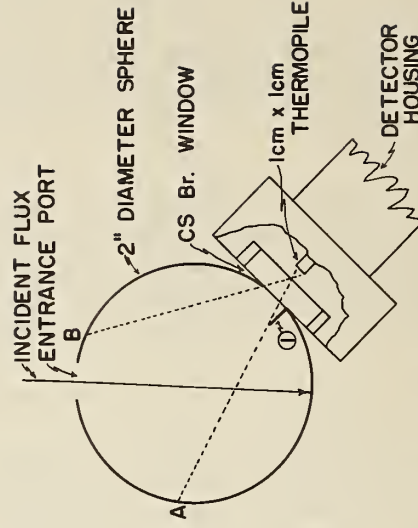
a) EXTERNAL SHIELD

A-B IS FIELD OF VIEW FOR THE DETECTOR
① BLACKENED .15" SHIELD

b) INTERNAL SHIELD

A-B IS FIELD OF VIEW FOR THE DETECTOR
① POLISHED PLATINUM SHIELD

Figure 30. Shield Configurations for Averaging Spheres

(1) 4" MgO SPHERE α 1.5μ
(2) 2" L-SHOT GOLD SPHERE α 2.4μ
(3) 2" HAND PRESSED SULFUR SPHERE α 2.4μ
(4) 2" GOLD SULFUR SPHERE α 2.4μ
(5) 2" SULFUR SPHERE α 2.4μ SHIELD #1
(6) 2" SULFUR SPHERE α 2.4μ SHIELD #2

Figure 29. Results of Size Sensitivity Tests of Coated Spheres

important that the sphere wall be a diffusing surface if a uniform irradiance across the detector port is to be attained.

High sphere efficiency is required in this application because the amount of flux available for measurement in the infrared is near the lower limit of the useful range of the available detectors, particularly at the longer wavelengths. Certain white paints, MgO, and $BaSO_4$ are good sphere coatings in the visible and near infrared, but they have low reflectance beyond 4 or 5 microns and are not suitable for use at longer wavelengths. Birkebak [24] showed that sulfur is both a good diffuser and reflector at 2 microns and 4 microns, and assumed that it is usable to 10 microns. However, he did not mention the specific form of sulfur that was used for his measurements, or his method of applying it to the sphere wall. Kronstein, et. al. [25], reported that mu sulfur and flowers of sulfur are good reflectors out to 15 microns, and gave spectral reflectance curves, but did not use sulfur as a sphere coating. Agnew and McQuistan [26] showed that sulfur is a diffuse reflector to the flux from a SiC source with wavelengths both shorter and longer than 4 microns. Data on the reflectance of mu sulfur are given in figure 17.

Polished metals have high reflectance at all wavelengths from the near infrared to the far infrared, but they are not suitable for use in integrating spheres, since they refelct specularly. Roughened polished metal, however, is a reasonably good diffuser. Hence, it may be possible to produce a usable sphere coating by first contouring a metal surface, and then applying a vacuum-deposited metal coating to increase the surface reflectance. In the present work, two general types of surfaces were considered for use as an averaging sphere coating in the infrared: (1) a roughened gold-plated surface, and (2) a sulfur coating.

Many spheres were built and coated. The following is a partial list of those tested:
(a) A 4-inch-diameter aluminum sphere coated with smoked MgO. The entrance and detector port areas were 0.188 in^2 and 0.875 in^2 respectively.
(b) A 2-inch-diameter sphere roughened by blasting with spherical glass shot. The sphere was then vapor plated with an opaque coating of gold. Entrance and exit port areas for all the 2-inch spheres described in this paper are 0.444 in^2 and 0.515 in^2 respectively.
(c) A 2-inch-diameter sphere coated with mu sulfur[14]. The sulfur was hand pressed onto a roughened sphere wall.
(d) The roughened, gold-plated wall of sphere (2) above, was over-coated with a very thin coat of mu sulfur. The sulfur was suspended in alcohol and sprayed with an ordinary paint sprayer.
(e) A 2-inch-diameter sphere was coated with a 1/8-inch-thick coating of mu sulfur, which had been sprayed from a suspension in alcohol.
(f) A 2-inch-diameter sphere was coated with a 1/8-inch-thick coating of mu sulfur, which was sprayed from a suspension in benzene.

8.2.1 Size Sensitivity: in order to establish the ability of the averaging sphere-detector combination to compare beams of flux of various sizes, the previously described size sensitivity test (test B) was performed.

The measured sphere position was experimentally correlated to the area of sphere wall irradiated by the incident beam, and each area was divided by the cross-sectional area of the beam at the focal plane of the spherical mirror to obtain the area ratio for each position. The detector response at each position was divided by the response at the position where the flux was focused on the sphere wall to obtain the curves shown in figures 29, 31 and 32.

This test simulates the conditions that exist when the detector is used to compare beams of flux of small and large areas. The maximum area ratio attainable with the described experimental arrangement was 12.15 to 1 for the 2-inch-diameter sphere, and about 2.36 to 1 for the 4-inch-diameter sphere.

---

[14] The sulfur used in this investigation was Crystex brand sulfur supplied by Stauffer Chemical Company. The analysis given by the supplier is 99.5% elemental sulfur, 90% mu (insoluble) sulfur, 0.10% ash, and the acidity is 0.05%. Mu (insoluble) sulfur comprises 90% of elemental sulfur.
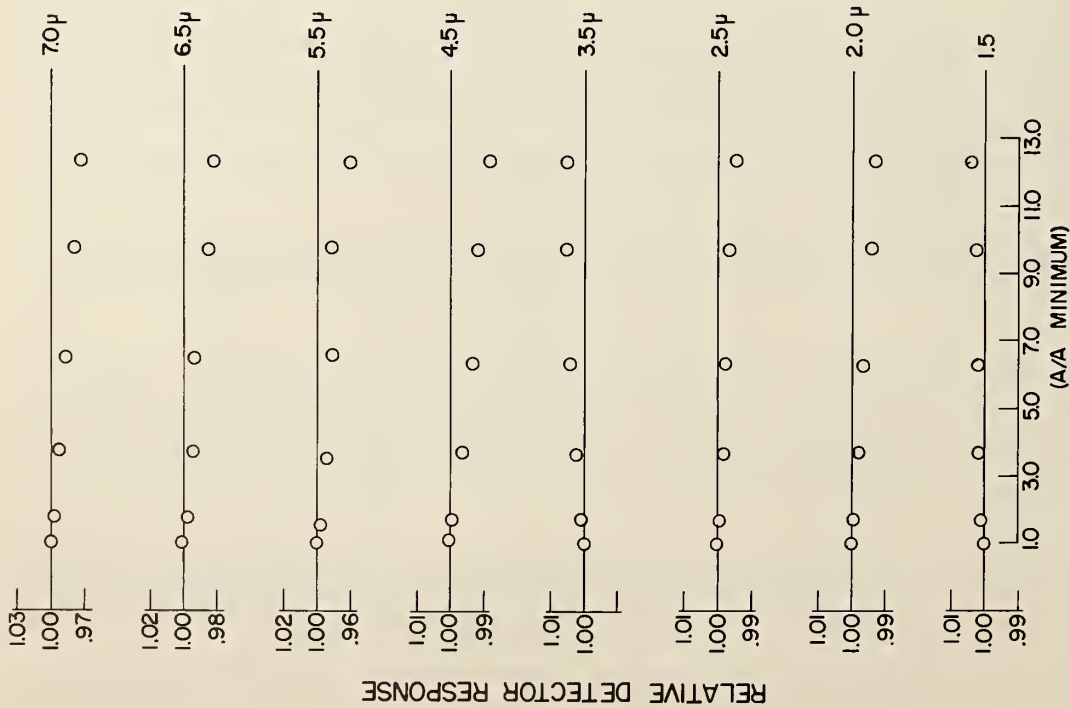
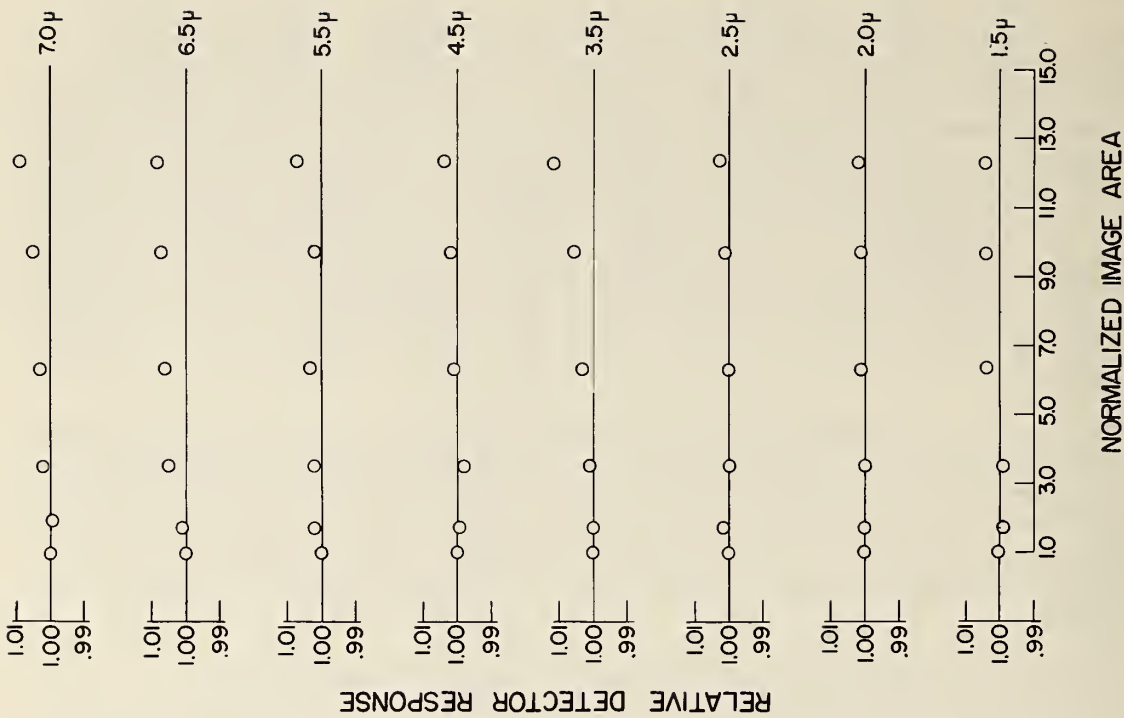Figure 32. Results of Size Sensitivity Test of Sulfur Coated Sphere with External Shield

Figure 31. Results of Size Sensitivity Tests for Sulfur Coated Sphere with Internal Shield

64

The size sensitivity test was applied to all the spheres considered for use as averaging devices. The data at the top of figure 29 represents the results for MgO at 1.5 microns, where it is known to be a good diffuser. R/R_0 varied by 0.8 percent for an area ratio 2.36 to 1. Since the sphere was 4 inches in diameter, the optics of the test system limited the area changes of the image on the sphere wall to a smaller ratio than for the 2-inch-diameter spheres used for the other materials in the test. The results indicate that the sphere does indeed reduce the size sensitivity of the detector. However, MgO is not suitable for general use as a coating in the infrared.

The second curve in figure 29 represents the results for a roughened sphere, which had been vapor-plated with gold; the roughness of the sphere wall was of the order of 25μin rms. The change in R/R_0 was 2 percent, indicating poorer diffuseness than for the MgO. Further, the efficiency of this sphere is almost identical to that of the other spheres tested, despite the very high reflectance of gold. In this design there is a large specular component of flux that passes out the entrance port of the sphere on the first reflection from the sphere wall. Thus, to increase the efficiency of a sphere of this design, the specular component of the first reflection must be kept in the sphere; on the other hand, it must be kept away from the detector's sensitive area, since slight variations in image placement would yield large changes in detector response.

Part 3 of figure 29 shows the data for mu sulfur, which was hand pressed onto the sphere wall. These data have a spread of 0.6 percent in R/R_0 and illustrate the usefulness of mu sulfur for an averaging sphere coating; however, the application technique yielded a surface that was extremely fragile and whose reflectance probably varied significantly from point to point over the sphere wall. Thus, other methods were tried to obtain a more uniform and mechanically durable surface. First, the gold sphere referred to above was coated with a very thin layer of mu sulfur. The sulfur was suspended in alcohol and applied with a paint spray gun. The results of the size sensitivity test indicate a variation in R/R_0 of 1.1 percent. Further, the efficiency of this sphere was nearly the same as that of the hand-pressed sulfur sphere. Since the efficiency was the same, and R/R_0 shows a greater change than that of the hand-pressed sulfur sphere, it was decided to try spraying an optically opaque 1/8-inch-thick coat of sulfur. This sphere exhibited the same change in R/R_0 as the hand-pressed sphere and the coating was less fragile.

To further reduce changes in R/R_0, two different methods of shielding the detector viewing area were tried. Shielding is useful because the detector does not view the entire sphere equally well, as is illustrated by its angular sensitivity. The primary function of a shield is to prevent the detector from viewing the directly irradiated area on the sphere wall for all image configurations. The first shield, which is illustrated in figure 30a, was a 0.15-inch-thick disk placed over the detector with a 1/2-inch-diameter hole centered over the detector sensing area. The sides of this hole were coated with Parson's black paint, and thus restricted the detector's field of view. The results are presented in the second to last graph in figure 29, and indicate an overall range in R/R_0 of 0.6 percent for an area ratio spread twice as large as for the hand-pressed sphere. The second shield tested is shown in figure 30b. This shield was tried because it yields a higher detector efficiency, since it only restricts the detector viewing field in the direction of the image on the sphere wall. The shield was constructed of 0.005-inch-thick polished platinum. The data for this sphere was plotted in the last graph of figure 29 and show a 0.4 percent variation in R/R_0. Thus these tests indicate that either of the spheres with detector shields are usable at 2.4 microns.

These two spheres were tested at other wavelengths in the range 1.5μm to 7.0μm. The results for the platinum shield (shield 2) are given in figure 31. Note that the scale of the graphs for the longer wavelengths is smaller. This figure shows that at the longer wavelengths, where sulfur's reflectance is lower, R/R_0 decreases with an increase in $A/(A_{min})$ as much as 2.8 percent. This could be caused (1) by the incident flux becoming trapped between the platinum shield and the sulfur wall (this would be more pronounced at the longer wavelengths, because the reflectance of the sulfur wall is lower), or (2) by atmospheric absorption in the increased path length due to water and CO_2 in the atmosphere. Such atmospheric absorption is not probable, since the wavelengths used were between the absorption bands (the results in figure 32 for the sphere with the circular disk shield subsantiate this conclusion).

Since the change in R/R_0 for the sphere with the platinum shield was quite large at the longer wavelengths, the sphere configuration using the circular disk was also tested at these wavelengths.[15] The results of the tests for variation of response with image size are given in figure 32. These results show an increase in detector sensitivity with image size, indicating that part of the flux is still reaching the detector on the first reflection for large images. However, the change in R/R_0 is limited to 0.9 percent for the longest wavelength. The reason that the change of R/R_0 varied with wavelength is that the reflectance of sulfur varied with wavelength. With low sphere wall reflectance (i.e., long wavelengths for sulfur), the flux from the first reflection is a major portion of the flux in the sphere, and if the detector views even a very small amount of this flux (which is the case for large images on the sphere wall), there is a significant increase in detector response [27]. This error can be eliminated by increasing the thickness of the shield shown in figure 30; however, this will reduce the efficiency of the sphere, which is intolerable, because the system is already energy limited in the 7-10 micron region when a thermopile detector is used.

The conslusions from this series of test are that a sulfur sphere with the circular disk shield provides the best averaging device of those tested for signals of different image sizes.

8.2.2 <u>Areal Sensitivity</u>: This test was designed to illustrate the required precision of incident image placement for comparing signals of nearly equal image area. The sphere entrance port was traversed across the incident beam, which was focused on the entrance port and had a 3mm by 3mm area.

The results for the sulfur sphere with the internal platinum shield are presented in figure 33. The data are arbitrarily normalized to one of the central readings and plotted as a function of position on the entrance port as measured from one edge. These data show variations exceeding 2 percent at the longer wavelengths.

Results for the sphere with the circular disk shield show variations of less than 0.4 percent for the wavelengths below 5.5 microns, and variations of about 0.8 percent for the longer wavelengths (figure 34). This again illustrates the effect of the first reflected flux, since at the long wavelengths, where the reflectance of sulfur is lower, the detector signal is higher for images between positions 0.4 and 0.6 on the entrance port of the sphere, which is where more of the once reflected flux could reach the detector (left hand side of sphere opening in figure 30).

The results of these tests indicate that for short wavelengths the position of the incident flux on the entrance port is not very critical, while at longer wavelengths more care must be taken in positioning the incident beam.

8.2.3 <u>Angular Sensitivity</u>: The general optical system for the angular sensitivity test is shown schematically in figure 28. In this test, the sphere was positioned with its entrance port at the center of rotation of the milling head, and the incident beam was centered on the entrance port. The sphere was then rotated, and the response of the detector was recorded as a function of the angular position of the sphere measured as the angle between the axial ray of the incident beam and the normal to the sphere entrance port.

If a perfect integrating sphere were tested in this way, and the detector viewed only a portion of the sphere wall, as illustrated in firgure 35, then the signal form the detector would change as the irradiated spot moves around the sphere, by an amount proportional to the difference in radiance of areas on the sphere wall that are and are not directly irradiated by the incident flux. If the area irradiated by the incident flux is not viewed by the detector, no flux that has been reflected only once will be received by the detector. Thus, for a surface that approaches an ideal integrating sphere coating, the curve of response as a function of angle should show two ranges of nearly constant response with a smooth monotonic transition between the two ranges. The lower range would represent those
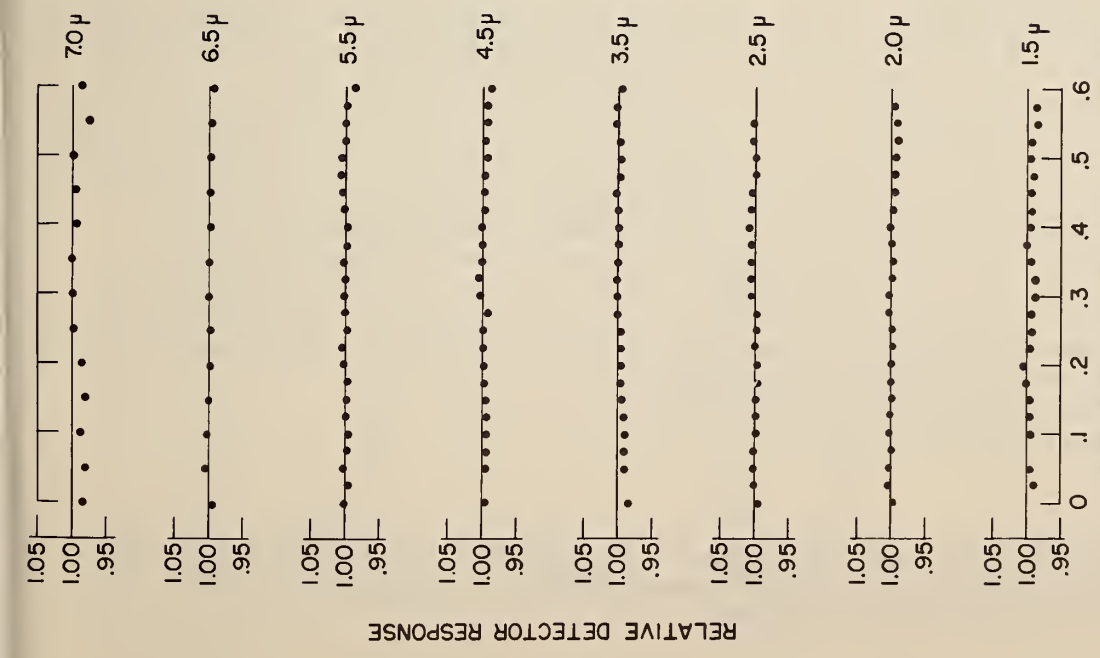
---

[15] Since the previous tests, this sphere had been recoated with sulfur sprayed from a benzene suspension, which yielded a coating that was more stable mechanically than that sprayed from an alcohol suspension.
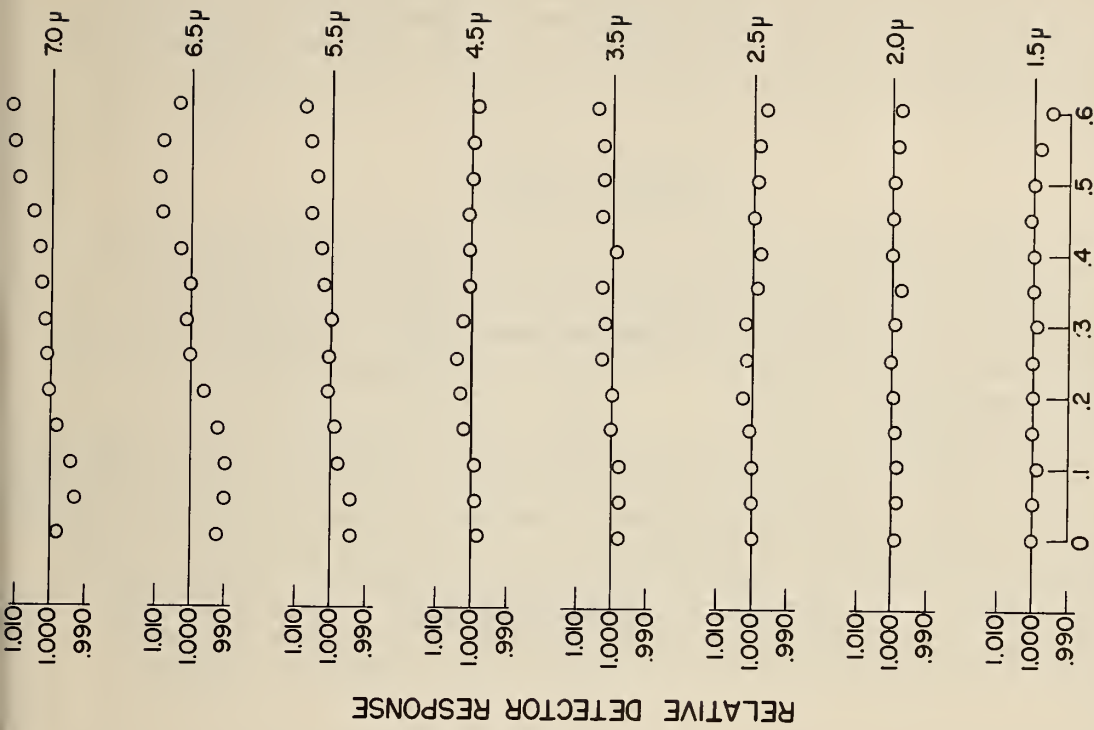
Figure 34. Results of Areal Sensitivity Test of Sulfur Coated
Sphere with External Shield

Figure 33. Results of Areal Sensitivity Test of Sulfur Coated
Sphere with Internal Shield

67

angles at which the detector views none of the irradiated area, and the higher level would represent those angles at which it views the entire irradiated area, and the transition would represent those angles at which the detector views an increasing fraction of the irradiated area. Reference 27 gives equation (91) as the quantitative description of this change for the perfect diffuser as the ratio (R) of the reading when the detector does not view the directly irradiated area to the reading when it views the directly irradiated area.

$$R = \cfrac{1}{1 + \cfrac{(f_2/f_1)[A_s - \rho_s A_{SH}]A_s}{\rho_s (A_{SH})(A_{Dv} - A_{H2})}}$$

(91)

where A is the total area of the sphere ($A = 4\pi R^2$), $A_{SH} = A_s - A_{H1}$ (A_{H1} and A_{H2} are the areas of the exit and entrance ports, respectively), A_{Dv} is the area of the sphere fully viewed by the detector $(A_{Dv} - A_{H2})/A_s$ is the proportion of the twice-reflected flux in the area viewed by the detector, f_1 is the diffuse configuration factor from area ($A_{Dv} - A_{H2}$) to the sensing element of the detector, f_2 is the configuration factor from the area irradiated by the beam to the detector sensing element, and ρ_s is the reflectance of the sphere wall.

Figure 36 shows results obtained with the gold-plated S-460 shot, 2-in-diameter sphere, at wavelengths of 2.2, 5 and 6 microns. In this case, the detector port is in the plane of incidence, and is diametrically opposite the entrance port. The curves indicate that there is a large specular component of the reflected flux reaching the detector when the angle is about 50°, and that the reflectance characteristics do not change appreciably with wavelength. The S-460 shot surface has a roughness of about 15 µin rms, hence no effect of wavelength would be expected in this range. This figure illustrates that the position of the incident beam on the inside of the sphere is quite critical and indicates the necessity of keeping the first reflection away from the detector port in a sphere with imperfectly diffuse walls.[16]

The sulfur coating outlined earlier was tested in this manner. Figure 37 illustrates the results of sulfur at 1.5, 2.2, 5.0 and 10.0 microns. Each of these curves has two flat regions with a smooth monotonic transition between the regions. These results gave a qualitative indication of the utility of sulfur as an averaging sphere coating. Further, the flatness of the flat regions suggests that the placement of a beam inside the sphere is not as critical as with the roughened metal sphere walls.

In addition, the ratios of the heights of the flat portions of these curves (figure 37) agree with the trends indicated in equation (91). However, the ratios calculated from the data in figure 37 were consistently lower by a factor of 2-3 than would be predicted by theory. Apparently, the experimental set-up did not entirely fit the theoretical model. Several possible sources of error are:

(a) the flux from the irradiated area when it is not directly viewed by the detector (i.e., when the incident flux is in area c-d in figure 37) could reach the detector by paths other than by being multiply reflected from the d-a-b-c area viewed by the detector, by (1) hitting the lip of the detector port and being diffused to the detector and (2) by being diffused to the detector by scratches on the CsBr window. The net effect would be to increase the height of the low flat portion of the curves in figure 37.

(b) the radiation of the a-b area of figure 35 is incident at near grazing angles, where even the best diffusers tend to become somewhat specular. Thus, some flux is reflected around the sphere wall into the area c-d, which is not viewed by the detector, instead of being diffusely reflected to the detector. The net effect would be to reduce the height of the high flat portion of the curves in figure 37.

(c) using the wrong value of A_{Dv} in equation (91).

(d) using the wrong value for the reflectance of the sulfur coating.

(e) Improper evaluation of f_1 and f_2.

---

[16] In addition, this test illustrates that roughened surfaces do not and can not follow the intergrating sphere model in any respect; thus, it does not appear promising as a true integrating sphere coating, as has been proposed by several investigators.
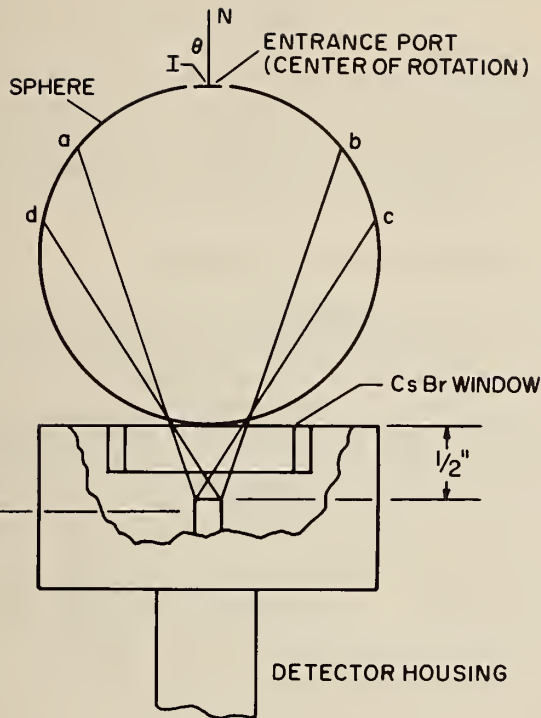
Figure 35. Model of Sphere for Angular Sensitivity Test
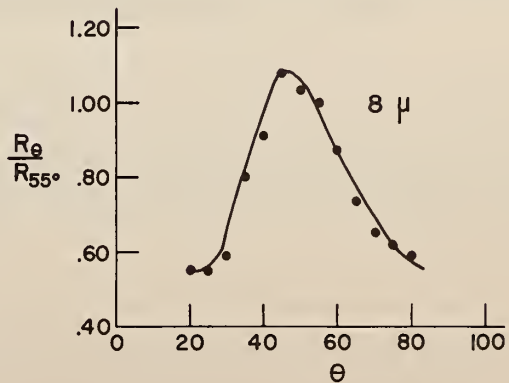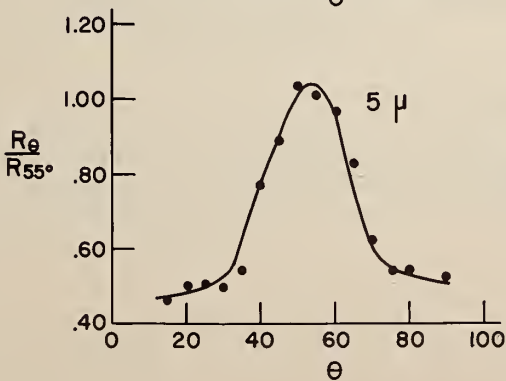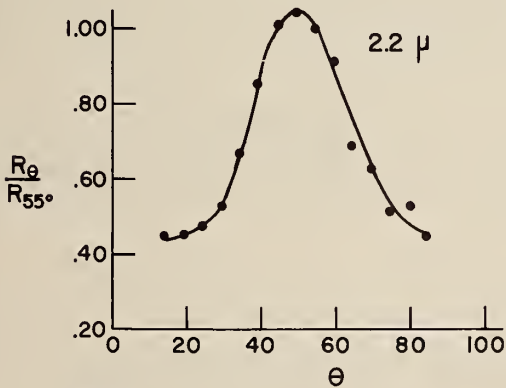
S-460 SHOT GOLD PLATED SPHERE (2" DIAMETER)

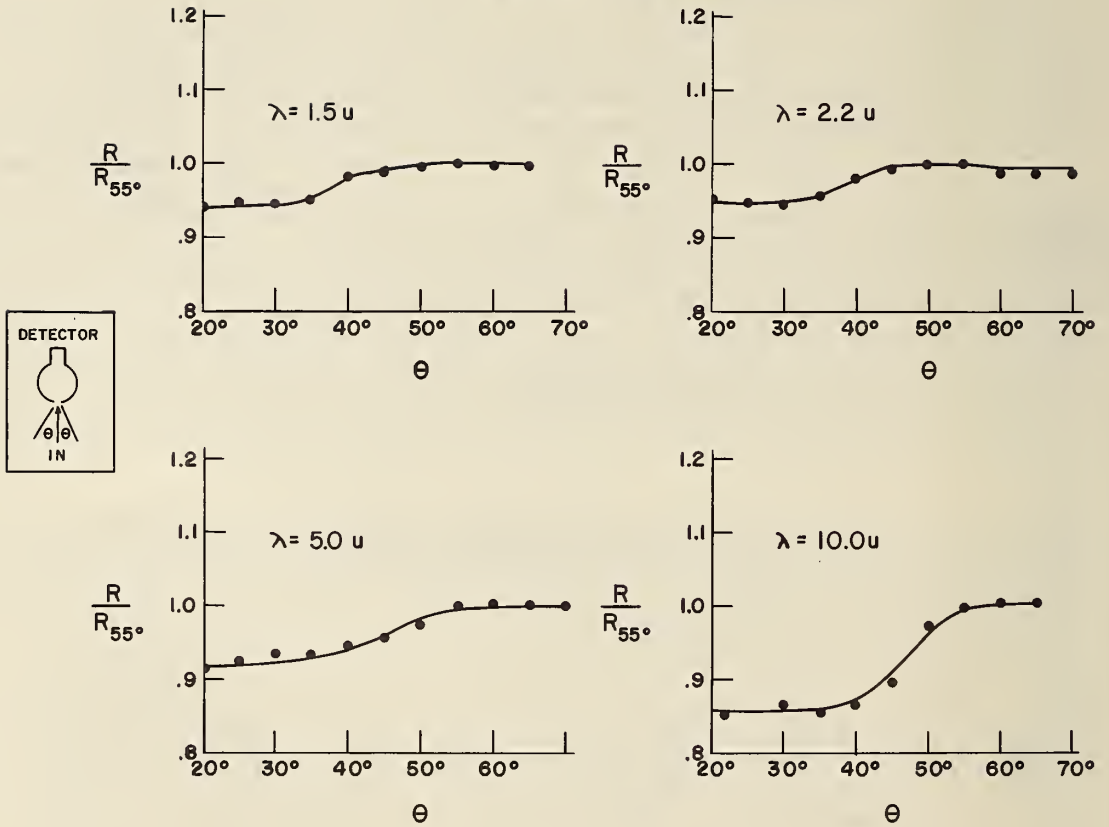Figure 36. Results of Angular Sensitivity Test of Roughened Gold Plated Sphere

69

Figure 37. Results of Angular Sensitivity Test of Sulfur Coated Sphere

The first two effects are largely responsible for the low ratio of the two signals, as compared to the ratio computed from equation (91).

From the results obtained it can be stated that the use of an averaging sphere can be extended at least to 7 microns by use of sulfur as a sphere wall coating. Further, the inherent advantage of this approach is the ability to accept images of varying size by use of a large entrance port and to measure accurately the total flux contained in various incident beams. The major disadvantage is the reduction (by 90 percent) of the flux that reaches the detector.

8.3 Summary

8.3.1 <u>The Sulfur-Coated Averaging Sphere</u>: the data presented indicate that, of the diffusers or averaging devices tested, the sulfur-coated sphere (with a shield restricting the viewing field of the detector) provides highest accuracy in comparing beams of different geometry. Additional advantages occurred through the use of an averaging sphere:(1) practically any detector geometry can be used to view the sphere regardless of sensitive area or type, (2) the use of an averaging sphere greatly reduces the problem of optical alignment, since minor variations in beam placement do not affect the signal output of the detector, and (3) the careful use of the averaging sphere with the detector will provide the capability to measure flux very accurately [more accurately than can be read from the commonly used 10-inch strip chart recorder]. Additional accuracy can be obtained by use of a digital readout.

The major disadvantages of the averaging sphere are the low efficiency of the sphere (the order of 1 to 10% for the spheres tested) and the fact that the sphere reflects flux back out the opening. The efficiency of the sulfur-coated averaging sphere decreases significantly at wavelengths beyond about 10μm, because of the decrease in wall reflectance. However, the tests on the sulfur sphere reported in this paper, combined with the data in references 2 and 8, indicate that sulfur is usable as an averaging sphere coating out to at least 10μm.

8.3.2 <u>Suggested Improvements to the Gold-Roughened Sphere</u>: Since a prime reason that the sulfur-coated sphere cannot be used beyond 10μm is sulfur's low reflectance between 10 and 15μm [24] it is desirable to improve the performance of the gold-roughened sphere. The following two methods are proposed to accomplish this: (1) design the sphere so that the first three specular reflections of the flux do not strike the detector or entrance port of the sphere (especially, keep them away from the detector viewing port), or (2) place an optically opaque coating of sulfur (or some other body scatterer for wavelengths longer than 20 microns, such as groundup CsBr) over the directly irradiated area of the sphere to diffuse the flux on the first reflection. For best results, care should be taken to prevent the detector from viewing any of the diffusing material.

8.3.3 <u>Other Averaging Devices or Techniques</u>: Several methods of averaging beams of flux that were not experimentally studied are (1) the use of lenses over the detector, (2) the use of condensing cones (which have inherent angular and areal sensitivity), (3) the viewing of diffusing blocks which have high areal sensitivity and low angular sensitivity, and (4) the use of statistical methods to compare various detector signals by traversing the sensitive area of the detector for each beam and cross-correlating the resulting sensitivity curves.

8.3.4 <u>Present Use of the Averaging Sphere in the Infrared</u>: The averaging sphere has been successfully used to improve the accuracy of the ellipsoidal-mirror reflectometer and to construct a simple, but accurate, multiple-reflection, infrared specular reflectometer. In both cases, an increased accuracy accompanied a decrease in the required precision of optical alignment. Reference 18 illustrates the use of the gold-roughened sphere to average flux from various sources over the entrance slits to a monochromator.

Effective Reflectance of the Ellipsoidal Mirror

The reflectance of the ellipsoidal mirror is needed in the analysis of the ellipsodial mirror reflectometer.   The effective reflectance accounts not only for the mirror absorptance and transmittance, but also for scattering due to surface roughness and aberrations due to improper construction of the ellipsoidal mirror.

The effective reflectances of various areas of the ellipsoidal mirror were measured because (1) in the absolute reflectance measurement it was necessary to know the reflectance of the ellipsoidal mirror, and (2) in the relative reflectance measurement it was necessary to know the change of reflectance with position of the reflected sample flux on the mirror.

Figure 38 illustrates the 13 areas of the mirror that were examined.   First, the reflectance of area 1 was measured by using a calibrated mirror and then the reflectances of the remaining 12 areas were compared to that of area No. 1 by using two of the calibrated mirrors described in a previous section.   These two calibrated mirrors were used to compare, for one pair of areas at a time, the flux reflected from one of the outer areas (area 2-13) to the flux reflected by area No. 1.   All of the areas on the mirror were larger than $\frac{1}{2}$ inch square, so that each reflected flux represented an average sampling of the reflectance over the particular region of the ellipsoidal mirror.

9. 1 Reflectance Measurement

The reflectance of area 1 was evaluated by taking two measurements; one with the averaging sphere-detector combination at the first focal point, to measure the incident flux F_1 , and the other with a calibrated aluminum mirror at the first focal point and the detector at the second conjugate focal point, to measure the flux F_1 reflected by the sample and the ellipsoidal mirror.   In both measurements the image of the flux to be measured was positioned on the same place in the averaging sphere, so that a very accurate comparison of the two fluxes could be made. Also, in both measurements, the sphere entrance was shielded to allow entrance of only the flux to be measured, eliminating any flux interchange between the sphere and the ellipsoidal mirror.

Since this is essentially an absolute reflectance measurement, the ellipsoidal mirror analysis can be used.   Equation 14 is

$$F_{ID} = F_1 \eta \tag{14}$$

and from equation (58)

$$F_{RD} = F_1 \eta \rho_M \rho_\epsilon \tag{92}$$

where the terms for the interchange between the ellipsoidal mirror and the sphere entrance are eliminated by the shielding described above.   Therefore

$$\bar{\rho}_\epsilon = \frac{F_{RD}}{F_{ID} \ \rho_M} \tag{93}$$

where ρ_M is given in Table X.   The values obtained from four sets of these measurements are listed in Table XII.   The arithmetic average of ρ_ϵ for area No. 1 for these four sets was used in computing the reflectance of the other areas of the mirror.

9. 2 Variation of Reflectance with Position

The change of reflectance as a function of position was measured by use of two of the calibrated mirrors.   These mirrors were placed on sample holders set at different angles to the first focal
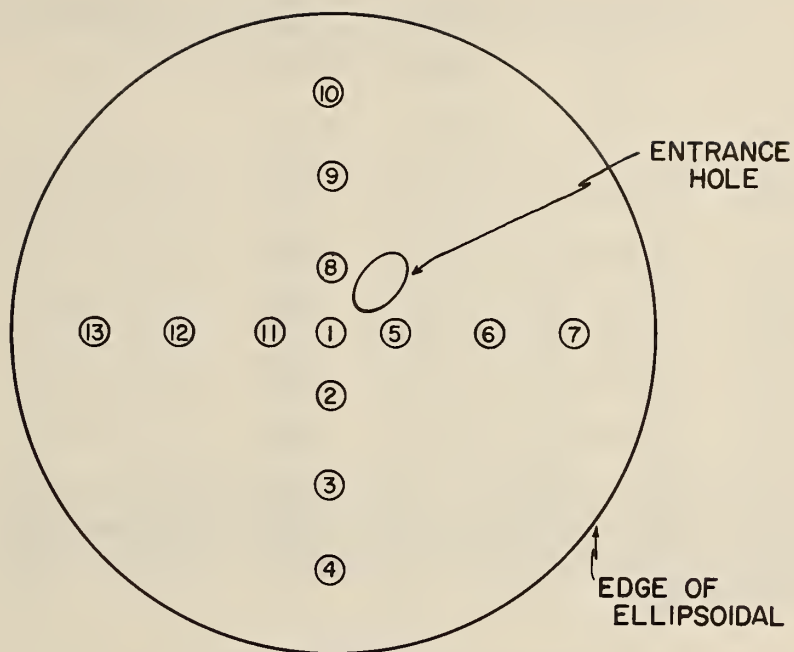
TOP VIEW OF ELLIPSOIDAL MIRROR
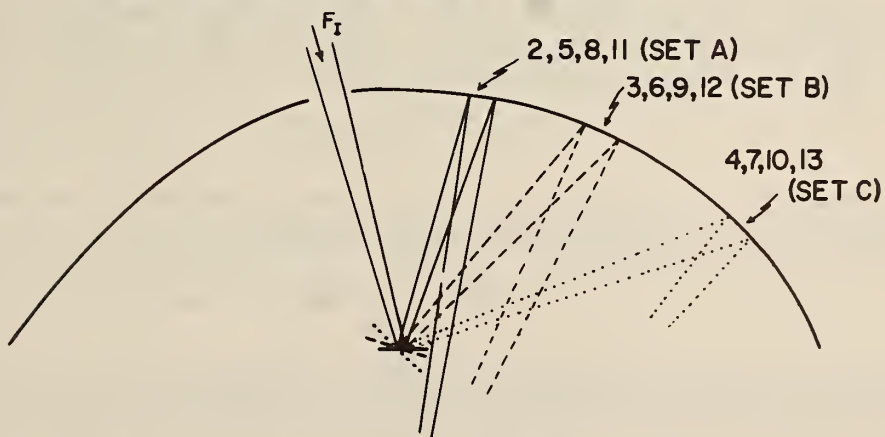
SIDE SECTION OF ELLISOIDAL MIRROR

Figure 38. Areas Measured for Ellipsoidal Mirror Reflectance

73

Table XIII Ellipsoidal Mirror Reflectance

λ, μm	Set 1	Set 2	Set 3	Set 4	Average
1.5	0.951	0.949	0.951	0.948	0.950
2.0	.964	.963	.959	.961	.962
2.5	.965	.969	.967	.963	.966
3.5	.969	.971	.969	.971	.970
4.5	.969	.971	.970	.973	.971
5.5	.970	.971	.973	.970	.971
6.5	.971	.973	.973	.974	.972
7.0	.972	.972	.974	.973	.972

plane of the ellipsoidal mirror (figure 38). Four measurements for each pair of areas were made. One of each pair of measurements was made with area No. 1 in the optical path. The detector was again shielded to prevent interchange between the averaging sphere and the ellipsoidal mirror. The flux viewed by the detector was

$$F_{1D} = \eta\ F_1\ \rho_{M1}\ \rho_{\epsilon 1} \tag{94}$$

where $\rho_{\epsilon 1}$ is the reflectance of area No. 1 and ρ_{M1} is the reflectance of the particular sample mirror. The second measurement was made with sample mirror 2 placed on another sample holder such that one of the remaining areas was in the optical path (areas No. 2-13). Again the averaging sphere was shielded to prevent interchange with the ellipsoidal mirror. The flux viewed by the detector was

$$F_{ND} = \eta\ F_1\ \rho_{M2}\ \rho_{\epsilon N} \tag{95}$$

where n represents one of the areas No 2 through 13. Since the efficiency of the averaging sphere (η) is the same for equations (94) and (95) the ratio of these fluxes is

$$\left[\frac{F_{ND}}{F_{1D}}\right]_{21} = \frac{\rho_{M2}}{\rho_{M1}}\frac{\rho_{\epsilon N}}{\rho_{\epsilon 1}} \tag{96}$$

To eliminate the effect of a possible difference in reflectance between ρ_{M2} and ρ_{M1}, the mirror samples were interchanged and measurements taken again to yield

$$\left[\frac{F_{ND}}{F_{1D}}\right]_{12} = \frac{\rho_{M1}}{\rho_{M2}}\frac{\rho_{\epsilon N}}{\rho_{\epsilon 1}} \tag{97}$$

From equations (96) and (97), the ratio of the two reflectances is given by

$$\frac{\rho_{\epsilon N}}{\rho_{\epsilon 1}} = \left(\left[\frac{F_{ND}}{F_{1D}}\right]_{21}\left[\frac{F_{ND}}{F_{1D}}\right]_{12}\right)^{\frac{1}{2}} \tag{98}$$

Table XIV presents the values obtained in this manner for the 13 positions and for the 8 wavelengths used in this work. The results indicate that $\rho_{\epsilon N}/\rho_{\epsilon 1}$ does not vary with wavelength and that $\rho_{\epsilon N}/\rho_{\epsilon 1}$ increases as one moves away from the apex of the ellipsoidal mirror. Thus it is apparent that the reflectance of the outermost parts of the mirror is about 1.5 percent higher than that of the apex at

Table XIV

The Change in Reflectance of the Ellipsoidal Mirror as a Function of Position
Values are all referred to Area No. 1.   For Location of the Areas on
The Ellipsoid, See Figure 39.

Wavelengths →

Areas	1.5μm	2.0μm	2.5μm	3.5μm	4.5μm	5.5μm	6.5μm	7.0μm
1	1.000	1.000	1.000	1.000	1.000	1.000	1.000	1.000
2	1.001	1.001	1.000	1.000	1.000	1.000	1.001	1.000
3	1.002	1.002	1.001	1.000	1.001	1.001	1.001	1.002
4	1.013	1.010	1.012	1.016	1.016	1.015	1.015	1.013
5	1.000	1.001	1.002	1.001	1.000	1.001	1.000	1.000
6	1.002	1.002	1.003	1.001	1.002	1.002	1.002	1.001
7	1.015	1.013	1.015	1.015	1.014	1.014	1.015	1.013
8	1.001	1.001	1.001	1.000	1.002	1.001	1.001	1.001
9	1.002	1.002	1.003	1.002	1.003	1.002	1.003	1.002
10	1.014	1.015	1.014	1.016	1.015	1.015	1.015	1.014
11	1.001	1.002	1.001	1.000	1.000	1.001	1.001	1.002
12	1.002	1.002	1.001	1.002	1.001	1.002	1.002	1.002
13	1.013	1.014	1.014	1.016	1.014	1.014	1.015	1.014

Average Values of Areas Equal Distance From the Apex of the Ellipsoid

	1.5μm	2.0μm	2.5μm	3.5μm	4.5μm	5.5μm	6.5μm	7.0μm
Set A*	1.001	1.001	1.001	1.000	1.001	1.001	1.001	1.001
Set B*	1.002	1.002	1.002	1.001	1.002	1.002	1.002	1.002
Set C*	1.014	1.013	1.014	1.016	1.015	1.015	1.015	1.014

*Set A is composed of areas 2, 5, 8, and 11; set B is composed of areas 3, 6, 9, and 12; and set C is composed of area 4, 7, 10, and 13.

all wavelengths. Therefore, the flux from a diffusing sample when measured with the ellipsoidal mirror reflectometer should be corrected for mirror reflectance depending on what part of the mirror is used to refocus the flux at the second focal point.

To increase the accuracy of this measurement, a scale expansion technique was used. With this technique, the scale is expanded by a factor of 5 by suppressing the zero by 400 percent. Hence, the error in reading the data from the recorded curve is reduced by about a factor of 5. This permits small changes in large signals to be measured with increased precision. The precision of these measurements is expected to be greater than that reported for the measurements on the specular mirror. This scale expansion technique could be used to increase the precision and accuracy of the values reported in specular reflectance measurements.

10   References

[1] Fragstein, C. V., On the formulation of Kirchhoff's law and its use for a suitable definition of diffuse reflection factors, Optik 12, 60-70 (1955).

[2] Nicodemus, F. E., Directional reflectance and emissivity of an opaque surface, Applied Optics 4, No. 7, 767-773 (July 1965).

[3] Torrance, K. E. and Sparrow, E. M., Off-specular peaks in the directional distribution of reflected thermal radiation, ASME Paper No. 65-WH/HT-19 and Journal of Heat Transfer 88 No. 2, 223-260 (1966).

[4] Wiebelt, J. A., Engineering Radiation Heat Transfer, Holt, Rinehart, & Winston, New York, New York (February 1966).

[5] Brandenberg, W. M., Focusing properties of hemispherical and ellipsoidal mirror reflectometers, Journal of the Optical Society of America 54, 1235-1237 (1964).

[6] Jakob, Max, Heat Transfer, John Wiley & Sons, Inc. 1, 52 (1949).

[7] Harrison, W. N., Richmond, J. C. Shorten, F. J., and Joseph, H. M., Standardization of thermal emittance measurements, WADC TR-59-510, Part IV (November 1963).

[8] Persky, M. J., Atmospheric infrared optics-flux measurements, AFCRL 63-439 (May 1963).

[9] Mertz, L., Transformations in Optics, John Wiley and Sons, New York, New York (1965).

[10] Fellgett, P., Journal de Physique et le Radium 19, 187 (1958).

[11] Connes, J., Spectroscopic studies using Fourier transformation, Revue d'Optique 40, 45-72, 116-140, 171-190 and 231-265 (1961).

[12] Bennett, J. M. and Ashley, E. J., Infrared reflectance and emittance of silver and gold evaporated in ultra-high vacuum, Applied Optics 4, 221-224 (1965).

[13] Gates, D. D., Shaw, C. C. and Beaumont, D., Infrared reflectance of evaporated metal films, Journal of the Optical Society of America 48, 88-89 (1958).

[14] Bennett, H. E. and Koehler, W. F., Precision measurement of absolute specular reflectance with minimized systematic errors, Journal of the Optical Society of America 50, 1-6 (1960)

[15] Bennett, H. E., Silver, M. and Ashley, E. J., Infrared reflectance of aluminum evaporated in Ultra-high vacuum, Journal of the Optical Society of America 53, 1089-1095 (1963).

[16] Hass, G., Optics Section, American Institute of Physics Handbook, Coordinating Editor: D. E. Gray, McGraw-Hill Book Company, Inc., New York, 6-19 (1957).

[17] Hass, G., Filmed surfaces for reflecting optics, Journal of the Optical Society of America 45, 945-952 (1954).

[18] Stair, R. and Schneider, W. E., Standards, sources, and detectors in radiation measurements, Symposium on Thermal Radiation of Solids, Editor: Dr. Samuel Katzoff. NASA SP-55, 217-231 (1965).

[19] Stair, R., Schneider, W. E., Waters, W. R. and Jackson, J. K., Some factors affecting the sensitivity and spectral response of thermoelectric (radiometric) detectors, Applied Optics 4, No. 6, 703-710 (June 1965).

[20] Coblentz, W. W., The radiation sensitivity as a function of area exposed, Bulletin of the Bureau of Standards 11, 142 (1915).

[21] Ronzhin, V. V., A photomultiplier for measuring radiant flux in lighted models with an absorbing medium, Iz vestis Vysshikh Uchebnykh Zavedeniy, Priborostroyeniye, No. 1, 94-98 (1961).

[22] Richmond, J. C., Dunn, S. T., Dewitt, D. P. and Hayes, W. D., Jr., Procedures for precise determination of thermal radiation properties, November 1963 to October 1964, National Bureau of Standards Technical Note 267 (1965).

[23] Jacques, J. A. and Kuppenheim, H. F., Theory of the integrating sphere, Journal of the Optical Society of America 45, 460-470 (1955).

[24] Birkebak, R. C., Monochromatic directional distribution of reflected thermal radiation from roughened surfaces, Ph. D. Thesis, University of Minnesota (1962).

[25] Kronstein, M., Kraushaar, R. J. and Deacle, R. E., Sulfur as a standard of reflectance in the infrared, Journal of the Optical Society of America 53, 458-465 (1963).

[26] Agnew, J. T. and McQuistan, R. B., Experiments concerning infrared diffuse reflectance standards in the range 0.8 to 20.0 microns, Journal of the Optical Society of America 43, 999-1007 (1953).

[27] Dunn, S. T., Design and analysis of an ellipsoidal mirror reflectometer, Ph. D. Thesis, Oklahoma State University, (May 1965).